J Stat Phys (2009) 134: 589–640
DOI 10.1007/s10955-009-9685-5

Statistical Properties of the Burgers Equation with Brownian Initial Velocity

Patrick Valageas

Received: 29 September 2008 / Accepted: 15 January 2009 / Published online: 5 February 2009

Abstract We study the one-dimensional Burgers equation in the inviscid limit for Brownian initial velocity (i.e. the initial velocity is a two-sided Brownian motion that starts from the origin $x = 0$). We obtain the one-point distribution of the velocity field in closed analytical form. In the limit where we are far from the origin, we also obtain the two-point and higher-order distributions. We show how they factorize and recover the statistical invariance through translations for the distributions of velocity increments and Lagrangian increments. We also derive the velocity structure functions and we recover the bifractality of the inverse Lagrangian map. Then, for the case where the initial density is uniform, we obtain the distribution of the density field and its n-point correlations. In the same limit, we derive the n-point distributions of the Lagrangian displacement field and the properties of shocks. We note that both the stable-clustering ansatz and the Press-Schechter mass function, that are widely used in the cosmological context, happen to be exact for this one-dimensional version of the adhesion model.

Keywords Inviscid Burgers equation · Turbulence · Cosmology: large-scale structure of the universe

1 Introduction

The Burgers equation [10] is a very popular nonlinear evolution equation that appears in many physical problems, see [6] for a recent review. It was first introduced as a simplified model of fluid turbulence, as it shares the same hydrodynamical (advective) nonlinearity and several conservation laws with the Navier-Stokes equation. Even though it was shown later on by [28] and [13] that it can be explicitly integrated and lacks the chaotic character associated with actual turbulence, it still retains much interest for hydrodynamical studies. In particular, it can serve as a useful benchmark to test various approximation schemes devised for turbulence studies, since the nonlinearity is the same for both dynamics [16]. On the

P. Valageas (✉)
Institut de Physique Théorique, CEA Saclay, 91191 Gif-sur-Yvette, France
e-mail: valag@spht.saclay.cea.fr

other hand, it has appeared in other physical situations, such as the propagation of nonlinear acoustic waves in non-dispersive media [22], the study of disordered systems and pinned manifolds [30], or the formation of large-scale structures in cosmology [25, 51]. There, in the limit of vanishing viscosity, it is known as the "adhesion model" and it provides a good description of the large-scale filamentary structure of the cosmic web [33]. In this context, one is interested in the statistical properties of the dynamics, starting with random Gaussian initial conditions [26, 29] (i.e. "decaying Burgers turbulence" in the hydrodynamical context). Moreover, in addition to the velocity field, one is also interested in the properties of the density field generated by this dynamics, starting with an initial uniform density.

This problem has led to many studies, focusing on power-law initial spectra (fractional Brownian motion), especially for the two peculiar cases of white-noise initial velocity [10, 17, 29, 41] or Brownian motion initial velocity [9, 41, 43]. The initial velocity fluctuations are dominated by short wavelengths in the former case and by large wavelengths in the latter case. In the present Universe, where the power spectrum is not a power law and converges at both ends, the velocity fluctuations are governed by scales that are somewhat larger than those where structures have already formed (thus the variance of the velocity field is still set by the linear theory) and this scale ratio was larger in the past (as the size of nonlinear structures was smaller). In this sense the case of Brownian initial conditions is closer to the cosmological scenario. From the viewpoint of hydrodynamics, this is also an interesting configuration since in many hydrodynamical systems the power is generated by the larger scales. For instance, the Kolmogorov spectrum of turbulence, $E(k) \propto k^{-5/3}$, displays such an infrared divergence. Thus, the case of Brownian initial velocity was recently used in [19] to address the issue of local homogeneity

In this article, we revisit the one-dimensional Burgers dynamics with two-sided Brownian initial velocity. In the spirit of the approach of [17], using analysis methods (Laplace transforms) we obtain closed analytical results for n-point distributions (mostly in the limit where we are far from the origin of the initial Brownian motion if $n \geq 2$). We check that our results agree with already known properties. In particular, we recover the property, derived by [9] through probabilistic tools for the one-sided Brownian initial velocity, that increments of the inverse Lagrangian map are independent and homogeneous. In our case this only holds for particles that are on the same side of the origin. We pay attention to issues that arise in the hydrodynamical context (e.g., velocity structure functions, Lagrangian displacement field) as well as the cosmological context (e.g., statistics of the density field, mass function of the collapsed structures associated with shocks). In particular, we compare our exact results with phenomenological models that are often used to describe the cosmological dynamics.

We first describe in Sect. 2 the initial Brownian conditions and the standard geometrical interpretation in terms of parabolas of the Hopf-Cole solution of the dynamics [10]. Adapting to our case the method presented in [17], this will allow us to express all statistical properties in terms of the transition kernel associated with Brownian particles moving above parabolic absorbing barriers. We present this propagator in Sect. 3, decomposed over a continuous set of eigenfunctions built from the Airy function (whereas the white-noise case leads to a discrete spectrum, that is also built from Airy functions). Then, we derive closed analytical expressions for the one-point velocity distribution $p_x(v)$ in Sect. 4, as well as the distribution, $p_x(q)$, of the initial Lagrangian position q of the particle that is located at the position x at time t. Next, we study the two-point and higher-order distributions in Sect. 5, and we obtain simple analytical results in the limit where all particles are far from the origin. This allows us to derive the distribution of the density field in Sect. 6, for the case of a uniform initial density. Next, we consider the statistics of the Lagrangian displacement

field in Sect. 7. In the same limit where the particles are far from the origin, we obtain the n-point distributions, $p_{q_i}(x_i)$, of the positions x_i at time t of the particles that were initially at positions q_i. We also derive the probability $\overline{p}_q^{\text{shock}}$ that two particles initially separated by a distance q have coalesced into a single shock by time t. Finally, we obtain in Sect. 8 the mass function of shocks and their spatial distribution.

The reader who is not interested in the technical details of our derivations may directly go to Sect. 5 to survey most of our practical results.

2 Initial Conditions and Geometrical Solution

We consider the one-dimensional Burgers equation for the velocity field $v(x,t)$ in the limit of zero viscosity,

$$\frac{\partial v}{\partial t} + v\frac{\partial v}{\partial x} = \nu\frac{\partial^2 v}{\partial x^2} \quad \text{with } \nu \to 0^+. \tag{1}$$

As is well-known [13, 28], introducing the velocity potential $\psi(x,t)$ and making the change of variable $\psi(x,t) = -2\nu \ln\theta(x,t)$ transforms the nonlinear Burgers equation into the linear heat equation. This gives the explicit solution

$$v(x,t) = \frac{\partial \psi}{\partial x} \quad \text{with } \psi(x,t) = -2\nu \ln \int_{-\infty}^{\infty} \frac{\mathrm{d}q}{\sqrt{4\pi\nu t}} \exp\left[-\frac{(x-q)^2}{4\nu t} - \frac{\psi_0(q)}{2\nu}\right], \tag{2}$$

where we introduced the initial condition $\psi_0(q) = \psi(q, t=0)$. Then, in the limit $\nu \to 0^+$ the steepest-descent method gives

$$\psi(x,t) = \min_q \left[\psi_0(q) + \frac{(x-q)^2}{2t}\right] \quad \text{and} \quad v(x,t) = \frac{x - q(x,t)}{t}, \tag{3}$$

where we introduced the Lagrangian coordinate $q(x,t)$ defined by

$$\psi_0(q) + \frac{(x-q)^2}{2t} \quad \text{is minimum at the point } q = q(x,t). \tag{4}$$

The Eulerian locations x where there are two solutions $q_- < q_+$ to the minimization problem (4) correspond to shocks (and all the matter initially between q_- and q_+ is gathered at x). The application $q \mapsto x(q,t)$ is usually called the Lagrangian map, and $x \mapsto q(x,t)$ the inverse Lagrangian map (which is discontinuous at shock locations). For the case of Brownian initial velocity that we consider in this paper, it is known that the set of regular Lagrangian points has a Hausdorff dimension of $1/2$ [43], whereas shock locations are dense in Eulerian space [41, 43].

In this article, we take for the initial velocity field $v_0(q)$ a bilateral Brownian motion starting from the origin $v_0(0) = 0$, and we also normalize the potential ψ_0 by $\psi_0(0) = 0$. Thus, introducing a Gaussian white noise $\xi(q)$, we can express the initial conditions by

$$v_0(q) = \int_0^q \mathrm{d}q'\xi(q'), \qquad \psi_0(q) = \int_0^q \mathrm{d}q' \int_0^{q'} \mathrm{d}q''\xi(q''). \tag{5}$$

All initial fields are Gaussian and fully determined by their two-point correlation, which we normalize by

$$\langle \xi(q) \rangle = 0, \qquad \langle \xi(q)\xi(q') \rangle = D\delta(q-q'), \tag{6}$$

where $\langle \ldots \rangle$ is the average over all realizations of ξ. This gives for instance

$$\langle v_0(q_1)v_0(q_2)\rangle = Dq_1, \qquad \langle \psi_0(q_1)\psi_0(q_2)\rangle = \frac{D}{2}\left[q_1^2 q_2 - \frac{q_1^3}{3}\right], \quad \text{for } 0 \le q_1 \le q_2, \tag{7}$$

and for the initial velocity distribution at location q,

$$t = 0: \quad p_q(v) = \frac{1}{\sqrt{2\pi}\sigma_{v_0}} e^{-v^2/(2\sigma_{v_0}^2)} \quad \text{with } \sigma_{v_0}^2(q) = Dq. \tag{8}$$

Note that the initial fields over the two sides $q < 0$ and $q > 0$ are independent. The initial velocity $v_0(q)$ is not homogeneous, since the origin $q = 0$ clearly plays a special role, but it has homogeneous increments, as seen from the equality,

$$\text{for any } q_1, q_2: \quad v_0(q_2) - v_0(q_1) = \int_{q_1}^{q_2} \mathrm{d}q\, \xi(q), \qquad \langle [v_0(q_2) - v_0(q_1)]^2 \rangle = D|q_2 - q_1|. \tag{9}$$

Then, the energy spectrum $E_0(k)$ of the initial velocity field is

$$E_0(k) = \frac{D}{4\pi} k^{-2}, \quad \text{with } \langle [v_0(q_2) - v_0(q_1)]^2 \rangle = 2\int_{-\infty}^{\infty} \mathrm{d}k (1 - e^{\mathrm{i}k(q_2 - q_1)}) E_0(k). \tag{10}$$

Thanks to the scale invariance of the Brownian motion, the scaled initial potential $\psi_0(\lambda q)$ has the same probability distribution as $\lambda^{3/2}\psi_0(q)$, for any $\lambda > 0$. Then, using the explicit solution (3) we obtain the scaling laws

$$\psi(x,t) \overset{\text{law}}{=} t^3 \psi(x/t^2, 1), \qquad v(x,t) \overset{\text{law}}{=} t\, v(x/t^2, 1), \qquad q(x,t) \overset{\text{law}}{=} t^2 q(x/t^2, 1), \tag{11}$$

where $\overset{\text{law}}{=}$ means that both sides have the same probability distribution. Thus, any equal-time statistics at a given time $t > 0$ can be expressed in terms of the same quantity at the time $t = 1$ through appropriate rescalings. In this article we only investigate equal-time statistics, so that t can be seen as a mere parameter in the explicit solution (2) from which we derive our results.

In the cosmological context, the time t in the Burgers equation (1) actually stands for the linear growing mode $D_+(t)$ of the density fluctuations, the spatial coordinate x is a comoving coordinate (that follows the uniform Hubble expansion) and, up to a time-dependent factor, the velocity v is the peculiar velocity (where the Hubble expansion has been subtracted), see [25, 51]. In these coordinates, the evolution of the density field is still given by the continuity equation (106) below, where the density ρ is the comoving density. If we take $\nu = 0$, that is we remove the right hand side in (1), this is the well-known Zeldovich approximation [47, 52], where particles always keep their initial velocity and merely follow straight trajectories. The diffusive term of (1) is then added as a phenomenological device to prevent particles from escaping to infinity after crossing each other and to mimic the gravitational trapping of particles within the potential wells formed by the overdensities [25]. Of course, this cannot describe the inner structure of collapsed objects (e.g., galaxies) but it provides a good description of the large-scale structure of the cosmic web [33].

As is well-known [10], the minimization problem (4) has a nice geometrical solution. Indeed, let us consider the downward[1] parabola $\mathcal{P}_{x,c}(q)$ centered at x and of maximum c,

[1] In the literature one usually defines the velocity potential as $v = -\partial_x \psi$, which leads to upward parabolas. Here we prefer to define $v = \partial_x \psi$ to simplify the interpretation of the process (q, ψ_0, v_0) in terms of the dynamics of a Brownian particle.

i.e. of vertex (x, c), of equation

$$\mathcal{P}_{x,c}(q) = -\frac{(q-x)^2}{2t} + c. \tag{12}$$

Then, starting from below with a large negative value of c, such that the parabola is everywhere well below $\psi_0(q)$ (this is possible thanks to the scaling $\psi_0(\lambda q) \overset{\text{law}}{=} \lambda^{3/2}\psi_0(q)$ which shows that $\psi_0(q)$ only grows as $|q|^{3/2}$ at large $|q|$), we increase c until the two curves touch one another. Then, the abscissa of the point of contact is the Lagrangian coordinate $q(x,t)$ and the potential is given by $\psi(x,t) = c$. (We show below in Fig. 1 the case where the Lagrangian coordinate $q'(x,t)$ is somewhere in the range $0 \le q' \le q$.)

3 Transition Kernel with Parabolic Absorbing Barrier

For the Brownian initial conditions (5), the process $q \mapsto \{\psi_0, v_0\}$ is Markovian, going from $q = 0$ towards positive or negative values. Then, following the approach of [17] (where it was applied to white-noise initial velocity), from the geometrical construction (12) we can see that a key quantity is the conditional probability density $K_{x,c}(q_1, \psi_1, v_1; q_2, \psi_2, v_2)$ for the Markov process $\{\psi_0(q), v_0(q)\}$, starting from $\{\psi_1, v_1\}$ at $q_1 \ge 0$, to end at $\{\psi_2, v_2\}$ at $q_2 \ge q_1 \ge 0$, while staying above the parabolic barrier, $\psi_0(q) > \mathcal{P}_{x,c}(q)$, for $q_1 \le q \le q_2$. It obeys the advective-diffusion equation

$$\left[\frac{\partial}{\partial q_2} + v_2\frac{\partial}{\partial \psi_2}\right] K_{x,c}(q_1, \psi_1, v_1; q_2, \psi_2, v_2) = \frac{D}{2}\frac{\partial^2}{\partial v_2^2} K_{x,c}(q_1, \psi_1, v_1; q_2, \psi_2, v_2) \tag{13}$$

over the domain $\psi \ge \mathcal{P}_{x,c}(q)$, with the initial condition at $q_2 = q_1$

$$K_{x,c}(q_1, \psi_1, v_1; q_1, \psi_2, v_2) = \delta(\psi_2 - \psi_1)\delta(v_2 - v_1), \tag{14}$$

and the boundary condition

$$K_{x,c}(q_1, \psi_1, v_1; q_2, \psi_2, v_2) = 0 \quad \text{at } \psi_2 = \mathcal{P}_{x,c}(q_2) \text{ for } v_2 \ge \frac{\mathrm{d}\mathcal{P}_{x,c}}{\mathrm{d}q}(q_2). \tag{15}$$

Equation (13) is also the Klein-Kramers equation for the distribution function $P(x, v; t)$ of Brownian particles, in the limit of zero external force and zero friction coefficient but finite diffusion coefficient, where we identify the position, velocity and time coordinates as $\{x, v; t\} = \{\psi_2, v_2; q_2\}$. The boundary condition (15) simply means that particles cannot come back from the absorbing region (i.e. curves that cross the parabola are "lost" and do not contribute to the probability density $K_{x,c}$).

In the case of white-noise initial velocity studied in [17], the velocity potential ψ itself is a Brownian motion so that the relevant propagator only involves one dependent variable, ψ, as $K^{\text{w.n.}}_{x,c}(q_1, \psi_1; q_2, \psi_2)$. In our case, since ψ is now the integral of the Brownian motion v, the propagator $K_{x,c}$ introduced in (13) involves the two dependent variables v and ψ. Thus, we have a diffusion in a two-dimensional $\{\psi, v\}$-space rather than the one-dimensional ψ-space as in [17]. As we shall see below, the propagator $K_{x,c}$ involves an expansion over a continuous spectrum of eigenfunctions that are built from the Airy function, whereas the white-noise case leads to a different expansion over eigenfunctions that are still built from the Airy function but form a discrete spectrum, see [17].

The conditional probability density $K_{x,c}$ associated with the left-handed Brownian motion $q_2 \leq q_1 \leq 0$ can be obtained from the symmetry $q \to -q$ as:

$$0 \leq q_1 \leq q_2 : \quad K_{x,c}(-q_1, \psi_1, v_1; -q_2, \psi_2, v_2) = K_{-x,c}(q_1, \psi_1, -v_1; q_2, \psi_2, -v_2), \quad (16)$$

hence we only need consider (13) for $0 \leq q_1 \leq q_2$. To solve this equation it is convenient to make the change of variables

$$K_{x,c}(q_1, \psi_1, v_1; q_2, \psi_2, v_2) = \mathcal{K}(q_1, y_1, w_1; q_2, y_2, w_2), \quad (17)$$

with

$$y = \psi - \mathcal{P}_{x,c}(q) = \psi + \frac{(q-x)^2}{2t} - c, \qquad w = v - \frac{\mathrm{d}\mathcal{P}_{x,c}}{\mathrm{d}q}(q) = v + \frac{q-x}{t}, \quad (18)$$

to obtain a simpler boundary at the fixed vertical half-line ($y = 0, w \geq 0$) in the (y, w) half-plane for $\mathcal{K}$, $y \geq 0$ and $-\infty < w < \infty$, instead of the parabolic boundary for K. From (13) the kernel $\mathcal{K}$ satisfies the equation with constant external force

$$\left[\frac{\partial}{\partial q_2} + w_2 \frac{\partial}{\partial y_2} + \frac{1}{t}\frac{\partial}{\partial w_2}\right]\mathcal{K} = \frac{D}{2}\frac{\partial^2}{\partial w_2^2}\mathcal{K}. \quad (19)$$

Then, making the transformation

$$\mathcal{K}(q_1, y_1, w_1; q_2, y_2, w_2) = \frac{2}{D} G(\tau; r_1, u_1; r_2, u_2) \exp\left[\frac{w_2 - w_1}{Dt} - \frac{q_2 - q_1}{2Dt^2}\right], \quad (20)$$

with

$$\tau = q_2 - q_1, \qquad r = \sqrt{\frac{2}{D}}\, y, \qquad u = \sqrt{\frac{2}{D}}\, w, \quad (21)$$

we obtain the simpler advective-diffusion equation for $\tau \geq 0$ and $x \geq 0$,

$$\frac{\partial G}{\partial \tau} + u_2 \frac{\partial G}{\partial r_2} = \frac{\partial^2 G}{\partial u_2^2}, \quad (22)$$

with the initial and boundary conditions

$$G(0; r_1, u_1; r_2, u_2) = \delta(r_2 - r_1)\delta(u_2 - u_1), \qquad G(\tau; r_1, u_1; 0, u_2) = 0 \quad \text{for } u_2 \geq 0. \quad (23)$$

Thus, $G(\tau; r_1, u_1; r_2, u_2)$ is the conditional probability density of Brownian particles with unit diffusion coefficient and absorbing barrier at $r = 0$. This quantity was obtained in [11] and we briefly recall below his procedure using our notations. We first take the Laplace transform of G as

$$\tilde{G}(s; r_1, u_1; r_2, u_2) = \int_0^\infty \mathrm{d}\tau e^{-s\tau} G(\tau; r_1, u_1; r_2, u_2), \quad (24)$$

hence (22) gives

$$\left(s + u_2 \frac{\partial}{\partial r_2} - \frac{\partial^2}{\partial u_2^2}\right)\tilde{G}(s; r_1, u_1; r_2, u_2) = \delta(r_2 - r_1)\delta(u_2 - u_1). \quad (25)$$

Next, to obtain an ordinary differential equation, it is convenient to expand over the eigenfunctions $e^{-\nu^3 r_2} g_{s,\nu}(u_2)$ associated with Schrödinger's equation

$$\left(s - \nu^3 u - \frac{\mathrm{d}^2}{\mathrm{d}u^2}\right) g_{s,\nu}(u) = 0, \quad \text{whence } g_{s,\nu}(u) = \mathrm{Ai}\left[-\nu u + \frac{s}{\nu^2}\right], \tag{26}$$

using the fact that the standard Airy function $\mathrm{Ai}(x)$ is the only solution of $\mathrm{Ai}''(x) = x\mathrm{Ai}(x)$ that vanishes at both ends $x \to \pm\infty$ [1]. We recall in Appendix A some useful properties of this entire function. Using the integral representation (165), we obtain the orthogonality property

$$\int_{-\infty}^{\infty} \mathrm{d}u u \mathrm{Ai}\left[-\nu u + \frac{s}{\nu^2}\right] \mathrm{Ai}\left[-\nu' u + \frac{s}{\nu'^2}\right] = \frac{1}{3\nu} \delta(\nu - \nu'), \tag{27}$$

and the closure relation

$$\int_{-\infty}^{\infty} \mathrm{d}\nu 3\nu \mathrm{Ai}\left[-\nu u + \frac{s}{\nu^2}\right] \mathrm{Ai}\left[-\nu u' + \frac{s}{\nu^2}\right] = \frac{1}{u} \delta(u - u'). \tag{28}$$

Therefore, we can see from (26)–(28) that (25) has the particular solution

$$\begin{aligned} \tilde{G}_0(s; r_1, u_1; r_2, u_2) = \int_{-\infty}^{\infty} \mathrm{d}\nu e^{-\nu^3 (r_2 - r_1)} 3\nu \mathrm{Ai}\left[-\nu u_1 + \frac{s}{\nu^2}\right] \mathrm{Ai}\left[-\nu u_2 + \frac{s}{\nu^2}\right] \\ \times \left[-\theta(-\nu)\theta(r_1 - r_2) + \theta(\nu)\theta(r_2 - r_1)\right] \end{aligned} \tag{29}$$

where θ is the Heaviside function. We can check that $\tilde{G}_0$ vanishes for $|r| \to \infty$ and for $|u| \to \infty$. Then, since we have not taken into account the boundary condition at $r_2 = 0$ of (23) yet, $\tilde{G}_0$ is the Laplace transform of the probability density of Brownian particles over the unbounded plane (r, u) (thus $\tilde{G}_0$ only depends on the length $|r_2 - r_1|$). Note that the solution to this unbounded problem is well known to be the Gaussian [11]

$$G_0(\tau; r_1, u_1; r_2, u_2) = \frac{\sqrt{3}}{2\pi\tau^2} e^{-\frac{3}{\tau^3}(r_2 - r_1 - u_1\tau)^2 + \frac{3}{\tau^2}(r_2 - r_1 - u_1\tau)(u_2 - u_1) - \frac{1}{\tau}(u_2 - u_1)^2}, \tag{30}$$

as can be checked by substitution into (22). Therefore, (30) is the inverse Laplace transform of (29).

Next, in order to satisfy the second constraint (23), we must subtract to $\tilde{G}_0$ an appropriate solution $\tilde{G}_1$ of the homogeneous form of (25). From (26), we can see that $\tilde{G}_1$ can be written as a combination of eigenfunctions $e^{-\mu^3 r_2} g_{s,\mu}(u_2)$, that must be restricted to $\mu > 0$ to ensure that $\tilde{G}$ vanishes for $r_2 \to +\infty$. Moreover, for $r_2 = 0$ only the first part $\theta(-\nu)\theta(r_1 - r_2)$ contributes to $\tilde{G}_0$ in (29). Therefore, to compensate for this term at $r_2 = 0$ for $u_2 \geq 0$, we must look for a function $\tilde{G}_1$ of the form

$$\tilde{G}_1(s; r_1, u_1; r_2, u_2) = \int_0^{\infty} \mathrm{d}\nu e^{-\nu^3 r_1} 3\nu \mathrm{Ai}\left[\nu u_1 + \frac{s}{\nu^2}\right] \phi_{s,\nu}(r_2, u_2), \tag{31}$$

where the function $\phi_{s,\nu}(r, u)$ can be written as

$$\phi_{s,\nu}(r, u) = \int_0^{\infty} \mathrm{d}\mu W_{s,\nu}(\mu) e^{-\mu^3 r} \mathrm{Ai}\left[-\mu u + \frac{s}{\mu^2}\right], \tag{32}$$

with some weight $W_{s,\nu}(\mu)$, and satisfies the constraint

$$\phi_{s,\nu}(r=0,u) = \mathrm{Ai}\left[\nu u + \frac{s}{\nu^2}\right] \quad \text{for } u \geq 0. \tag{33}$$

This is a half-range problem as we must decompose a given function (here $\mathrm{Ai}[\nu u + s/\nu^2]$) over half the domain ($u \geq 0$) using only half of the eigenfunctions $g_{s,\mu}(u)$. Using the results of [31], who studied the Klein-Kramers equation, and taking the limit of zero friction but non-zero diffusion, [11] obtained:

$$\nu > 0: \quad \phi_{s,\nu}(r,u) = \int_0^\infty \frac{\mathrm{d}\mu}{2\pi} \frac{3\nu^{1/2}\mu^{3/2}}{\nu^3+\mu^3} e^{-\frac{2}{3}s^{3/2}(\nu^{-3}+\mu^{-3})} e^{-\mu^3 r} \mathrm{Ai}\left[-\mu u + \frac{s}{\mu^2}\right]. \tag{34}$$

Substituting into (31), we obtain for the solution $\tilde{G}$ of (25), with the boundary conditions (23),

$$\tilde{G} = \tilde{G}_0 - \tilde{G}_1, \quad \text{with} \tag{35}$$

$$\tilde{G}_1 = \int_0^\infty \frac{\mathrm{d}\nu\mathrm{d}\mu}{2\pi} \frac{9\nu^{3/2}\mu^{3/2}}{\nu^3+\mu^3} e^{-\frac{2}{3}s^{3/2}(\nu^{-3}+\mu^{-3})} e^{-\nu^3 r_1 - \mu^3 r_2} \mathrm{Ai}\left[\nu u_1 + \frac{s}{\nu^2}\right] \mathrm{Ai}\left[-\mu u_2 + \frac{s}{\mu^2}\right]. \tag{36}$$

We describe in Appendix B how the solution (34) can be directly obtained for the half-range expansion problem (32)–(33), associated with the Brownian dynamics (22), rather than first solving the problem associated with the Klein-Kramers dynamics and next taking the limit of zero friction, see (188). This also allows us to derive the more general identities (187), (189), that we need in the following sections.

We can see from the explicit expressions (29), (36), that the kernel G also satisfies the backward evolution equations (compare with (22), (25))

$$\left(\frac{\partial}{\partial\tau} - u_1\frac{\partial}{\partial r_1} - \frac{\partial^2}{\partial u_1^2}\right) G(\tau; r_1, u_1; r_2, u_2) = 0, \tag{37}$$

$$\left(s - u_1\frac{\partial}{\partial r_1} - \frac{\partial^2}{\partial u_1^2}\right) \tilde{G}(s; r_1, u_1; r_2, u_2) = \delta(r_2 - r_1)\delta(u_2 - u_1), \tag{38}$$

as well as the boundary condition (compare with (23))

$$G(\tau; 0, u_1; r_2, u_2) = 0 \quad \text{for } u_1 \leq 0. \tag{39}$$

Equation (39) merely states that the trajectory $r(\tau)$ starting on the absorbing barrier at $r_1 = 0$ must start in the upward direction $u_1 > 0$ not to be immediately absorbed.

For later calculations we also need two kernels Δ and H that are derived from G. Thus, we define the propagator Δ, that will be associated with Brownian particles that come within a small distance ϵ from the parabolic absorbing barrier, by

$$\Delta(\tau; r_1, u_1; r_2, u_2) = \lim_{\epsilon\to 0} \frac{1}{\epsilon}[G(\tau; r_1+\epsilon, u_1; r_2+\epsilon, u_2) - G(\tau; r_1, u_1; r_2, u_2)]. \tag{40}$$

From (29) and (36) we have for its Laplace transform $\tilde{\Delta}$

$$\tilde{\Delta}(s; r_1, u_1; r_2, u_2) = \int_0^\infty \frac{\mathrm{d}\nu\mathrm{d}\mu}{2\pi} 9\nu^{3/2}\mu^{3/2} e^{-\frac{2}{3}s^{3/2}(\nu^{-3}+\mu^{-3})} e^{-\nu^3 r_1 - \mu^3 r_2}$$

$$\times \mathrm{Ai}\left[\nu u_1 + \frac{s}{\nu^2}\right]\mathrm{Ai}\left[-\mu u_2 + \frac{s}{\mu^2}\right]. \tag{41}$$

Next, we define the kernel $H_\infty(r_1, u_1)$, associated with Brownian particles that stay forever above the parabolic absorbing barrier, by

$$H_\infty(r_1, u_1) = \lim_{\tau\to+\infty} e^{-\tau/\gamma^2} H(\tau; r_1, u_1), \tag{42}$$

with

$$H(\tau; r_1, u_1) = \int_0^\infty \mathrm{d}r_2 \int_{-\infty}^\infty \mathrm{d}u_2 e^{u_2/\gamma} G(\tau; r_1, u_1; r_2, u_2). \tag{43}$$

Using (29) and (36), and the property (172), we obtain after integration over r_2 and u_2 for the Laplace transform $\tilde{H}$,

$$\begin{aligned}\tilde{H}(s; r_1, u_1) = &\int_{-\infty}^\infty \mathrm{d}\nu \frac{3}{\nu^3}\mathrm{Ai}\left[-\nu u_1 + \frac{s}{\nu^2}\right] e^{(\frac{s}{\gamma} - \frac{1}{3\gamma^3})/\nu^3}\left[\theta(\nu) - \theta(-\nu)(1 - e^{\nu^3 r_1})\right] \\ &- \int_0^\infty \frac{\mathrm{d}\nu\mathrm{d}\mu}{2\pi} \frac{9\nu^{3/2}\mu^{-5/2}}{\nu^3 + \mu^3} e^{-\frac{2}{3}s^{3/2}(\nu^{-3} + \mu^{-3})} e^{-\nu^3 r_1} \mathrm{Ai}\left[\nu u_1 + \frac{s}{\nu^2}\right] e^{(\frac{s}{\gamma} - \frac{1}{3\gamma^3})/\mu^3}.\end{aligned} \tag{44}$$

The behavior for $\tau \to \infty$ of $H(\tau; r_1, u_1)$ is determined by the rightmost singularity of $\tilde{H}$, which is located at $s = 1/\gamma^2$. At this point, the first integral in (44) diverges for $\nu \to 0^+$ whereas the second integral diverges for $\mu \to 0^+$. Therefore, the singularity is governed by the behavior of the integrand for $\nu \to 0^+$ and $\mu \to 0^+$, so that we can expand the first Airy function and the ratio $1/(\nu^3 + \mu^3)$, which yields

$$s \to \gamma^{-2}: \quad \tilde{H} \sim \frac{1}{s - \gamma^{-2}}\left\{e^{u_1/\gamma} - \int_0^\infty \frac{\mathrm{d}\nu}{\sqrt{\pi}} 3\nu^{-3/2} e^{-\frac{2}{3}\nu^{-3} - \nu^3 r_1/\gamma^3} \mathrm{Ai}\left[\nu\frac{u_1}{\gamma} + \frac{1}{\nu^2}\right]\right\}. \tag{45}$$

This gives for the function $H_\infty(r_1, u_1)$:

$$H_\infty(r_1, u_1) = e^{u_1/\gamma} - \int_0^\infty \frac{\mathrm{d}\nu}{\sqrt{\pi}} 3\nu^{-3/2} e^{-\frac{2}{3}\nu^{-3} - \nu^3 r_1/\gamma^3} \mathrm{Ai}\left[\nu\frac{u_1}{\gamma} + \frac{1}{\nu^2}\right]. \tag{46}$$

Finally, using the transformations (17) and (20), we obtain in terms of the original variables

$$K_{x,c}(q_1, \psi_1, v_1; q_2, \psi_2, v_2)\mathrm{d}\psi_2\mathrm{d}v_2 = e^{-\tau/\gamma^2 + (u_2 - u_1)/\gamma} G(\tau; r_1, u_1; r_2, u_2)\mathrm{d}r_2\mathrm{d}u_2, \tag{47}$$

with

$$\tau = \gamma^2(Q_2 - Q_1), \qquad r_i = 2\gamma^3\left[\Psi_i + \frac{(Q_i - X)^2}{2} - C\right], \qquad u_i = 2\gamma(V_i + Q_i - X). \tag{48}$$

Here we introduced the dimensionless spatial coordinates (which we shall note by capital letters in this article)

$$Q = \frac{q}{\gamma^2} = \frac{q}{2Dt^2}, \qquad X = \frac{x}{\gamma^2} = \frac{x}{2Dt^2}, \quad \text{with } \gamma = \sqrt{2D}t, \tag{49}$$

and the dimensionless velocity

$$V = \frac{tv}{\gamma^2} = \frac{v}{2Dt}, \quad \text{whence } X = Q + V \text{ for regular points.} \tag{50}$$

In a similar fashion, the dimensionless velocity potential coordinates in (48) are

$$\Psi = \frac{t\psi}{\gamma^4} \quad \text{and} \quad C = \frac{tc}{\gamma^4}. \tag{51}$$

Next, from (42) the kernel associated with Brownian particles that remain forever above the parabola $\mathcal{P}_{x,c}$ reads as

$$\lim_{q_2 \to +\infty} \int \mathrm{d}\psi_2 \mathrm{d}v_2 K_{x,c}(q_1, \psi_1, v_1; q_2, \psi_2, v_2) = e^{-u_1/\gamma} H_\infty(r_1, u_1), \tag{52}$$

whereas the propagator associated with Brownian particles that come within a small distance δc from the parabolic absorbing barrier is from (40)

$$\begin{aligned} &\lim_{\delta c \to 0} \frac{1}{\delta c} [K_{x,c}(q_1, \psi_1, v_1; q_2, \psi_2, v_2) - K_{x,c+\delta c}(q_1, \psi_1, v_1; q_2, \psi_2, v_2)] \mathrm{d}\psi_2 \mathrm{d}v_2 \\ &\quad = 2\frac{t}{\gamma} e^{-\tau/\gamma^2 + (u_2-u_1)/\gamma} \Delta(\tau; r_1, u_1; r_2, u_2) \mathrm{d}r_2 \mathrm{d}u_2. \end{aligned} \tag{53}$$

4 One-Point Distributions

4.1 Results for Arbitrary Eulerian Location x

In this section we consider the one-point velocity distribution $p_x(v)$ at the Eulerian location x. From the explicit solution (3), it can be derived from the probability distribution $p_x(q)$ of the Lagrangian coordinate $q(x,t)$. Thus, we have from (3)

$$p_x(v) = t p_x(q) \quad \text{and} \quad q = x - vt, \tag{54}$$

where we note $p_x(v)$ and $p_x(q)$ the probability distributions of the velocity v and of the Lagrangian coordinate q, at the Eulerian location x and time t. Here we used the property that $q(x,t)$ is well defined for any x except over a set of zero measure in Eulerian space associated with shocks [41].

Then, from the geometrical construction (12), we are led to consider the bivariate probability distribution, $p_x(0 \le q' \le q, c)\mathrm{d}c$, that the first contact point of the potential $\psi_0(q')$ with the family of downward parabolas $\mathcal{P}_{x,c}(q')$, with c increasing from $-\infty$, occurs at an abscissa q' in the range $0 \le q' \le q$, with a parabola of height between c and $c + \mathrm{d}c$. This will give us in turn the cumulative distribution $p_x(0 \le q' \le q)$ by integrating over c. Then, for $q \ge 0$, we can write this probability distribution as

$$\begin{aligned} p_x(0 \le q' \le q, c)\mathrm{d}c = \lim_{q_\pm \to \pm\infty} \int &\mathrm{d}\psi_- \mathrm{d}v_- \mathrm{d}\psi \mathrm{d}v \mathrm{d}\psi_+ \mathrm{d}v_+ K_{x,c}(0,0,0; q_-, \psi_-, v_-) \\ &\times [K_{x,c}(0,0,0; q, \psi, v) - K_{x,c+\mathrm{d}c}(0,0,0; q, \psi, v)] \\ &\times K_{x,c}(q, \psi, v; q_+, \psi_+, v_+), \end{aligned} \tag{55}$$

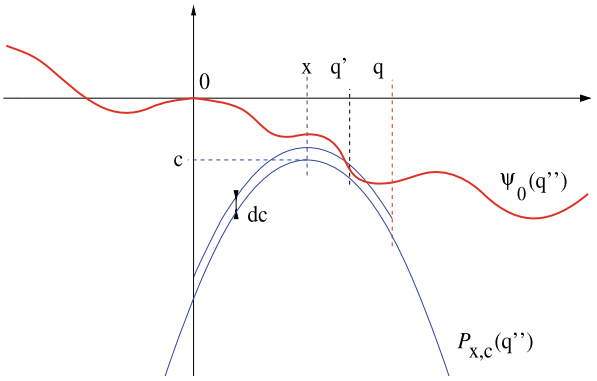

Fig. 1 (Color online) Geometrical interpretation of the initial conditions $\psi_0(q'')$ associated with the probability $p_x(0 \le q' \le q, c)\mathrm{d}c$. The Brownian curve $\psi_0(q'')$ is everywhere above the parabola $\mathcal{P}_{x,c}$ and goes below $\mathcal{P}_{x,c+\mathrm{d}c}$ somewhere in the range $0 \le q'' \le q$. From the constraints $\psi_0(0) = 0$ and $\psi_0'(0) = 0$, see (5), it goes through the origin with an horizontal tangent. To obtain the cumulative probability, $p_x(0 \le q' \le q)$, we must then integrate over the height c of the parabola

where we used the Markovian character of the process $q \mapsto \{\psi, v\}$. Thus, we could factorize in (55) the probability $p_x(0 \le q' \le q, c)\mathrm{d}c$ into three terms, which correspond to the probabilities that i) $\psi_0(q')$ stays above $\mathcal{P}_{x,c}$ for $q' < 0$, ii) $\psi_0(q')$ stays above $\mathcal{P}_{x,c}$, but does not everywhere remain above $\mathcal{P}_{x,c+\mathrm{d}c}$, over the range $0 \le q' \le q$, while reaching an arbitrary value $\{\psi, v\}$ at q, over which we will integrate, and iii) $\psi_0(q')$ stays above $\mathcal{P}_{x,c}$ for $q' > q$. We show in Fig. 1 the geometrical interpretation of (55) (where we did not try to draw an actual Brownian curve $\psi_0(q)$ which has no finite second-derivative).

We can easily check that in the limit $x \to +\infty$ and $q \to +\infty$ with $q \gg x$, the integral over c of (55) gives unity as it should. It is convenient to first compute cumulative probabilities as in (55) and to take the derivatives afterwards to derive the probability densities. This ensures that probabilities are well normalized and it avoids coming across ill-defined expressions. Indeed, since the curve $\psi_0(q)$ has a continuous derivative, it is tangent to the parabola $\mathcal{P}_{x,c}$ at the first contact point. Then, this point corresponds to $r = 0$ and $u = 0$ in terms of the reduced variables (21), where the Brownian kernels are singular. For instance, the expression (29) is not well defined if we naively put $r_1 = r_2 = 0$. Other ambiguities or seemingly divergent quantities appear if we try to directly compute probability densities by using Taylor expansions.

Then, using the relations (47)–(53), we obtain

$$p_x(0 \le q' \le q, r_0)\mathrm{d}r_0 = e^{-q/\gamma^2}\mathrm{d}r_0 \int \mathrm{d}r\mathrm{d}u\, H_\infty(r_0, \hat{u})\Delta(q; r_0, -\hat{u}; r, u)H_\infty(r, u), \qquad (56)$$

where we defined

$$\hat{u} = \sqrt{\frac{2}{D}}\frac{x}{t} = \frac{2x}{\gamma}. \qquad (57)$$

Using the results of Sect. 3, the integration over r and r_0 gives

$$p_x(0 \le q' \le q) = \int_{-i\infty}^{+i\infty} \frac{\mathrm{d}s}{2\pi\mathrm{i}} e^{(s-1)Q} I(s)J(s, 2X), \qquad (58)$$

where we introduced the dimensionless variables Q and X as in (49) and we defined the functions

$$I(s) = \int_{-\infty}^{\infty} \mathrm{d}z\, J(s, 2z), \tag{59}$$

and

$$J(s,y) = e^y \int_0^\infty \frac{\mathrm{d}\nu}{\sqrt{\pi}} 3\nu^{-3/2} e^{-\frac{2}{3}s^{3/2}\nu^{-3}} \mathrm{Ai}\left[-\nu y + \frac{s}{\nu^2}\right] - \int_0^\infty \frac{\mathrm{d}\nu \mathrm{d}\mu}{\pi} \frac{9\nu^{-3/2}\mu^{3/2}}{\nu^3+\mu^3} e^{-\frac{2}{3}(\nu^{-3}+s^{3/2}\mu^{-3})} \mathrm{Ai}\left[\nu y + \frac{1}{\nu^2}\right] \mathrm{Ai}\left[-\mu y + \frac{s}{\mu^2}\right]. \tag{60}$$

For $y \geq 0$, we obtain using (187)–(190),

$$y \geq 0: \quad J(s,y) = s^{-1/4} e^{(1-\sqrt{s})y} - 6\int_0^\infty \frac{\mathrm{d}\nu}{\nu^2} e^{\frac{2}{3}(s^{3/2}-1)\nu^{-3}} \mathrm{Ai}\left[\nu y + \frac{1}{\nu^2}\right] \mathrm{Ai}\left[\nu y + \frac{s}{\nu^2}\right]. \tag{61}$$

For $y \leq 0$, using (189) in the second term of (60), we obtain

$$y \leq 0: \quad J(s,y) = 6\int_0^\infty \frac{\mathrm{d}\mu}{\mu^2} e^{-\frac{2}{3}(s^{3/2}-1)\mu^{-3}} \mathrm{Ai}\left[-\mu y + \frac{1}{\mu^2}\right] \mathrm{Ai}\left[-\mu y + \frac{s}{\mu^2}\right]. \tag{62}$$

Therefore, since we have the primitive

$$\int \mathrm{d}u \mathrm{Ai}\left[\nu u + \frac{s_1}{\nu^2}\right] \mathrm{Ai}\left[\nu u + \frac{s_2}{\nu^2}\right] = \frac{\nu}{s_1 - s_2} \left\{ \mathrm{Ai}'\left[\nu u + \frac{s_1}{\nu^2}\right] \mathrm{Ai}\left[\nu u + \frac{s_2}{\nu^2}\right] - \mathrm{Ai}\left[\nu u + \frac{s_1}{\nu^2}\right] \mathrm{Ai}'\left[\nu u + \frac{s_2}{\nu^2}\right] \right\}, \tag{63}$$

the integral (59) reads as

$$I(s) = \frac{s^{-1/4}}{2(\sqrt{s}-1)} + \frac{3}{s-1} \int_{-\infty}^{\infty} \frac{\mathrm{d}\nu}{\nu} e^{\frac{2}{3}(s^{3/2}-1)\nu^{-3}} \left[\mathrm{Ai}'\left(\frac{s}{\nu^2}\right) \mathrm{Ai}\left(\frac{1}{\nu^2}\right) - \mathrm{Ai}\left(\frac{s}{\nu^2}\right) \mathrm{Ai}'\left(\frac{1}{\nu^2}\right) \right]. \tag{64}$$

Using (199) this yields the simple result

$$I(s) = \frac{1}{s-1}. \tag{65}$$

Therefore, in terms of dimensionless variables, the cumulative probability (58) reads as

$$P_X(0 \leq Q' \leq Q) = \int_{-i\infty}^{+i\infty} \frac{\mathrm{d}s}{2\pi \mathrm{i}} e^{(s-1)Q} \frac{J(s,2X)}{s-1}. \tag{66}$$

On the other hand, since the system is statistically invariant through reflection about the origin, we have the symmetry $p_x(0 \leq q' \leq q) = p_{-x}(-q \leq q' \leq 0)$. This implies that the cumulative probability distribution associated with a Lagrangian coordinate q' on the negative real axis reads as

$$P_X(-Q \leq Q' \leq 0) = \int_{-i\infty}^{+i\infty} \frac{\mathrm{d}s}{2\pi \mathrm{i}} e^{(s-1)Q} \frac{J(s,-2X)}{s-1}. \tag{67}$$

We can also check (67) through an explicit calculation similar to (55).

From (54) and (66)–(67), the cumulative velocity distribution is given by

$$v \le \frac{x}{t}: \quad p_x(v \le v' \le x/t) = p_x(0 \le q' \le x - vt) = P_X(0 \le Q' \le X - V), \tag{68}$$

$$v \ge \frac{x}{t}: \quad p_x(x/t \le v' \le v) = p_x(x - vt \le q' \le 0) = P_{-X}(0 \le Q' \le V - X), \tag{69}$$

where we introduced the dimensionless velocity V defined as in (50). Of course, (66)–(69) agree with the scalings (11).

Letting $|Q| \to \infty$ in (66)–(67), or $|V| \to \infty$ in (68)–(69), we obtain the probabilities that the Lagrangian coordinate q, associated with the Eulerian coordinate x, is located on either side of the origin (or that the velocity v is smaller or greater than x/t):

$$p_x(q \ge 0) = p_x(v \le x/t) = J(1, 2X), \tag{70}$$

$$p_x(q \le 0) = p_x(v \ge x/t) = J(1, -2X). \tag{71}$$

Here we used the fact that the large-Q behavior of (66)–(67) is set by the rightmost singularity of the ratio $J(s, \pm 2X)/(s-1)$, which is the simple pole at $s = 1$. From (61)–(62) we obtain for $x \ge 0$:

$$x \ge 0: \quad p_x(q \le 0) = \int_0^\infty \mathrm{d}\nu \frac{6}{\nu^2} \mathrm{Ai}\left[\nu 2X + \frac{1}{\nu^2}\right]^2, \qquad p_x(q \ge 0) = 1 - p_x(q \le 0). \tag{72}$$

We can check that the sum of these two probabilities is equal to unity. As expected, (72) shows that $p_x(q \le 0)$ decreases as x gets larger and it goes to zero for $x \to +\infty$. For $x = 0$, both quantities are equal to $J(1, 0) = 1/2$, as can be checked from the explicit computation of the integral in (72).

Finally, from (66)–(67) the probability densities are given by:

$$Q \ge 0: \quad P_X(Q) = \int_{-i\infty}^{+i\infty} \frac{\mathrm{d}s}{2\pi \mathrm{i}} e^{(s-1)Q} J(s, 2X), \quad P_X(-Q) = \int_{-i\infty}^{+i\infty} \frac{\mathrm{d}s}{2\pi \mathrm{i}} e^{(s-1)Q} J(s, -2X). \tag{73}$$

This also gives the velocity distributions through the relation (50).

4.2 Velocity Distribution at the Origin $x = 0$

We consider here the one-point distribution at the origin $x = 0$. From (73) we can check that the distribution is even (we have $Q = -V$ at $X = 0$). For $V \ge 0$ it is given by

$$V \ge 0: \quad P_0(V) = \int_{-i\infty}^{+i\infty} \frac{\mathrm{d}s}{2\pi \mathrm{i}} e^{(s-1)V} J(s, 0), \qquad P_0(-V) = P_0(V). \tag{74}$$

The behavior for $V \to 0^+$ is determined by the behavior at $s \to +\infty$ of $J(s, 0)$. From (62) and using (177) we obtain

$$s \to +\infty: J(s, 0) \sim \frac{\sqrt{3}}{\pi} s^{-1/2}, \tag{75}$$

which leads to

$$V \to 0^+: P_0(V) \sim \frac{1}{\pi} \sqrt{\frac{3}{\pi V}}. \tag{76}$$

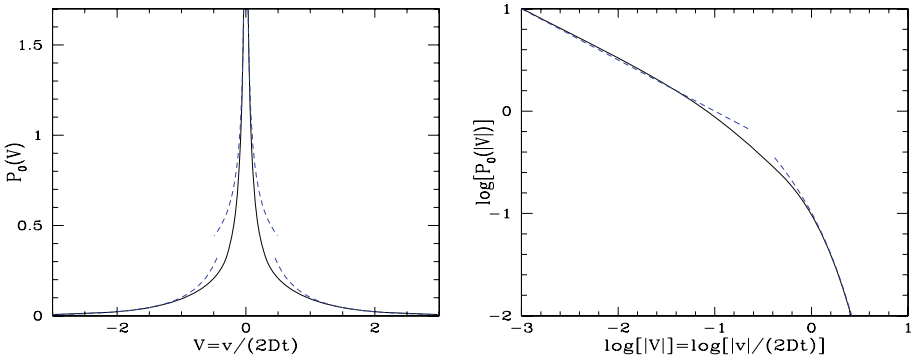

Fig. 2 (Color online) *Left panel:* The probability distribution $P_0(V)$ of the reduced velocity $V = v/(2Dt)$ at the origin $x = 0$, from (74). The *dashed lines* show the asymptotic behaviors (76) and (77). *Right panel:* Same as *left panel* but on a logarithmic scale

Thus, we obtain an inverse square-root divergence for $P_0(V)$ at $V \to 0$.

The behavior of $P_0(V)$ for large V is governed by the rightmost singularity of $J(s, 0)$, located at $s = 0$ (associated with the branch cut along the negative real axis). There, $J(s, 0)$ behaves as $J(s, 0) \sim s^{-1/4}$, because of the first term in (61). This yields

$$V \to +\infty : \quad P_0(V) \sim \frac{1}{\Gamma[1/4]} V^{-3/4} e^{-V}. \tag{77}$$

Note that initially, at time $t = 0$, the velocity at the origin is not random as it is equal to zero, see (5). Then, for $t > 0$ the nonlinear evolution of the velocity field $v(x, t)$ broadens this initial Dirac peak and gives rise to the exponential tail (77) at large velocities and to the power-law peak (76) at low velocities. We show in Fig. 2 the velocity distribution $P_0(V)$, as well as the asymptotic behaviors (76) and (77), that happen to describe very well most of the distribution.

We can note that since all quantities can be expressed in terms of the scaling variables (49)–(50), the exponential tail (77) can be understood from simple scaling arguments applied to the initial velocity field. Thus, for a particle of initial Lagrangian position $q > 0$ to reach the Eulerian position $x = 0$ at time t, we can expect its initial velocity to be of order $v_0 \sim -q/t$. From (8) this corresponds to a probability of order $e^{-v_0^2/(2\sigma_{v_0}^2(q))} \sim e^{-q/t^2} \sim e^{-Q}$, where we did not write factors of order unity in the exponent, which cannot be obtained by such arguments. Thus, we recover the exponential tail (77) (at $X = 0$ we have $V = -Q$).

4.3 Velocity Distribution for $|x| \to \infty$

Finally, we consider the one-point velocity distribution at large $|x|$. By symmetry, we only need consider $x \to +\infty$. Using the relation $X = Q + V$ and (73), we can write the velocity distribution in terms of the reduced variables X and V as

$$V \le X : \quad P_X(V) = \int_{-i\infty}^{+i\infty} \frac{\mathrm{d}s}{2\pi \mathrm{i}} e^{(s-1)(X-V)} J(s, 2X). \tag{78}$$

We now consider the limit $X \to +\infty$ at fixed V. Then, making the change of variable $s = 1 + ik$, we obtain at leading order (k being of order $X^{-1/2}$)

$$P_X(V) \sim \int_{-\infty}^{\infty} \frac{\mathrm{d}k}{2\pi} e^{ik(X-V)} e^{(1-\sqrt{1+ik})2X} \sim \int_{-\infty}^{\infty} \frac{\mathrm{d}k}{2\pi} e^{-ikV - Xk^2/4} = \frac{e^{-V^2/X}}{\sqrt{\pi X}}. \tag{79}$$

Therefore, in terms of the variable v, we recover as expected the initial Gaussian (8). This can be understood as follows. A remote region $[x - L/2, x + L/2]$, with $L \ll x$, has a mean initial velocity $v_0 \sim \sqrt{Dx}$ that is much larger than its initial velocity dispersion $\Delta v_0 \sim \sqrt{DL}$, see (9). Then, this domain remains well-defined and not strongly disturbed by neighboring regions until times of order t_* with $\Delta v_0 t_* = L$, that is $Dt_*^2 = L$. Conversely, at any time t, for $x \gg Dt^2$ (i.e. $X \gg 1$) it is possible to make such a separation of scales and to identify a region of size L around x, with $Dt^2 \ll L \ll x$, that moves in a collective fashion with a mean velocity $\simeq v_0(x)$ that is set by the initial velocity. Therefore, we recover at leading order the initial Gaussian velocity distribution, of variance $\sigma_v = \sqrt{Dx}$ (i.e. $\sigma_V = \sqrt{X/2} \gg 1$), and the nonlinear evolution only modifies the velocity distribution by changes of order $\Delta v \sim Dt$ (i.e. $\Delta V \sim 1$). The result (79) confirms this simple scaling argument. This is an illustration of the "principle of permanence of large eddies" [26], that holds for more general energy spectra, $E_0(k) \propto k^n$, with $n < 1$. As suggested by this discussion, and as checked in numerical simulations [2, 23], the stability of large-scale structures is not only a statistical property but actually holds on an individual basis, that is for each random realization of the velocity field.

Of course, this reasoning does not apply to rare events, such as those where the displacement $x - q$ remains of order x. In particular, from (72), we obtain for the cumulative probability to have a negative Lagrangian coordinate q the asymptotic behavior

$$x \to +\infty : \quad p_x(q \le 0) = p_x(v \ge x/t) \sim \left(8\pi\sqrt{3}X\right)^{-1/2} e^{-4\sqrt{3}X}. \tag{80}$$

Thus, we obtain an exponential tail for these very rare events. It can again be understood from simple scaling arguments, as for the exponential tail (77). Thus, for a particle with Lagrangian coordinate $q < 0$ to reach the position $x \gg 2Dt^2$, we can associate the initial velocity $v_0 = (x - q)/t$ and the probability $e^{-(x-q)^2/(t^2|q|)}$, using (8) without writing numerical factors. Then, the maximum over $q < 0$ of this exponential weight is reached for $q = -x$, which gives a weight $\sim e^{-x/t^2} \sim e^{-X}$ that agrees with (80). We show in Fig. 3 the probability $p_x(q \le 0)$, as well as the asymptotic decay (80).

5 Two-Point and Higher-Order Distributions

5.1 General Results for $x_1 < x_2$ and $0 < q_1 < q_2$

We now study the two-point Eulerian velocity distribution $p_{x_1,x_2}(v_1, v_2)$, with $x_1 < x_2$. As in Sect. 4, we first consider the distribution $p_{x_1,x_2}(q_1, q_2)$ of the Lagrangian coordinates q_1, q_2, associated with the Eulerian positions x_1, x_2. For the Brownian initial conditions (5)–(6) shocks are dense [41, 43]. Therefore, for $x_1 < x_2$ there is almost surely a shock between x_1 and x_2 and these two Eulerian points are associated with two different Lagrangian coordinates $q_1 \ne q_2$. This can also be understood from the fact that at the contact point q_1 (resp. q_2) the curve $\psi_0(q)$ is tangent to a parabola $\mathcal{P}_{x_1,c_1}(q)$ (resp. $\mathcal{P}_{x_2,c_2}(q)$), from the geometric construction recalled in (12). Then, since two parabolas $\mathcal{P}_{x_1,c_1}$ and $\mathcal{P}_{x_2,c_2}$ with $x_1 \ne x_2$ have

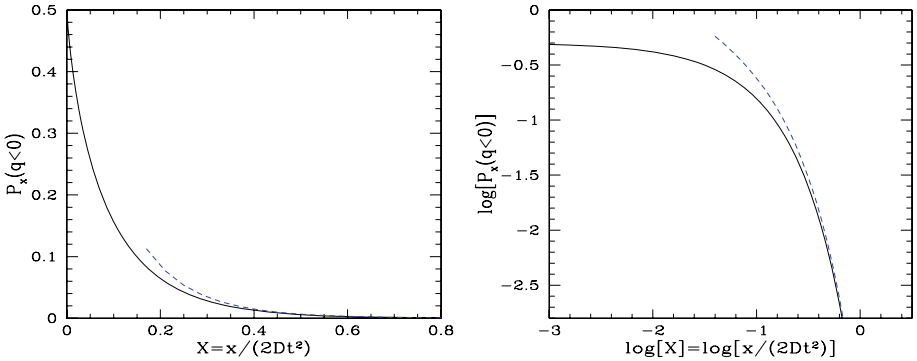

Fig. 3 (Color online) *Left panel:* The probability $p_x(q \leq 0)$ (equal to the reduced cumulative probability $P_X(Q \leq 0)$), that a particle, located at a position $x > 0$ at time t, was initially located on the negative real axis, $q < 0$, from (72). The *dashed line* is the asymptotic behavior (80). *Right panel:* Same as *left panel* but on a logarithmic scale

different tangents at any point q (indeed $\mathrm{d}\mathcal{P}_{x,c}/\mathrm{d}q = -(q-x)/t$), the curve $\psi_0(q)$ cannot be tangent to both parabolas at a common point $q_1 = q_2$ (in both steps we used the property that the derivative $\psi_0'(q)$ is continuous, being a Brownian motion). Therefore, we almost surely have $q_1 \neq q_2$. Then, since particles do not cross each other we have $q_1 < q_2$ for $x_1 < x_2$.

As in Sect. 4.1, we first consider the cumulative probability distribution, $p_{x_1,x_2}(0 \leq q_1' \leq q_1; q_2' \geq q_2)$, that the Lagrangian coordinates q_1', q_2', associated with the Eulerian positions x_1, x_2, are within the ranges $0 \leq q_1' \leq q_1$ and $q_2 \leq q_2' < +\infty$. Let us consider this probability in two steps. First, as for (55), we consider the initial conditions such that $\psi_0(q)$ stays everywhere above a parabola $\mathcal{P}_{x_1,c_1}$ but goes below $\mathcal{P}_{x_1,c_1+\mathrm{d}c_1}$ somewhere in the range $0 \leq q_1' \leq q_1$. Integrating over the height c_1 this will take care of the first constraint $0 \leq q_1' \leq q_1$ for the Lagrangian coordinate associated with x_1. Second, we must only count among those initial conditions the ones that also satisfy $q_2' \geq q_2$. We split them into two contributions as follows. Let us note q_* the unique abscissa where the two contact parabolas $\mathcal{P}_{x_1,c_1}$ and $\mathcal{P}_{x_2,c_2}$ intersect. From (12) it is given by

$$q_* = \frac{x_1+x_2}{2} - \frac{c_2-c_1}{x_2-x_1}t. \tag{81}$$

Then, we note $p^>$ the first contribution, associated with initial conditions such that $q_* > q_2$ (which implies $q_2' > q_* > q_2$). Clearly, this actually corresponds to curves $\psi_0(q)$ that at some point go below the parabola $\mathcal{P}_{x_2,c_*}$ where c_* is such that $q_* = q_2$ (i.e. the second parabola intersects $\mathcal{P}_{x_1,c_1}$ at q_2). We note $p^<$ the second contribution, associated with $q_1 < q_* < q_2$ (since afterwards we shall consider the probability density $p_{x_1,x_2}(q_1; q_2' \geq q_2)$ we only need to include the cases with $q_* > q_1$). We show in Figs. 4 and 5 the geometrical interpretation of these two contributions $p^>$ and $p^<$.

We describe in Appendix C the computation of the two-point distribution $p_{x_1,x_2}(q_1,q_2)$ from these two contributions $p^>$ and $p^<$. As for the one-point distribution computed in Sect. 4.1, we first express the kernels K in terms of the Brownian propagator G obtained in Sect. 3 and we use various properties of the Airy functions, described in Appendices A and B, to simplify the integrals. We finally obtain for the sum of both contributions the

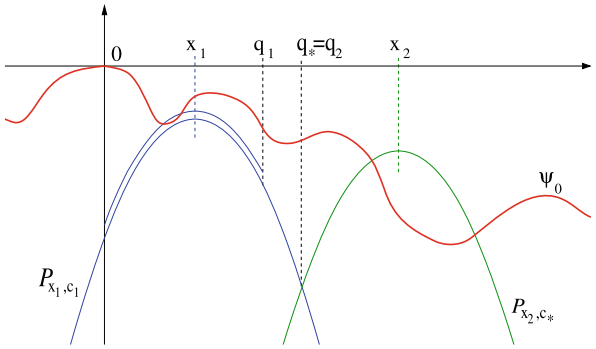

Fig. 4 (Color online) Geometrical interpretation of the initial conditions $\psi_0(q)$ associated with the contribution $p^{>}_{x_1,x_2}(0 \le q_1' \le q_1, c_1; q_2' \ge q_2)\mathrm{d}c_1$. The Brownian curve $\psi_0(q)$ is everywhere above the parabola $\mathcal{P}_{x_1,c_1}$, it goes below $\mathcal{P}_{x_1,c_1+\mathrm{d}c_1}$ somewhere in the range $0 \le q_1' \le q_1$, and it goes below the parabola $\mathcal{P}_{x_2,c_*}$, of center x_2, that intersects $\mathcal{P}_{x_1,c_1}$ at $q_* = q_2$. This counts all paths with a first-contact parabola $\mathcal{P}_{x_2,c_2}$ such that $c_2 \le c_*$ and $q_* \ge q_2$ (which implies $q_2' \ge q_2$)

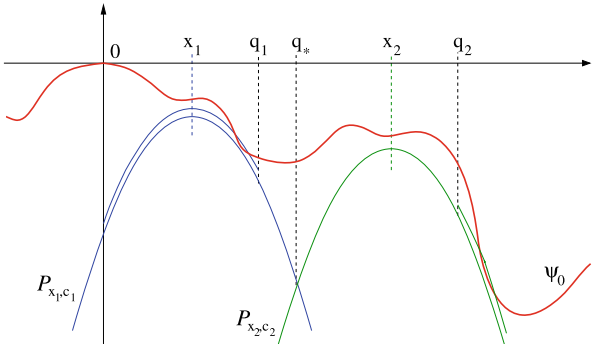

Fig. 5 (Color online) Geometrical interpretation of the initial conditions $\psi_0(q)$ associated with the contribution $p^{<}_{x_1,x_2}(0 \le q_1' \le q_1, c_1; q_2' \ge q_2, c_2)\mathrm{d}c_1\mathrm{d}c_2$. The Brownian curve $\psi_0(q)$ is everywhere above the parabolas $\mathcal{P}_{x_1,c_1}$ and $\mathcal{P}_{x_2,c_2}$, it goes below $\mathcal{P}_{x_1,c_1+\mathrm{d}c_1}$ somewhere in the range $0 \le q_1' \le q_1$, and below the parabola $\mathcal{P}_{x_2,c_2+\mathrm{d}c_2}$ somewhere in the semi-infinite range $q_2' \ge q_2$. The height c_2 of the second parabola is such that both parabolas intersect at q_* in the range $q_1 \le q_* \le q_2$

probability density

$$P_{X_1,X_2}(Q_1, Q_2) = \int_{-i\infty}^{+i\infty} \frac{\mathrm{d}s_1 \mathrm{d}s_2}{(2\pi \mathrm{i})^2} e^{(s_1-1)Q_1+(s_2-1)Q_{21}} J(s_1, 2X_1) e^{-(\sqrt{s_2}-1)2X_{21}}. \tag{82}$$

Comparing with the one-point probability density (73), we find that for $0 \le Q_1 \le Q_2$ the two-point probability density factorizes as

$$X_1 \le X_2, 0 \le Q_1 \le Q_2 : \quad P_{X_1,X_2}(Q_1, Q_2) = P_{X_1}(Q_1)\overline{P}_{X_{21}}(Q_{21}), \tag{83}$$

where we introduced

$$\overline{P}_X(Q) = \int_{-i\infty}^{+i\infty} \frac{\mathrm{d}s}{2\pi \mathrm{i}} e^{(s-1)Q} e^{-(\sqrt{s}-1)2X}. \tag{84}$$

Therefore, the conditional probability $P(X_2, Q_2|X_1, Q_1)$ obeys the property

$$X_1 \leq X_2, 0 \leq Q_1 \leq Q_2 : \quad P(X_2, Q_2|X_1, Q_1) = \frac{P_{X_1,X_2}(Q_1, Q_2)}{P_{X_1}(Q_1)} = \overline{P}_{X_{21}}(Q_{21}), \quad (85)$$

that is, it only depends on the relative distances X_{21} and Q_{21}, and no longer on Q_1 and X_1, over the range $Q_1 \geq 0$. Thus, the system is statistically homogeneous with respect to Lagrangian and velocity increments as long as we remain on either side of the origin $Q = 0$. Indeed, by symmetry through reflection about the origin we also have

$$\begin{aligned} X_1 \leq X_2, Q_1 \leq Q_2 \leq 0 : \quad P_{X_1,X_2}(Q_1, Q_2) &= P_{-X_2,-X_1}(-Q_2, -Q_1) \\ &= P_{-X_2}(-Q_2)\overline{P}_{X_{21}}(Q_{21}) \\ &= P_{X_2}(Q_2)\overline{P}_{X_{21}}(Q_{21}). \end{aligned} \quad (86)$$

Then, in the limits $X_1 \to +\infty$, or $X_2 \to -\infty$, where the weight of configurations such that Q_1 and Q_2 have different signs vanishes, we recover the invariance through translation of the probability distributions of relative displacements and velocity increments. Of course, this is related to the fact that the initial conditions have homogeneous velocity increments, see (9). However, the invariance through translation is only recovered in the exact nonlinear velocity distribution if we go infinitely far from the origin $Q = 0$. As we get closer to the origin it is broken by the increasing weight of configurations, such that Q_1 and Q_2 are on different sides of the origin, which do not satisfy the factorizations (83) or (86). Indeed, note that (86) shows that the factorization (83) cannot be extended to $Q_1 < 0$, as for $Q_1 < 0$ and $Q_2 < 0$ we must reach the other regime (86) that cannot hold simultaneously.

Thus, at finite distance from the origin the invariance through translation is always partly broken for the distribution $P_{x_1,x_2}(q_1, q_2)$ considered over the full range $-\infty < q_1 \leq q_2 < \infty$. Nevertheless, the invariance is exactly recovered over either the partial range $0 \leq q_1 \leq q_2 < \infty$, or $-\infty < q_1 \leq q_2 \leq 0$. This can be understood as follows, focussing on the case $q_1 > 0$ with again $x_1 < x_2$. The probability density $p_{x_1}(q_1)$ counts the configurations $\psi_0(q)$ that are tangent at q_1 with the highest first contact parabola $\mathcal{P}_{x_1,c_1}$, from the geometric construction described below (12). Then, the conditional probability density $p(x_{21}, q_{21}|x_1, q_1)$ only counts among those the configurations that are also tangent at q_2 with the highest first contact parabola $\mathcal{P}_{x_2,c_2}$. Independently of the behavior of the curve ψ_0 on either side of q_1, the first-contact height parameter c_2 must be smaller than the value c_* such that $\mathcal{P}_{x_2,c_*}$ runs through the point $\{q_1, \psi_0(q_1)\}$. Then, for any $c_2 < c_*$, we clearly have $\mathcal{P}_{x_2,c_2}(q) < \mathcal{P}_{x_1,c_1}(q)$ for all $q < q_1$ (using $x_1 < x_2$), whence $\mathcal{P}_{x_2,c_2}(q) < \psi_0(q)$ for all $q < q_1$ since we have already selected those configurations associated with $p_{x_1}(q_1)$ that are above $\mathcal{P}_{x_1,c_1}$ (and make contact at q_1). (In other words, the additional requirement $q(x_2) = q_2$ does not bring any additional constraint on $\psi_0(q)$ over $q < q_1$.) Therefore, we are only sensitive to the behavior of ψ_0 to the right of q_1. For the Brownian initial conditions (5), the latter is fully determined by $\{\psi_0(q_1), v_0(q_1)\}$ and the white noise $\xi(q)$ at $q \geq q_1$ (which is statistically homogeneous). Next, $p(x_{21}, q_{21}|x_1, q_1)$ does not depend on $\psi_0(q_1)$ since a vertical translation of the curves ψ_0 and $\mathcal{P}_{x_1,c_1}$ is fully absorbed by the same vertical translation of the parabola $\mathcal{P}_{x_2,c_2}$, without affecting spatial coordinates q and x. On the other hand, through Galilean invariance the relative displacements of the particles only depend on their relative velocities, hence $p(x_{21}, q_{21}|x_1, q_1)$ only depends on the relative velocity field $v_0(q) - v_0(q_1)$ over $q \geq q_1$. For the Brownian initial conditions (5), with homogeneous velocity increments, the statistical properties of this relative velocity field $v_0(q) - v_0(q_1)$ do not depend on $v_0(q_1)$, but only

on the distance $q - q_1$, see (9). Therefore, the distributions $p(x_{21}, q_{21}|x_1, q_1)$, of the Lagrangian position increment q_{21}, and $p(x_{21}, v_{21}|x_1, v_1)$, of the velocity increment v_{21}, only depend on x_{21}, as in (85) and in (89) below.

In agreement with (86), we can check that this argument fails for $q_1 < 0$. Indeed, again we are only sensitive to the behavior of $\psi_0(q)$ to the right of q_1, but this range now includes the special point $q = 0$ with the constraints $\psi_0(0) = 0$ and $v_0(0) = 0$ that prevent us from absorbing $\psi_0(q_1)$ and $v_0(q_1)$. For instance, we now have the new constraint that the first-contact parabola $\mathcal{P}_{x_2,c_2}$ cannot go upward of the point $\{0, \psi_0(0) = 0\}$ (which was irrelevant in the previous case $q_1 > 0$, since we already had $\mathcal{P}_{x_2,c_2} < \mathcal{P}_{x_1,c_1}$ over $q < q_1$ and $\mathcal{P}_{x_1,c_1}(0) \leq 0$ by construction, being everywhere below ψ_0).

The property that the increments of the inverse Lagrangian map, $q(x_2) - q(x_1)$, are independent and homogeneous, as in (85), and the probability distribution (84), were already obtained by [12] for intrinsic statistical solutions, and by [9] through probabilistic tools for $x \geq 0$ in the case of one-sided Brownian initial conditions (i.e. $v_0(q) = 0$ for $q \leq 0$). The latter work involves a similar reasoning to the one described above, using the property that the distribution of a Markov process after last passage at a given point does not depend on its previous path, but this mathematical proof uses the convex hull of the Lagrangian potential rather than the parabolas construction used here. For one-sided Brownian initial conditions, it is clear that if we consider Eulerian locations at $x \geq 0$, the particles can only come from the right side $q \geq 0$ so that we recover the configuration analyzed above for particles that are all located on the same side of the origin. The agreement with the results of [9] provides a nice check of our calculations. The probabilistic proof is remarkably concise, as it first shows that the increments q_{21} are independent and homogeneous and next derives their distribution. However, the analysis method presented in the present work has the advantage of a large range of applicability. Thus, it allowed us to obtain the one-point distributions in closed form in Sect. 4 and it could also be applied to different-time statistics, where the parabolas would have different curvatures. Another application of the method described in this paper is presented in [48], where we study ballistic aggregation for one-sided Brownian initial velocity.

The previous discussion can be extended to n-point distributions, which thus factorize as

$$\begin{aligned} &X_1 \leq \ldots \leq X_n, 0 \leq Q_1 \leq \ldots \leq Q_n : \\ &\quad P_{X_1,\ldots,X_n}(Q_1, \ldots, Q_n) \\ &\qquad = P_{X_1}(Q_1)\overline{P}_{X_2-X_1}(Q_2 - Q_1)\overline{P}_{X_3-X_2}(Q_3 - Q_2)\ldots\overline{P}_{X_n-X_{n-1}}(Q_n - Q_{n-1}). \end{aligned} \tag{87}$$

We obtain a similar identity for $Q_1 \leq \ldots \leq Q_n \leq 0$ by reflection through the origin, as for (86). This also extends to the general case where the Lagrangian coordinates are located on both sides of the origin as

$$\begin{aligned} &X'_m \leq \ldots \leq X'_1 \leq X_1 \leq \ldots \leq X_n, Q'_m \leq \ldots \leq Q'_1 \leq 0 \leq Q_1 \leq \ldots \leq Q_n : \\ &\quad P_{X'_i;X_j}(Q'_i; Q_j) = P_{X'_1,X_1}(Q'_1, Q_1)\prod_{i=2}^{m}\overline{P}_{X'_{i-1,i}}(Q'_{i-1,i})\prod_{j=2}^{n}\overline{P}_{X_{j,j-1}}(Q_{j,j-1}), \end{aligned} \tag{88}$$

where we defined relative distances such as $X_{j,j-1} = X_j - X_{j-1}$. However, it appears that the probability distribution $P_{X'_1,X_1}(Q'_1, Q_1)$, with $Q'_1 \leq 0 \leq Q_1$, does not greatly simplify and is given by intricate multiple integrals. Therefore, we shall not consider it further in this article. Note that for practical purposes one is mostly interested in the behavior far from the origin, where the invariance through translations is fully restored.

In terms of velocities, using the relation (50) for the dimensionless velocities V_i, we obtain from the previous results the factorization

$$X'_m \le \ldots \le X'_1 \le X_1 \le \ldots \le X_n, V'_1 \ge X'_1, V'_{i,i-1} \ge X'_{i,i-1}, V_1 \le X_1, V_{j,j-1} \le X_{j,j-1}:$$

$$P_{X'_i;X_j}(V'_i; V_j) = P_{X'_1,X_1}(V'_1, V_1) \prod_{i=2}^{m} \overline{P}_{X'_{i-1,i}}(V'_{i-1,i}) \prod_{j=2}^{n} \overline{P}_{X_{j,j-1}}(V_{j,j-1}), \tag{89}$$

where the various factors are the velocity probabilities that may be obtained from the Lagrangian Q-probability densities through (50). As noticed above, the factorizations (88)–(89) also follow from the analysis of [9]. However, although this provides the conditional distribution $\overline{P}_{X_2-X_1}(Q_2 - Q_1)$ of the Lagrangian increment it does not give the distributions $P_{X'_i;X_j}(Q'_i; Q_j)$ or $P_{X'_1,X_1}(V'_1, V_1)$ that appear in these n-point distributions. Nevertheless, in the limit where we are far from the origin, we only need the one-point distribution $P_{X_1}(Q_1)$, which goes to the Gaussian (79), as would also be the case for one-sided initial conditions, besides in that limit we are mostly interested in the distributions of relative increments.

We can note that the Burgers equation with Brownian initial velocity which we study in this paper was also used in a recent article [19] to discuss the concept of local homogeneity that is used in turbulence studies. Indeed, for systems which are not strictly homogeneous (the energy shows an infrared divergence) it is customary to assume incremental homogeneity so that the physical quantities of interest (e.g. velocity increments) remain homogeneous. However, as noticed in [19] this is not fully consistent because initial incremental homogeneity is destroyed at later times by the nonlinearity of the equations of hydrodynamics (the quadratic advective term). Then, they used numerical simulations and perturbative analysis of the 1-D Burgers dynamics with two-sided Brownian initial velocity to illustrate this point and to note that local homogeneity is only asymptotically recovered far from the reference point. The results (88) and (89) above explicitly show how the incremental homogeneity is indeed destroyed at finite distance from the origin but asymptotically recovered at large distances. A peculiarity of this system is that at finite distance it is already exactly recovered over a partial range of velocities. In fact, for the case of one-sided initial conditions ($v_0(q) = 0$ for $q \le 0$) the system is exactly homogeneous over $x > 0$, as shown by the previous discussion and [9].

The factorizations (88) and (89) also show that small scales are largely decoupled from long-wavelength modes. Note that this key property is usually assumed in hydrodynamical systems (so that one can ignore the details of the large-scale boundary conditions) but is often difficult to prove in a precise manner.

5.2 Distribution of Lagrangian Increments (i.e. of Relative Initial Lagrangian Distance)

We now study in more details the probability distribution, $\overline{P}_X(Q)$, of the relative Lagrangian positions (i.e. relative initial distance q between particles that are separated by distance x at time t), that is, of the increments of the inverse Lagrangian map (here we omit the subscripts "21" to simplify the notations). The following results apply far from the origin, or at any location on the right side of the origin if we have one-sided initial conditions ($v_0(q) = 0$ at $q \le 0$).

We can check from the integral representation (84) that for $X \to 0$ we obtain as expected the Dirac distribution $\overline{P}_X(Q) \to \delta(Q)$ (whence $Q_2 \to Q_1$ for $X_2 \to X_1$). In fact, (84) is a well-known inverse Laplace transform [1] which gives the explicit expression

$$X \ge 0, Q \ge 0: \quad \overline{P}_X(Q) = \frac{X}{\sqrt{\pi}} Q^{-3/2} e^{2X-Q-X^2/Q} = \frac{X}{\sqrt{\pi}} Q^{-3/2} e^{-(\sqrt{Q}-X/\sqrt{Q})^2}. \tag{90}$$

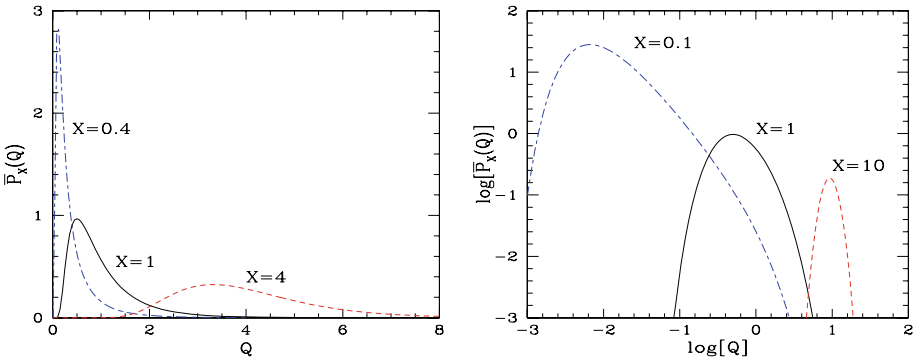

Fig. 6 (Color online) *Left panel:* The probability density $\overline{p}_x(q)$ that two particles, separated by the distance $x > 0$ at time t, were initially separated by a distance q (in the limit where the particles are far from the origin, or anywhere on the right side for one-sided initial conditions). This is the distribution of the increments of the inverse Lagrangian map, $x \mapsto q$. We show the reduced probabilities, $\overline{P}_X(Q)$, in terms of the dimensionless variables $X = x/(2Dt^2)$ and $Q = q/(2Dt^2)$, for three values of X, from (90). The probability is zero for $Q < 0$. For large relative distance X we recover a Gaussian of center X and variance $\langle (Q-X)^2 \rangle = X/2$. *Right panel:* The probability density $\overline{P}_X(Q)$ on a logarithmic scale, for three values of X

Therefore, we obtain an exponential tail at large Q, as $\sim e^{-Q}$, and a strong falloff at small Q, as $\sim e^{-X^2/Q}$. For large relative distance X this gives the Gaussian

$$X \to +\infty, |Q-X| \ll X : \quad \overline{P}_X(Q) \sim \frac{1}{\sqrt{\pi X}} e^{-(Q-X)^2/X}. \tag{91}$$

This agrees with the expectation that over large distances particles are still governed by the initial velocity field, as discussed in Sect. 4.3 for (79). This is again an illustration of the "principle of permanence of large eddies" [26], see the discussion below (79).

We show the probability density $\overline{P}_X(Q)$ obtained for three relative distances X in Fig. 6. We clearly see that for large X, which corresponds to large scales or small times, we recover a Gaussian centered on X, whereas for small X we obtain a skewed distribution with an intermediate power-law regime $Q^{-3/2}$.

From (90) we obtain the moments of the Lagrangian increments Q as [21]

$$\langle Q^n \rangle = \frac{2}{\sqrt{\pi}} X^{n+1/2} e^{2X} K_{n-1/2}(2X) = X^n \sum_{k=0}^{n-1} \frac{(n-1+k)!}{k!(n-1-k)!(4X)^k}, \tag{92}$$

where the last equality only holds for $n \geq 1$, and K_ν is the modified Bessel function of the second kind. This gives for the first few moments

$$\langle Q \rangle = X, \qquad \langle Q^2 \rangle = X^2 + \frac{X}{2}, \qquad \langle Q^3 \rangle = X^3 + \frac{3X^2}{2} + \frac{3X}{4}. \tag{93}$$

We can note that the mean of the relative displacement, $\chi = X - Q$, is zero: the mean distance between particles does not change (far from the origin). On the other hand, if we define the usual moment-generating function $\Psi(y)$ by

$$\Psi(y) = \sum_{n=0}^{\infty} \frac{(-y)^n}{n!} \langle Q^n \rangle = \int_0^\infty \mathrm{d}Q e^{-yQ} \overline{P}_X(Q), \qquad \overline{P}_X(Q) = \int_{-i\infty}^{+i\infty} \frac{\mathrm{d}y}{2\pi \mathrm{i}} e^{Qy} \Psi(y), \tag{94}$$

we obtain from (84), making the change of variable $s = 1 + y$,

$$\Psi(y) = e^{-(\sqrt{1+y}-1)2X}. \tag{95}$$

Therefore, the cumulant-generating function $\Phi(y)$, which satisfies the standard relation

$$\Phi(y) = \sum_{n=1}^{\infty} \frac{(-y)^n}{n!} \langle Q^n \rangle_c = \ln[\Psi(y)], \tag{96}$$

is given by

$$\Phi(y) = -(\sqrt{1+y}-1)2X = -Xy + 2X \sum_{n=2}^{\infty} \frac{(2n-3)!!}{2^n n!} (-y)^n. \tag{97}$$

This yields the simple results

$$\langle Q \rangle_c = X, \quad \text{and for } n \geq 2: \quad \langle Q^n \rangle_c = \frac{(2n-3)!!}{2^{n-1}} X. \tag{98}$$

We can note that the first equality in (92) also holds for non-integer n, and we obtain for small Eulerian distance, $(x_2 - x_1) \to 0^+$,

$$\nu > \frac{1}{2}: \quad \langle (q_2 - q_1)^\nu \rangle \sim (2Dt^2)^{(\nu-1)} \frac{\Gamma[\nu - \frac{1}{2}]}{\sqrt{\pi}} (x_2 - x_1), \tag{99}$$

$$\nu < \frac{1}{2}: \quad \langle (q_2 - q_1)^\nu \rangle \sim (2Dt^2)^{-\nu} \frac{\Gamma[-\nu + \frac{1}{2}]}{\sqrt{\pi}} (x_2 - x_1)^{2\nu}. \tag{100}$$

Note that the second scaling also holds for any negative ν. Indeed, the strong cutoff, $e^{-X^2/Q}$, of the probability distribution (90), ensures that all negative moments are finite. Equations (99)–(100) show that we recover the bifractality of the inverse Lagrangian map, that was already derived in [3] for $\nu \geq 0$. As is well-known [18], the scaling (99) is universal as it is due to shocks. Indeed, if we have a shock of finite Lagrangian increment δq at position x, it gives a contribution $[q(x + \ell/2) - q(x - \ell/2)]^n \sim (\delta q)^n$ which remains of order unity for $\ell \to 0^+$ for any n. Next, the probability to have a shock of a given finite strength δq in a small Eulerian interval ℓ scales as ℓ at small distances, which gives rise to the factor $(x_2 - x_1)$ in (99). Note that in our case, the total number of shocks per unit length is actually infinite [41, 43], see Sect. 8.1 below, as the shock mass function (154) leads to a divergence at low mass, but the number of shocks above a finite mass threshold is finite and this is sufficient to make the scaling (99) universal. However, the behavior observed at $\nu < 1$ (the critical value $\nu_c = 1/2$ and the exponent 2ν observed below ν_c in (100)) depends on the initial energy spectrum, through the low-mass tail of the shock mass function, see also [3] for more detailed discussions.

5.3 Distribution of Eulerian Velocity Increments

We now consider the probability distribution, $\overline{P}_X(V)$, of the relative Eulerian velocities, that is of the velocity increments $V(X_2) - V(X_1)$. From (90) we obtain

$$X \geq 0, V \leq X: \quad \overline{P}_X(V) = \frac{X}{\sqrt{\pi}} (X - V)^{-3/2} e^{-(\sqrt{X-V} - X/\sqrt{X-V})^2}. \tag{101}$$

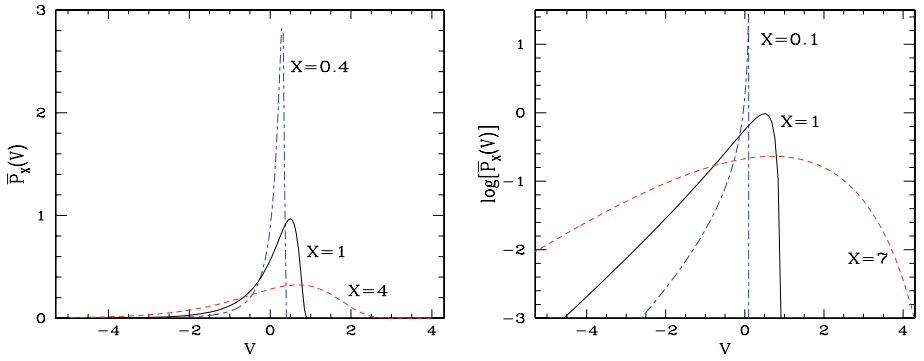

Fig. 7 (Color online) *Left panel:* The probability density $\overline{p}_x(v)$ of the velocity increment $v = v(x_2) - v(x_1)$ for two positions separated by the distance $x = x_2 - x_1$ (in the limit where we are far from the origin, or anywhere on the right side for one-sided initial conditions). We show the reduced probabilities, $\overline{P}_X(V)$ in terms of the dimensionless variables $X = x/(2Dt^2)$ and $V = v/(2Dt)$, for three values of X, from (101). The probability is zero for $V > X$. At large relative distance X we recover a symmetric Gaussian of variance $\langle V^2 \rangle = X/2$. *Right panel:* The probability density $\overline{P}_X(V)$ on a semi-logarithmic scale, for three values of X

In the limit of large relative Eulerian distance $X \to \infty$, at fixed V, the distribution (101) can be expanded around the maximum of the exponent at $V = 0$ (corresponding to $Q = X$) and we again recover the initial Gaussian

$$|V| \ll X : \quad \overline{P}_X(V) \sim \frac{1}{\sqrt{\pi X}} e^{-V^2/X}, \tag{102}$$

in agreement with the fact that over large distances particles are still governed by the initial velocity field (see also Sect. 4.3). We show in Fig. 7 the velocity distribution $\overline{P}_X(V)$ for three values of X. We can again check that we recover a Gaussian for large X (i.e. large scales or small times), whereas for smaller X the upper bound $V \leq X$ is increasingly apparent while a power law develops at intermediate negative velocities.

From (98) the velocity cumulants are given by

$$n \geq 2 : \quad \langle V^n \rangle_c = (-1)^n \frac{(2n-3)!!}{2^{n-1}} X, \quad \text{whence } \langle V \rangle = 0, \langle V^2 \rangle = \frac{X}{2}, \langle V^3 \rangle = -\frac{3X}{4}. \tag{103}$$

We can note that the first moment exactly vanishes whereas the variance $\langle V^2 \rangle$ remains equal to that of the initial Gaussian field, see (9), even though $\overline{P}_X(V)$ is no longer Gaussian. Thus, in terms of the dimensional variables the velocity energy spectrum remains equal to the initial one,

$$\langle [v(x_2,t) - v(x_1,t)]^2 \rangle = D|x_2 - x_1|, \qquad E(k,t) = E_0(k) = \frac{D}{4\pi} k^{-2}. \tag{104}$$

Finally, in the limit of small separations we obtain from (103)

$$n \geq 2, (x_2 - x_1) \to 0^+ : \quad \langle (v_2 - v_1)^n \rangle \sim \frac{(2Dt^2)^{n-1}}{t^n} (-1)^n \frac{(2n-3)!!}{2^{n-1}} (x_2 - x_1). \tag{105}$$

Therefore, we recover the universal scaling at small distances of the structure functions [18], $\langle [v(x+\ell) - v(x)]^n \rangle \propto \ell$, that was also observed in the numerical simulations of [41]. This is

due to the contribution from shocks, as discussed below (99)–(100). Thus, if we have a shock of finite velocity jump $-\delta v = \delta q/t$ at location x, then $[v(x+\ell/2) - v(x-\ell/2)]^n \sim (-\delta v)^n$ for $\ell \to 0^+$. Note that δv is positive, since a shock is associated with particles from the left overtaking particles on the right, so that $v(x^-) > v(x^+)$, which agrees with the factor $(-1)^n$ in (105). Again, the factor $(x_2 - x_1)$ in (105) comes from the probability to encounter a shock of strength larger than some finite threshold δq in a small Eulerian interval $[x_1, x_2]$.

6 Density Field

6.1 Overdensity within Finite Size Domains

We consider here the evolution of a density field $\rho(x,t)$ that evolves through the usual continuity equation,

$$\frac{\partial \rho}{\partial t} + \frac{\partial}{\partial x}(\rho v) = 0, \tag{106}$$

whereas the velocity field $v(x,t)$ evolves through the Burgers equation (1). The initial conditions for the velocity are set by (5) as in previous sections, whereas the initial density is a constant ρ_0. Thus, the mass m between particles q_1 and q_2, with $q_1 < q_2$, is $m = \rho_0(q_2 - q_1)$. This quantity is conserved by the dynamics since particles do not cross each other (though it is ambiguous at shock locations, but the latter have zero measure in Eulerian space). Then, the overall overdensity, $\eta = m/(\rho_0 x)$, over the length $x = x_2 - x_1$, is $\eta = (q_2 - q_1)/(x_2 - x_1)$ by conservation of matter, where q_i is the initial Lagrangian position of the particle that is located at x_i at time t. In terms of dimensionless variables this reads as the ratio of relative distances $\eta = Q/X$. Therefore, far from the origin ($|x_1| \to \infty$), or on the right side of the origin for one-sided initial conditions, we obtain from (90) the probability distribution of the overdensity at scale X as

$$\eta = \frac{m}{\rho_0 x}, \eta \geq 0: \quad P_X(\eta) = \sqrt{\frac{X}{\pi}} \eta^{-3/2} e^{-X(\sqrt{\eta} - 1/\sqrt{\eta})^2} = \sqrt{\frac{X}{\pi}} e^{2X} \eta^{-3/2} e^{-X(\eta + 1/\eta)}. \tag{107}$$

Over large scales we recover a Gaussian distribution, as for the variables Q and V, while on small scales, $X \to 0$, we obtain the power law $\eta^{-3/2}$ between the low and high density cutoffs at $\eta_- \sim x/(2Dt^2)$ and $\eta_+ \sim (2Dt^2)/x$, as we can see in Fig. 8 where we show the overdensity distribution $P_X(\eta)$ for three values of X. We can note that this is very similar to the behavior that is observed in cosmological numerical simulations for gravitational clustering [4, 14, 49].

From (92) and (98) we obtain for the moments and the cumulants of the overdensity at scale X:

$$n \geq 1: \quad \langle \eta^n \rangle = \sum_{k=0}^{n-1} \frac{(n-1+k)!}{k!(n-1-k)!(4X)^k}, \quad \text{and for} \quad n \geq 2: \quad \langle \eta^n \rangle_c = \frac{(2n-3)!!}{(2X)^{n-1}}, \tag{108}$$

whence for the lowest orders

$$\langle \eta \rangle = 1, \qquad \langle \eta^2 \rangle_c = \frac{1}{2X}, \qquad \langle \eta^3 \rangle_c = \frac{3}{4X^2} = 3\langle \eta^2 \rangle_c^2. \tag{109}$$

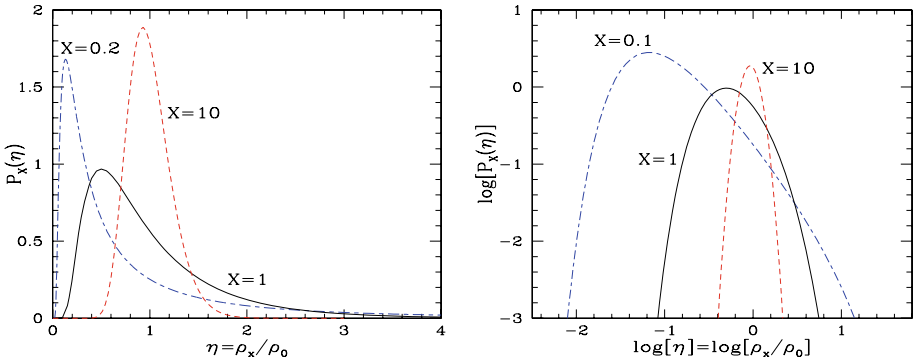

Fig. 8 (Color online) *Left panel:* The probability distribution $p_x(\eta)$ of the overdensity, $\eta = m/(\rho_0 x)$, over a region of length x. We show $P_X(\eta)$ for three values of the reduced length $X = x/(2Dt^2)$, from (107). Thus larger X corresponds to larger scale or smaller time. For large X we recover a Gaussian of mean 1 and variance $\langle(\eta-1)^2\rangle = 1/(2X)$. For small X the distribution becomes skewed and an intermediate power-law region develops. *Right panel:* The probability density $P_x(\eta)$ on a logarithmic scale, for three values of X

We can note that the second result (108) gives the cumulant hierarchy

$$S_n = \frac{\langle\eta^n\rangle_c}{\langle\eta^2\rangle_c^{n-1}} = (2n-3)!! \quad \text{and} \quad \varphi(y) = \sum_{n=1}^{\infty}(-1)^{n-1}S_n\frac{y^n}{n!} = \sqrt{1+2y}-1, \tag{110}$$

which shows that the ratios S_n are constants that do not depend on time nor scale. We can note that in the cosmological context, associated with a gravitational dynamics in a 3-dimensional expanding Universe, for the case of an initial power-law density power spectrum, the coefficients S_n, still defined as in (110), only show a weak dependence on scale in the highly nonlinear regime, and they also asymptotically reach (different) finite values at large scales in the quasi-linear regime [8, 14]. Then, it has been proposed to use the approximation of constant S_n to describe the highly nonlinear regime [37]. Moreover, the form (110) of the reduced cumulant generating function $\varphi(y)$ is one of the possibilities that have been studied in this context [4]. This phenomenological ansatz is known as the "stable clustering model" as it was derived by assuming that on small physical scales, after nonlinear collapse and gravitational relaxation, overdensities decouple from the Hubble expansion and keep a constant physical size [15]. In the present case, collapsed objects are actually Dirac peaks (shocks) of vanishing size. Then, it is easy to see from a multifractal analysis that shocks lead to finite ratios S_n in the small-scale limit [5, 44], so that the hierarchy (110) is universal, in the sense that the generating function $\varphi(y)$ has a finite limit at small scale, $x \to 0$. However, this non-trivial limit depends on the initial energy spectrum. A specific property of the Brownian initial conditions studied in this paper is that the ratios S_n are actually constant over all scales, from the linear to highly nonlinear scales. Thus, it is interesting to note that the 1-D Burgers equation with Brownian initial velocity provides an exact physical realization of this ansatz.

6.2 Density Correlations

We now consider the unsmoothed density field $\rho(x)$ itself (again in the limit where we are far from the origin so that the previous results apply). It is related to the smoothed overdensity

η over scale x introduced above through

$$\eta = \int_{x_1}^{x_1+x} \frac{\mathrm{d}x'}{x} \frac{\rho(x')}{\rho_0}. \tag{111}$$

Then, introducing the density power spectrum, $\mathcal{P}(k)$, by going to Fourier space as

$$\rho(x) - \rho_0 = \int_{-\infty}^{\infty} \mathrm{d}k e^{\mathrm{i}kx} \rho(k), \qquad \langle \rho(k_1)\rho(k_2)\rangle = \delta(k_1+k_2)\rho_0^2 \mathcal{P}(k_1), \tag{112}$$

we obtain using the second (109) and (111)–(112)

$$\frac{Dt^2}{x} = \langle \eta^2 \rangle_c = \int_{-\infty}^{\infty} \mathrm{d}k \mathrm{sinc}^2\left(\frac{kx}{2}\right) \mathcal{P}(k), \quad \text{and} \quad \mathcal{P}(k,t) = \frac{Dt^2}{2\pi}, \tag{113}$$

where $\mathrm{sinc}(x) = \sin(x)/x$ is the cardinal sine. Thus, we obtain a white-noise density power spectrum, with an amplitude that grows as t^2. This yields the connected density two-point correlation

$$\langle \rho(x_1,t)\rho(x_2,t)\rangle_c = \rho_0^2 C_2(x_1,x_2), \quad \text{with } C_2(x_1,x_2) = Dt^2 \delta(x_2-x_1), \tag{114}$$

which remains a Dirac function at all times.

In fact, the factorization (87) implies a similar factorization for the multivariate distributions of the smoothed density field, far from the origin ($X_1 \to +\infty$),

$$X_1 \le \ldots \le X_n : \; P_{X_{2,1};\ldots;X_{n,n-1}}(\eta_{2,1};\ldots;\eta_{n,n-1}) = P_{X_{2,1}}(\eta_{2,1}) \ldots P_{X_{n,n-1}}(\eta_{n,n-1}), \tag{115}$$

where $\eta_{i,i-1}$ is the mean overdensity over the interval $[X_{i-1}, X_i]$. Thus, the densities within non-overlapping domains are completely independent random variables. This agrees with the Dirac obtained in (114) for the connected density two-point correlation. Moreover, this can be extended to all higher orders. Indeed, let us consider the density n-point connected correlation, defined as

$$\langle \rho(x_1)\ldots\rho(x_n)\rangle_c = \rho_0^n C_n(x_1,\ldots,x_n). \tag{116}$$

If there exists a position x_i that is different from all other positions x_j, with $j \neq i$, then we can build a small region $[x_i-\epsilon, x_i+\epsilon]$ where the density is independent from the density at all other points x_j, using the property (115) and $\epsilon \to 0^+$. Therefore, by definition of connected correlations, C_n must vanish. Then, the n-point connected correlation can be written as the product of $n-1$ Dirac factors

$$C_n(x_1,\ldots,x_n) = (2n-3)!!(Dt^2)^{n-1}\delta(x_2-x_1)\delta(x_3-x_1)\ldots\delta(x_n-x_1) \tag{117}$$

$$= (2n-3)!! C_2(x_1,x_2)C_2(x_1,x_3)\ldots C_2(x_1,x_n), \tag{118}$$

where the amplitude is obtained from (108), as well as (111) which implies the relation $\langle \eta^n \rangle_c = x^{-n} \int_0^x \mathrm{d}x_1 \ldots \mathrm{d}x_n C_n(x_1,\ldots,x_n)$.

We can note that $(2n-3)!!$ also counts the number of heap ordered trees with n nodes, that is, rooted trees where the n nodes are labelled as $\{1,2,\ldots,n\}$ and each path from the root has increasing labels [39]. In our case, we can therefore construct the following combinatorial interpretation of (117). First, the points $x_1,\ldots,x_n$, are ordered such that $x_1 \le x_2 \le \ldots \le x_n$ (we choose one among several possibilities if several positions are equal).

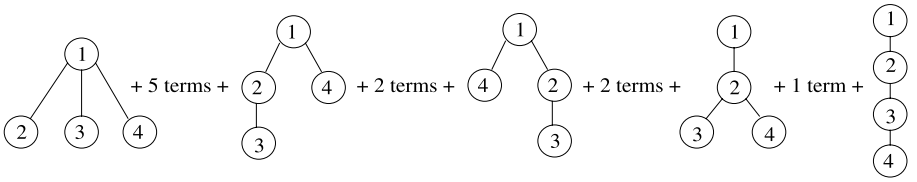

Fig. 9 The 15 heap ordered trees that can be associated with the 4-point correlation $C_4(x_1, \ldots, x_4)$. The labels refer to the positions x_i, which are ordered as $x_1 \le x_2 \le x_3 \le x_4$. We only show the 5 tree structures, as the additional terms can be obtained from the previous diagram by permutations over the labels that satisfy the ordering constraint that each path from the root has increasing labels as we proceed down to the leaves. Each link between nodes i and j yields a contribution $C_2(x_i, x_j)$ and the contribution of a tree is the product of the 3 factors C_2 associated with its 3 links. This gives C_4 as the sum over all these tree contributions

Then, the n-point connected correlation (117) is obtained as the sum of the contributions of all heap ordered trees, where the contribution of each tree is simply the product of the $n-1$ factors $C_2(x_i, x_j)$ associated with the $n-1$ links between nodes x_i and x_j.

Of course, we may also write (117) as the sum over the products of $C_2(x_i, x_j)$ associated with any other class of N trees, multiplied by a weight $(2n-3)!!/N$. However, this no longer recovers the amplitude $(2n-3)!!$ of (117) in a natural manner. We note that in the cosmological context, within the stable-clustering ansatz discussed above, it has been proposed to use as a phenomenological model a diagrammatic description such as Fig. 9, where the connected n-point density correlation is written as the sum over trees of each product of $(n-1)$ factors $C_2(x_i, x_j)$ associated with the internal links [20, 40]. However, the tree diagrams used in this context are usually not ordered, and each topology may have an additional multiplicative weight. In the present case of the 1-dimensional Burgers dynamics, we can note that the concept of ordering naturally arises since particles do not cross each other and one can order both Lagrangian and Eulerian positions on the line (this would no longer be the case for higher dimensions).

Thus, the 1-D Burgers dynamics with Brownian initial velocity provides a physical realization of the hierarchical structure such as (118) for the many-body correlation functions. It is an interesting question to ask whether other real dynamical systems can be built that display the same factorization property (possibly over other classes of trees) with other two-point correlations C_2.[2] On the other hand, one may wonder whether a factorization such as (118), and a diagrammatic construction such as Fig. 9, could be generalized, as an exact asymptotic solution or as a useful phenomenological model, to the 1-dimensional Burgers dynamics with other initial conditions, where C_2 would no longer be the simple Dirac function (114).[3]

[2] In fact, as for the weaker property of constant ratios S_n, the author is not aware of other dynamical systems that exactly obey such a factorization property. In view of the many phenomenological works that have used such a diagrammatic construction for many-body correlations, it is satisfying to find that it is at least obeyed by one truly dynamical system, even though the expression in terms of Dirac factors and the lack of large distance correlation make this a very simple and specific case.

[3] The results of [9] show that the Brownian case can be generalized to Levy processes with no positive jumps, where the increments of the inverse Lagrangian map again remain homogeneous and independent at all times. However, this does not provide another hierarchy for the many-body correlations as they remain of the Dirac type.

6.3 Comparison with a Perturbative Approach

We can note that the exact (far from the origin) nonlinear results (113)–(114) are identical to the perturbative predictions that would be obtained at linear order from (106). Indeed, if we linearize the continuity and inviscid Burgers equations, we obtain at lowest order for the density field $\partial\rho_L/\partial t = -\rho_0\partial v_L/\partial x = -\rho_0\partial v_0/\partial x = -\rho_0\xi$, where ξ is the initial white-noise of (5). This gives $\rho_L(x,t) = \rho_0(1 - t\xi(x))$, which leads in turn to (113)–(114). The fact that for these Brownian initial conditions the nonlinear Burgers dynamics preserves the linear density power spectrum is reminiscent of the invariance of the energy velocity spectrum (104). In both cases, one needs to consider higher-order correlations (or the full distribution) to measure the effects of the nonlinearities.

In fact, the agreement of the exact density two-point function with the linear theory actually extends to all order cumulants $\langle\eta^n\rangle_c$, computed at leading order from quasi-linear theory. Indeed, at tree-order in perturbation theory, in the inviscid limit, it can be shown that the cumulant-generating function $\varphi(y)$, defined as in (110), is given by the implicit system

$$\begin{cases} \tau = -y\mathcal{G}'(\tau) \\ \varphi(y) = y\mathcal{G}(\tau) + \frac{\tau^2}{2} \end{cases} \quad \text{with } \mathcal{G}(\tau) = \mathcal{F}\left[-\tau\frac{\sigma(\mathcal{G}x)}{\sigma(x)}\right] = \mathcal{F}[-\tau\mathcal{G}^{-1/2}], \tag{119}$$

where $\sigma(x)^2 = \langle\delta_L^2\rangle = Dt^2/x$ is the variance of the linear density contrast δ_L at scale x, and the function $\mathcal{F}(\delta_L)$ describes the evolution of spherical (here symmetric) density fluctuations (see [7, 8, 45] for the similar case of the cosmological gravitational dynamics). The system $\{\tau, \mathcal{G}\} \leftrightarrow \{y, \varphi\}$ in (119) is actually a Legendre transform and it arises from a saddle-point approximation. Indeed, in the quasi-linear limit (i.e. $\sigma \to 0$, which also corresponds to $t \to 0$ or $x \to \infty$) the cumulant ratios S_n are governed by the tails of the density distribution and the generating function $\varphi(y)$ can be obtained from a steepest-descent method[4] [45]. (In a somewhat similar fashion, the minimization problem (3), that also arises from a saddle-point method, can be written in terms of a Legendre transform of the Lagrangian potential, see [6].) As compared with (69) of [45] we made the change $\sigma[(1+\mathcal{G})^{1/3}x] \to \sigma(\mathcal{G}x)$ by taking $1 + \mathcal{G} \to \mathcal{G}$ and the exponent $1/3$ is changed to unity as we go from 3-D to 1-D. For the present 1-D Burgers dynamics, we have:

$$\eta = \frac{q}{x} = \frac{q}{q+tv}, \quad \text{whence at linear order } \eta_L = 1 - \frac{tv}{q} \text{ and } \delta_L = -t\frac{v}{q}. \tag{120}$$

This yields

$$\mathcal{F}(\delta_L) = \frac{1}{1-\delta_L}, \quad \text{whence } \mathcal{G}(\tau) = \frac{(-\tau + \sqrt{\tau^2+4})^2}{4} \text{ and } \varphi(y) = \sqrt{1+2y} - 1. \tag{121}$$

Thus, we recover at tree-order the exact result (110). Therefore, for Brownian initial velocity the Burgers dynamics happens to preserve the density cumulant-generating function $\varphi(y)$ that would be obtained at leading order (tree-order) from a perturbative approach,

[4] In fact, the steepest-descent method described in [45] is a non-perturbative approach, which can also be applied to the other limit of rare events at finite σ, where it allows to go beyond perturbative methods [46]. However, in the quasi-linear limit $\sigma \to 0$ it gives the same results for $\varphi(y)$ as the usual perturbative expansion over powers of the linear growing mode of the density field (provided the latter gives finite results in this limit).

which does not take into account collisions between particles (shell-crossings). This is also why the ratios S_n are constants that apply to all scales, from the quasi-linear to the highly nonlinear scales. Note that the perturbative approach breaks down beyond leading order as next-to-leading corrections actually involve divergent integrals (which means that one can no longer discard shocks, which requires non-perturbative methods). For other initial conditions the coefficients S_n would no longer remain equal to their tree-order values. However, they still asymptote to finite values in the highly nonlinear regime, because of the contribution from shocks, just as the Lagrangian and velocity increments scale linearly with ℓ for small distances $\ell \to 0$, as discussed below (99)–(100) and (105).

7 Lagrangian Displacement Field

7.1 One-Point Distributions

We now consider the dynamics associated with the Burgers equation (1) from a Lagrangian point of view. That is, labelling particles by their initial position q at time $t = 0$, we follow their trajectory $x(q,t)$ and we note $\chi(q,t) = x(q,t) - q$ their displacement with respect to their initial location. Note that for regular points, which have kept their initial velocity, we have $\chi = tv$, see (2). Since particles do not cross each other they remain well-ordered. Then, it is clear that the probability, $p_q(x' \geq x)$, for the particle q to be to the right of the Eulerian position x, at time t, is equal to the probability, $p_x(q' \leq q)$, for the Eulerian location x to be "occupied" by particles that were initially to the left of particle q. (Since shocks have zero measure in Eulerian space there are no ambiguities.) Therefore, we obtain in terms of dimensionless variables, for the case $q \geq 0$,

$$\begin{aligned} Q \geq 0: \quad P_Q(X' \geq X) &= P_X(Q' \leq Q) = P_X(Q' \leq 0) + P_X(0 \leq Q' \leq Q) \\ &= J(1,-2X) + \int_{-i\infty}^{+i\infty} \frac{\mathrm{d}s}{2\pi \mathrm{i}} e^{(s-1)Q} \frac{J(s,2X)}{s-1}, \end{aligned} \tag{122}$$

where we used the results of Sect. 4.1 and the integration contour runs to the right of the pole $s = 1$. Therefore, the probability density of the Eulerian position X of particle Q reads as

$$\begin{aligned} Q \geq 0: \quad P_Q(X) &= -\frac{\partial}{\partial X} P_Q(X' \geq X) \\ &= -\frac{\partial}{\partial X}\left[J(1,-2X) + \int_{-i\infty}^{+i\infty} \frac{\mathrm{d}s}{2\pi \mathrm{i}} e^{(s-1)Q} \frac{J(s,2X)}{s-1} \right]. \end{aligned} \tag{123}$$

The case $Q < 0$ can be obtained from (123) through a reflection about the origin.

Let us consider more precisely the case of the particle that was initially at rest at the origin, $q = 0$. Following the previous discussion, we have $p_0(x' \geq x) = p_x(q' \leq 0)$, hence we can directly use (70)–(72) which give

$$X \geq 0: \quad P_0(X) = -\frac{\partial}{\partial X} \int_0^\infty \mathrm{d}\nu \frac{6}{\nu^2} \mathrm{Ai}\left[\nu 2X + \frac{1}{\nu^2} \right]^2, \qquad P_0(-X) = P_0(X). \tag{124}$$

At small X, we obtain from (124) the asymptotic

$$X \to 0^+: \quad P_0(X) \sim -\frac{4\sqrt{3}}{\pi} \ln X, \tag{125}$$

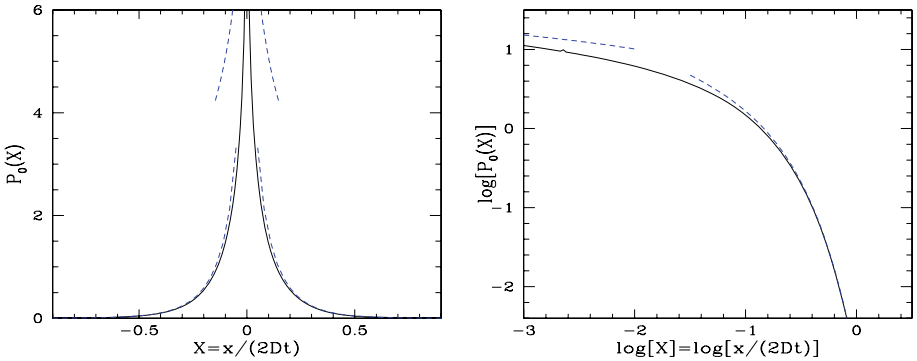

Fig. 10 (Color online) *Left panel:* The probability distribution, $P_0(X)$, of the reduced position $X = x/(2Dt)$ of the particle that was initially at the origin, $q = 0$, from (124). The *dashed lines* show the asymptotic behaviors (125) and (126). *Right panel:* Same as left panel but on a logarithmic scale

whereas the behavior for large displacement X is set by the asymptotic (80), which yields

$$X \to +\infty : \quad P_0(X) \sim \left(\pi X/(2\sqrt{3})\right)^{-1/2} e^{-4\sqrt{3}X}. \tag{126}$$

Thus, the central particle $q = 0$, that was initially at rest ($v_0(0) = 0$), has moved by time t by a distance $\chi = X$ whose distribution shows an exponential tail at large $|X|$ and a logarithmic peak at low $|X|$. We can note that both the large-X tail and the low-X divergence are different from the asymptotics of the distribution of the Lagrangian coordinate, $Q = -V$, of the particle located at the Eulerian location $X = 0$ at the same time, see (76)–(77). We show in Fig. 10 the distribution $P_0(X)$ as well as the asymptotic behaviors (125) and (126). It appears that the logarithmic asymptote is only reached at very low X.

Finally, far away from the origin, in the limit $Q \to \infty$ at fixed $\chi = X - Q$, we obtain from (123) the asymptotic behavior (making the change of variable $s = 1 + ik$ as for (79))

$$Q \to +\infty, \ |\chi| \ll Q : \quad P_Q(\chi) \sim \frac{e^{-\chi^2/Q}}{\sqrt{\pi Q}}. \tag{127}$$

Therefore, we recover the property that far from the origin the displacement of the particles is governed at leading order by the Gaussian distribution of the initial velocity field $v_0(q)$. This agrees with the discussion presented below (79) in Sect. 4.3. Again, this expresses the fact that at very large distances, where the initial velocity becomes increasingly large as $\sqrt{|q|}$, the motion with respect to the origin is dominated by the "large-scale flow" and the local fluctuations of the initial velocity field have only produced local subdominant shifts, see also [2, 23].

7.2 Two-Point Distributions

We now investigate the two-point probability distribution of the Lagrangian displacement field. As for the one-point distribution (122), it is related to its Eulerian counterpart through

$$P_{Q_1,Q_2}(X_1' \geq X_1, X_2' \geq X_2) = P_{X_1,X_2}(Q_1' \leq Q_1, Q_2' \leq Q_2). \tag{128}$$

Using (79), (84), we obtain far away from the origin, in the limit $Q_1 \to +\infty$ at fixed $Q_{21} = Q_2 - Q_1 > 0$,

$$Q_1 \to +\infty, Q_{21} > 0: \quad P_{Q_1,Q_2}(X_1' \geq X_1, X_2' \geq X_2) \sim \int_0^{Q_1} \mathrm{d}Q_1' \int_{Q_1'}^{Q_2} \mathrm{d}Q_2' \int_{-\infty}^{\infty} \frac{\mathrm{d}k}{2\pi} e^{-\mathrm{i}k(X_1 - Q_1') - X_1 k^2/4} \times \int_{-i\infty}^{+i\infty} \frac{\mathrm{d}s}{2\pi \mathrm{i}} e^{(s-1)(Q_2' - Q_1')} e^{-(\sqrt{s}-1)2X_{21}}. \tag{129}$$

Integrating over Q_1' and Q_2' gives the cumulative distribution

$$Q_1 \to +\infty, Q_{21} > 0: \quad P_{Q_1,Q_2}(X_1' \geq X_1, X_2' \geq X_2) \sim \int \frac{\mathrm{d}k}{2\pi} \int_{-i\infty}^{+i\infty} \frac{\mathrm{d}s}{2\pi \mathrm{i}} \frac{e^{-\mathrm{i}kX_1 - X_1 k^2/4 - (\sqrt{s}-1)2X_{21}}}{(s-1)(\mathrm{i}k - s + 1)} \times \left[e^{\mathrm{i}kQ_1 + (s-1)Q_{21}} - e^{(s-1)Q_2} \right]. \tag{130}$$

Then, taking the derivatives with respect to X_1 and X_2, and integrating over k, gives in the limit $Q_1 \to +\infty$, at finite $\chi_1 = X_1 - Q_1$, the probability density

$$Q_1 \to +\infty, Q_{21} > 0: \quad P_{Q_1,Q_2}(X_1, X_2) \sim \frac{e^{-\chi_1^2/Q_1}}{\sqrt{\pi Q_1}} \int_{-i\infty}^{+i\infty} \frac{\mathrm{d}s}{2\pi \mathrm{i}} e^{(s-1)Q_{21} - (\sqrt{s}-1)2X_{21}} \frac{4}{(\sqrt{s}+1)^2}. \tag{131}$$

Thus, the comparison with (127) shows that we obtain as expected a factorization of the form

$$Q_1 \to +\infty, Q_{21} > 0: \quad P_{Q_1,Q_2}(X_1, X_2) \sim P_{Q_1}(X_1) \overline{P}_{Q_{21}}(X_{21}), \tag{132}$$

where the distribution, $\overline{P}_{Q_{21}}(X_{21})$, of the relative Eulerian distance X_{21} of the particles that were initially separated by the distance Q_{21} reads as

$$Q \geq 0, X > 0: \quad \overline{P}_Q(X) = \int_{-i\infty}^{+i\infty} \frac{\mathrm{d}s}{2\pi \mathrm{i}} e^{(s-1)Q - (\sqrt{s}-1)2X} \frac{4}{(\sqrt{s}+1)^2}. \tag{133}$$

Therefore, we recover a factorization of the form (83) that was obtained in the Eulerian framework. However, it is no longer exact at a finite distance from the origin and only applies in the limit $Q_1 \to \infty$ (again, by symmetry we have a similar result for $Q_2 \to -\infty$).

Multiplying (133) by e^{-4X} and taking the derivative with respect to X we obtain a standard inverse Laplace transform [1]

$$\frac{\mathrm{d}}{\mathrm{d}X}\left[e^{-4X}\overline{P}_Q(X)\right] = -\int_{-i\infty}^{+i\infty} \frac{\mathrm{d}s}{2\pi \mathrm{i}} e^{(s-1)Q} \frac{8e^{-(\sqrt{s}+1)2X}}{\sqrt{s}+1} = -8\left[\frac{1}{\sqrt{\pi Q}} e^{-(\frac{X}{\sqrt{Q}} + \sqrt{Q})^2} - \mathrm{erfc}\left(\frac{X}{\sqrt{Q}} + \sqrt{Q}\right)\right], \tag{134}$$

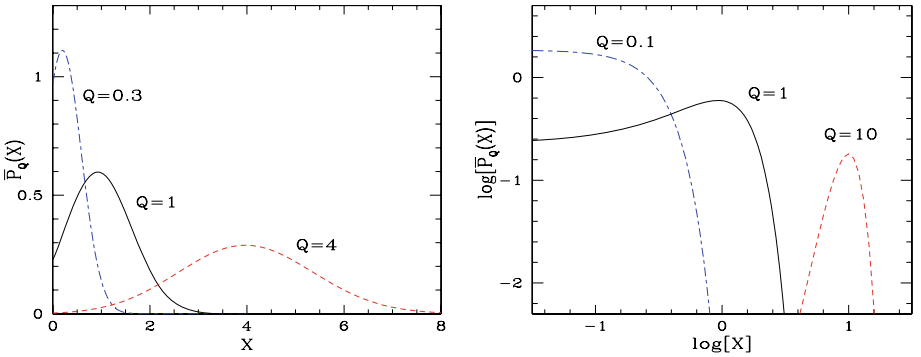

Fig. 11 (Color online) *Left panel:* The probability density $\overline{p}_q(x)$ that two particles, that were initially separated by a distance q, are separated by the distance $x > 0$ at time t (in the limit where the particles are far from the origin). We show the reduced probabilities, $\overline{P}_Q(X)$, in terms of the dimensionless variables $Q = q/(2Dt^2)$ and $X = x/(2Dt^2)$, for three values of Q, from (135). The probability is zero for $X < 0$. For large initial relative distance Q we recover a Gaussian of center Q and variance $\langle (X-Q)^2 \rangle = Q/2$. *Right panel:* The probability density $\overline{P}_Q(X)$ on a logarithmic scale, for three values of Q

where $\mathrm{erfc}(z)$ is the complementary error function. This can be integrated to give

$$\overline{P}_Q(X) = 8\left(X+Q+\frac{1}{2}\right)e^{4X}\mathrm{erfc}\left(\frac{X}{\sqrt{Q}}+\sqrt{Q}\right) - 8\sqrt{\frac{Q}{\pi}}e^{-(\frac{X}{\sqrt{Q}}-\sqrt{Q})^2}. \tag{135}$$

Using the asymptotic expansion of the complementary error function [1] we obtain for large Lagrangian separation, Q, and fixed relative displacement, $\chi = X - Q$,

$$Q \to +\infty : \quad \overline{P}_Q(\chi) \sim \frac{1}{\sqrt{\pi Q}} e^{-\chi^2/Q}. \tag{136}$$

As for (79), (102), (127), we recover as expected the property that over large distances particles are still governed at leading order by the initial Gaussian velocity field. Next, (135) yields for the asymptotic behavior at large X for finite Q,

$$X \to +\infty : \quad \overline{P}_Q(X) \sim \sqrt{\frac{Q}{\pi}}\frac{4}{X} e^{-(\frac{X}{\sqrt{Q}}-\sqrt{Q})^2} = 4\sqrt{\frac{Q}{\pi}} e^{-Q} X^{-1} e^{2X-X^2/Q}, \tag{137}$$

whereas $\overline{P}_Q(X)$ remains finite for $X \to 0^+$. We show our results for three values of Q in Fig. 11, that clearly illustrate the evolution of $\overline{P}_Q(X)$ with scale or time (smaller Q corresponds to smaller scale or larger time). As for the Eulerian probability distribution, the Gaussian tail (137) can be understood from a simple scaling argument applied to the initial velocity field. Thus, the expansion of the initial Lagrangian interval q up to a very large size x at time t requires an initial velocity increment of order $v_0 \sim x/t$ (since $x \gg q$) which gives rise to a probability of order $e^{-(x/t)^2/q} \sim e^{-X^2/Q}$, using (8), which agrees with the large-X tail (137).

From (135) we also obtain for the asymptotic behaviors of $\overline{P}_Q(0^+)$ with respect to Q

$$Q \to 0 : \quad \overline{P}_Q(0^+) \to 4, \qquad Q \to +\infty : \quad \overline{P}_Q(0^+) \sim \frac{4}{\sqrt{\pi}} Q^{-3/2} e^{-Q}. \tag{138}$$

However, note that the limits $X \to 0$ and $Q \to 0$ do not commute. Indeed, it is clear from (135) that for any $X > 0$ we have $\overline{P}_Q(X) \to 0$ for $Q \to 0$. As we shall see below, this is the signature of the contribution due to shocks. Thus, from (133) we obtain the cumulative distribution as

$$Q \geq 0, X > 0: \quad \overline{P}_Q(X' \geq X) = \int_{-i\infty}^{+i\infty} \frac{\mathrm{d}s}{2\pi \mathrm{i}} e^{(s-1)Q} \frac{2e^{-(\sqrt{s}-1)2X}}{(s-1)(\sqrt{s}+1)}, \quad \Re(s) > 1, \quad (139)$$

where the integration path is located to the right of the pole at $s = 1$, so that $\overline{P}_Q(X' \geq X) \to 0$ for $X \to +\infty$. However, we note that it does not reach unity in the limit $X \to 0^+$, since we have

$$Q \geq 0: \quad \lim_{X \to 0^+} \overline{P}_Q(X' \geq X) = 1 + \int_{-i\infty}^{+i\infty} \frac{\mathrm{d}s}{2\pi \mathrm{i}} e^{(s-1)Q} \frac{2}{(s-1)(\sqrt{s}+1)}, \quad 0 < \Re(s) < 1, \quad (140)$$

where the integration path crosses the real axis in the range $0 < s < 1$. This means that there is a non-zero contribution due to shocks, where particles that were initially located at different positions, $q_1 \neq q_2$, have collided by time t and are now located at the same Eulerian position, $x_1 = x_2$, in the same massive shock. Therefore, to the contribution (133) we must add the contribution from shocks, that reads as

$$Q \geq 0: \quad \overline{P}_Q^{\text{shock}}(X) = \overline{P}_Q^{\text{shock}} \delta(X - 0^+), \quad \text{with the amplitude}$$
$$\overline{P}_Q^{\text{shock}} = \int_{-i\infty}^{+i\infty} \frac{\mathrm{d}s}{2\pi \mathrm{i}} e^{(s-1)Q} \frac{2}{(1-s)(\sqrt{s}+1)}, \quad 0 < \Re(s) < 1, \quad (141)$$

so that the full probability is normalized to unity, see (140). Thus, the amplitude $\overline{P}_Q^{\text{shock}}$ is the probability that two particles, that were initially separated by the (dimensionless) distance Q, are both located in the same shock at time t (in the limit where the particles are far from the origin, or anywhere on the right side for one-sided initial conditions). At large initial Lagrangian separation Q, we obtain from (141) the exponential decay (that again can be understood from simple scaling arguments)

$$Q \to +\infty: \quad \overline{P}_Q^{\text{shock}} \sim \frac{1}{\sqrt{\pi}} Q^{-3/2} e^{-Q}, \quad (142)$$

whereas for small initial distance Q we have

$$Q \to 0: \quad \overline{P}_Q^{\text{shock}} \sim 1 - 4\sqrt{\frac{Q}{\pi}}. \quad (143)$$

Therefore, in the limit $Q \to 0$ the probability that both particles are within the same shock reaches unity whereas the weight associated with the "regular" contribution (135) vanishes (while its cutoff decreases as Q). This agrees with the well-known result that the set of regular Lagrangian points has a Hausdorff dimension equal to $1/2$ [41, 43], so that with probability 1 a random Lagrangian point q belongs to a shock at any given time $t > 0$. This clearly implies that $\overline{P}_Q^{\text{shock}} \to 1$ for $Q \to 0$, as in (143). Moreover, the behavior $1 - \overline{P}_Q^{\text{shock}} \propto Q^{1/2}$ also shows that the set of regular Lagrangian points has a box-counting dimension equal to $1/2$, in agreement with these works.

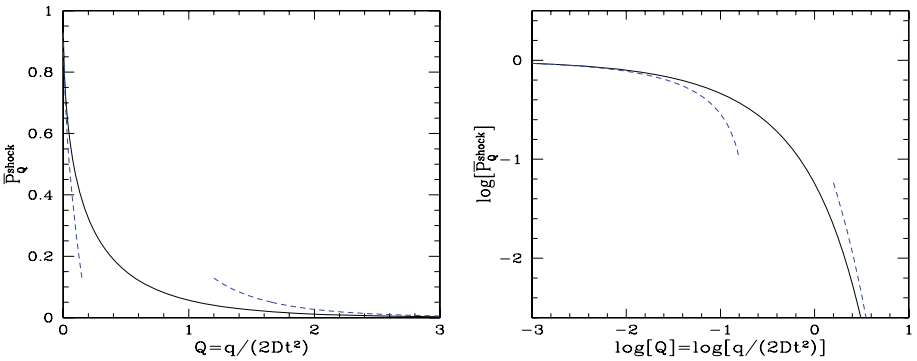

Fig. 12 (Color online) *Left panel:* The probability, $\overline{p}_q^{\rm shock}$, that two particles, that were initially separated by a distance q, have coalesced within a single shock by time t (in the limit where the particles are far from the origin). We show the reduced probability, $\overline{P}_Q^{\rm shock}$, from (144). The *dashed lines* are the asymptotic behaviors (142) and (143). *Right panel:* The probability $\overline{P}_Q^{\rm shock}$ on a logarithmic scale

Taking the derivative of (141) yields again a standard inverse Laplace transform [1] that provides a convenient integral expression for $\overline{P}_Q^{\rm shock}$,

$$\frac{{\rm d}\overline{P}_Q^{\rm shock}}{{\rm d}Q} = 2\left[{\rm erfc}(\sqrt{Q}) - \frac{e^{-Q}}{\sqrt{\pi\,Q}}\right], \quad \text{hence } \overline{P}_Q^{\rm shock} = 2\int_Q^\infty {\rm d}Q' \left(\frac{e^{-Q'}}{\sqrt{\pi\,Q'}} - {\rm erfc}(\sqrt{Q'})\right). \tag{144}$$

We show in Fig. 12 the same-shock probability $\overline{P}_Q^{\rm shock}$ as a function of Q, as well as the asymptotic behaviors (142) and (143).

7.3 Higher-Order Distributions

We can obtain the higher-order n-point distributions $p_{q_1,\ldots,q_n}(x_1,\ldots,x_n)$ by the same method which we applied in the previous section for the two-point distribution. Thus, as in (128), we can related the Lagrangian and Eulerian cumulative probabilities by

$$P_{Q_1,\ldots,Q_n}(X_1' \geq X_1, \ldots, X_n' \geq X_n) = P_{X_1,\ldots,X_n}(Q_1' \leq Q_1, \ldots, Q_n' \leq Q_n), \tag{145}$$

with $Q_1 < Q_2 < \ldots < Q_n$ and $X_1 < X_2 < \ldots < X_n$. Then, in the limit $Q_1 \to +\infty$, using again the factorization (87) and the expressions (79) and (84), we can integrate over $Q_1', \ldots, Q_n'$. Differentiating with respect to $X_1, \ldots, X_n$, gives the n-point probability density (compare with (131))

$$\begin{aligned} Q_1 \to \infty: \quad & P_{Q_1,\ldots,Q_n}(X_1,\ldots,X_n) \\ & \sim \frac{e^{-\chi_1^2/Q_1}}{\sqrt{\pi\,Q_1}} \int_{-i\infty}^{+i\infty} \frac{{\rm d}s_2 \ldots {\rm d}s_n}{(2\pi{\rm i})^{(n-1)}} e^{(s_2-1)Q_{2,1}+\ldots+(s_n-1)Q_{n,n-1}} \\ & \quad \times \frac{2^n e^{-(\sqrt{s_2}-1)2X_{2,1}-\ldots-(\sqrt{s_n}-1)2X_{n,n-1}}}{(1+\sqrt{s_2})(\sqrt{s_2}+\sqrt{s_3})\ldots(\sqrt{s_{n-1}}+\sqrt{s_n})(\sqrt{s_n}+1)}, \end{aligned} \tag{146}$$

with $X_{i,i-1} = X_i - X_{i-1}$, $Q_{i,i-1} = Q_i - Q_{i-1}$, $\Psi_1 = X_1 - Q_1$. Note that this n-point distribution does not factorize.

From (146) we can obtain the contributions associated with shocks in the same manner as in Sect. 7.2. For instance, far from the origin ($Q_1 \gg 1$), the probability density, $\overline{P}^{\rm shock}_{Q_{21},Q_{32},Q_{43}}(X_{32})$, that each pair $\{Q_1, Q_2\}$, and $\{Q_3, Q_4\}$, has coalesced within two shocks that are separated by a distance in the range $[X_{32}, X_{32} + \mathrm{d}X_{32}]$, reads as

$$\overline{P}^{\rm shock}_{Q_{21},Q_{32},Q_{43}}(X_{32}) = \int_{-i\infty}^{+i\infty} \frac{\mathrm{d}s_2\mathrm{d}s_3\mathrm{d}s_4}{(2\pi\mathrm{i})^3} e^{(s_2-1)Q_{21}+(s_3-1)Q_{32}+(s_4-1)Q_{43}} \times \frac{4e^{-(\sqrt{s_3}-1)2X_{32}}}{(s_2-1)(\sqrt{s_2}+\sqrt{s_3})(\sqrt{s_3}+\sqrt{s_4})(s_4-1)}, \tag{147}$$

where the integration contour is such that $\Re(s_2) < 1$, $\Re(s_3) > 1$ and $\Re(s_4) < 1$.

7.4 Computing the Density Power Spectrum from the Lagrangian Statistics

Finally, it is interesting to note that the statistics of the Lagrangian displacement field also allow us to compute the Eulerian density power spectrum and to recover the result (113). Indeed, as is well-known the conservation of matter implies that the density $\rho(x)$ may be written as

$$\rho(x) = \rho_0 \left(\frac{\partial x}{\partial q}\right)^{-1} = \rho_0 \int \mathrm{d}q \delta(x - q - \chi(q)), \tag{148}$$

where $\chi(q) = x(q) - q$ is the Lagrangian displacement of particle q. Note that the last expression is still valid when there are shocks, as may be seen by computing the mass within some interval $[x_1, x_2]$. Going to Fourier space as in (112), we can write

$$\langle \rho(k_1)\rho(k_2)\rangle = \rho_0^2 \int \frac{\mathrm{d}q_1\mathrm{d}q_2}{(2\pi\mathrm{i})^2} e^{-\mathrm{i}(k_1q_1+k_2q_2)} \langle e^{-i(k_1\chi_1+k_2\chi_2)}\rangle. \tag{149}$$

Then, in the regime where the invariance through translations is recovered (i.e. far from the origin), making the changes of variables $q_2 = q_1 + q$ and $\chi_2 = \chi_1 + \chi$, we obtain

$$\mathcal{P}(k) = \int_0^\infty \frac{\mathrm{d}q}{\pi} \int_0^\infty \mathrm{d}x \overline{p}_q(x) \cos(kx) \tag{150}$$

$$= \gamma^2 \int_0^\infty \frac{\mathrm{d}Q}{\pi} \int_{0^+}^\infty \mathrm{d}X \overline{P}_Q(X) \cos(\gamma^2 kX) + \gamma^2 \int_0^\infty \frac{\mathrm{d}Q}{\pi} \overline{P}^{\rm shock}_Q. \tag{151}$$

In the second line, written in terms of dimensionless variables, we separated the two contributions associated with the regular part (135) and with the singular part (141) of the distribution of the relative Eulerian distance X. Using (133), we can check that the first contribution actually vanishes (as expected since all the mass is enclosed within shocks, see (153) below and [41, 43]), whereas the shock contribution is obviously independent of k and using (141) we recover the amplitude (113).

8 Properties of Shocks

8.1 Shock Mass Function

From the probability $\overline{p}^{\rm shock}_q$ that two particles, initially separated by a distance q, are located in the same shock at a time $t > 0$, we can now derive the mass function of shocks. First, we

note that if a shock has Lagrangian end-points q_- and q_+, its mass is simply $m = \rho_0(q_+ - q_-)$, where ρ_0 is the uniform initial density, as discussed in Sect. 6. Then, within an interval of length $\mathcal{Q}$ in Lagrangian space, we now count the number, $\mathcal{Q}n_{\mathcal{Q}}(m)\mathrm{d}m$, of shock-intervals of length in the range $[q, q + \mathrm{d}q]$, whence of mass in $[m, m + \mathrm{d}m]$, with $m = \rho_0 q$. The limit $\mathcal{Q} \to \infty$ gives the probability density $n(m)$ for a Lagrangian point to belong to a shock of mass m. Since on large scales particles are still governed by the initial Gaussian velocity field and have only moved by a relative distance $\chi \sim \sqrt{\mathcal{Q}}$, see for instance (136), the corresponding Eulerian relative distance, $\mathcal{X}$, obeys $\mathcal{X}/\mathcal{Q} \to 1$ for $\mathcal{Q} \to \infty$. Therefore, $n(m)\mathrm{d}m$ is also the mean number of shocks, per unit Eulerian length, with a mass in the range $[m, m + \mathrm{d}m]$.

Let us now relate the mass function $n(m)$ to the shock probability $\overline{p}_q^{\,\mathrm{shock}}$ that we obtained in (141). The latter is the probability that a Lagrangian interval, $q = q_2 - q_1$, chosen at random, has coalesced by time t within a single shock. This clearly means that this shock has a length q^{s} larger than q and that q_1 is located within a distance smaller than $q^{\mathrm{s}} - q$ from its left boundary. Therefore, in terms of dimensionless variables, we have the relation

$$\overline{P}_Q^{\,\mathrm{shock}} = \int_Q^\infty \mathrm{d}M N(M)(M - Q), \quad \text{with } M = \frac{m}{\rho_0 \gamma^2}. \tag{152}$$

Here $N(M)$ is the dimensionless mass function. From (152) and (143), taking $Q = 0$, we obtain at once the normalization

$$\int_0^\infty \mathrm{d}M M N(M) = 1, \tag{153}$$

which means that all the mass is included within shocks, at any time $t > 0$. This agrees with previous results discussed below (143), see [41] and [43]. Differentiating twice (152) with respect to Q, and using the first (144), gives the simple expression

$$N(M) = \left.\frac{\mathrm{d}^2 \overline{P}_Q^{\,\mathrm{shock}}}{\mathrm{d}Q^2}\right|_{Q=M}, \quad \text{whence } N(M) = \frac{1}{\sqrt{\pi}} M^{-3/2}\, e^{-M}. \tag{154}$$

Thus, we recover the low-mass power law $M^{-3/2}$ that was already obtained in [41, 43]. At large masses we obtain the exponential falloff that was heuristically derived in [51], following the same scaling arguments as those described in previous sections for the tails of the Eulerian or Lagrangian distributions. The full mass function (154) was also obtained in [9] for the one-sided Brownian initial velocity. Indeed, in that case the Lagrangian increments q_{21} have the same distribution for $x \geq 0$, as discussed in Sect. 5.1, which clearly leads to identical shock properties.

It is interesting to compare the exact result (154) with the Press-Schechter ansatz that is widely used in the cosmological context to count the number of collapsed objects [38]. This model attempts to identify such objects from the properties of the linear fields, obtained from the linearization of the equations of motion. For our case, this heuristic approach would state that the fraction of matter, $F(> m)$, that is enclosed within collapsed objects (here infinitesimally thin shocks, as we consider the Burgers equation in the inviscid limit) of mass larger than m, with $m = \rho_0 q$, is given by the probability that, choosing a Lagrangian point q_c at random, the linear-theory Eulerian relative distance x_L at time t between the particles $q_c + q/2$ and $q_c - q/2$ vanishes. (For a 3-dimensional Universe one considers the probability the a sphere of mass m centered on q_c has collapsed to a point.) In terms of

dimensionless variables this reads as

$$F^{\rm PS}(\geq M) = P_Q^L(X_L \leq 0) \quad \text{at } M = Q, \text{ with } P_Q^L(X_L) = \frac{e^{-(X_L-Q)^2/Q}}{\sqrt{\pi\, Q}}, \tag{155}$$

where P^L refers to the distribution obtained by linear theory, where particles always keep their initial velocity and shocks are discarded. This gives

$$F^{\rm PS}(\geq M) = \int_{\sqrt{M}}^{\infty} {\rm d}y \frac{e^{-y^2}}{\sqrt{\pi}}. \tag{156}$$

As usual, (156) implies $F^{\rm PS}(\geq 0) = 1/2$, which means that only half of the mass would be within collapsed structures. Therefore, it is customary to multiply this by a somewhat ad-hoc factor 2 [38]. Thus, differentiating with respect to M, the standard Press-Schechter recipe gives in our case the mass function

$$2F^{\rm PS}(\geq M) = \int_M^{\infty} {\rm d}M\, M N^{\rm PS}(M), \quad \text{whence } N^{\rm PS}(M) = \frac{1}{\sqrt{\pi}} M^{-3/2}\, e^{-M}. \tag{157}$$

Therefore, we find that for the 1-D Burgers dynamics with Brownian initial velocity the Press-Schechter ansatz happens to give the exact mass function (154). The agreement of the Press-Schechter mass function at both small and large masses for the one-dimensional case was already noticed in [51], for more general power-law initial velocity energy spectra (although there were no exact results available at large masses but heuristic predictions). This can be somewhat surprising in view of the many effects that could have made the Press-Schechter ansatz fail (especially at the low-mass tail), such as the so-called "cloud-in-cloud problem", associated here with the fact that, even though particles $q_c \pm q/2$, evolved according to linear theory, may have not collided yet, on a larger scale $\ell > q$ it may happen that particles $q_c \pm \ell/2$ had very large inward velocities and have formed by time t a massive shock that includes the smaller scale q. Nevertheless, in the cosmological context, numerical simulations have shown that, even though the Press-Schechter mass function is not exact, is usually gives reasonably good estimates (e.g., [42]), so that it is still widely used today. It is satisfying to find out that in a related dynamical system, it actually happens to coincide with the exact result. This makes the reasonable agreement observed in other cases somewhat less surprising than would be expected at first sight. As found in [51], this also suggests that it could provide a reasonable estimate for the Burgers dynamics itself with more general initial conditions.

8.2 Spatial Distribution of Shocks

Finally, from the n-point distributions (146) we can derive the many-body distributions of shocks, far from the origin. Thus, in a fashion similar to (152), we can relate the trivariate mass function, $N(M_1, M, M_2; X){\rm d}M_1{\rm d}M{\rm d}M_2{\rm d}X_1{\rm d}X$, that counts the probability to have a shock of mass M_1 within $[X_1, X_1+{\rm d}X_1]$, another shock of mass M_2 at distance $[X, X+{\rm d}X]$, and a mass M in-between both shocks, to the three-point conditional shock probability, $\overline{P}_{Q_{21},Q_{32},Q_{43}}$, of (147). This reads as

$$\overline{P}_{Q_{21},Q_{32},Q_{43}}(X) = \int_0^{Q_{32}} {\rm d}M \int_{Q_{21}}^{\infty} {\rm d}M_1 \int_{Q_{43}}^{\infty} {\rm d}M_2 N(M_1, M, M_2; X) \int_0^{M_1-Q_{21}} {\rm d}Q_1 \times \theta(Q_1+Q_{21}+Q_{32}-M_1-M)\theta(M_1+M+M_2-Q_1-Q_{21}-Q_{32}-Q_{43}), \tag{158}$$

where the two Heaviside factors ensure that Q_3 and Q_4 are within the second shock of mass M_2. Then, differentiating with respect to Q_{21} and Q_{43} yields

$$\frac{\partial^2 \overline{P}_{Q_{21},Q_{32},Q_{43}}}{\partial Q_{21}\partial Q_{43}} = \int_0^{Q_{32}} \mathrm{d}M \int_{Q_{43}}^{Q_{43}+Q_{32}-M} \mathrm{d}M_2 N(Q_{21}+Q_{32}+Q_{43}-M-M_2, M, M_2; X). \tag{159}$$

Taking the shifted Laplace transform of both quantities, in the form

$$N(M_1, M, M_2; X) = \int_{-i\infty}^{+i\infty} \frac{\mathrm{d}s_1 \mathrm{d}s \mathrm{d}s_2}{(2\pi \mathrm{i})^3} e^{(s_1-1)M_1+(s-1)M+(s_2-1)M_2} \tilde{N}(s_1, s, s_2; X), \tag{160}$$

and using (147), we obtain

$$\tilde{N}(s_1, s, s_2; X) = \frac{4(s-s_1)(s-s_2)e^{-(\sqrt{s}-1)2X}}{(\sqrt{s_1}+\sqrt{s})(\sqrt{s}+\sqrt{s_2})}. \tag{161}$$

If we now consider the multiplicity of shocks at positions X_1 and X_2, independently of the mass M in-between, we integrate over M and s, which gives the bivariate mass function of shocks separated by a distance X:

$$N(M_1, M_2; X) = \int_{-i\infty}^{+i\infty} \frac{\mathrm{d}s_1 \mathrm{d}s_2}{(2\pi \mathrm{i})^2} e^{(s_1-1)M_1+(s_2-1)M_2} \frac{4(1-s_1)(1-s_2)}{(\sqrt{s_1}+1)(1+\sqrt{s_2})} = N(M_1)N(M_2), \tag{162}$$

where we used (154) and (141) to recognize the product $N(M_1)N(M_2)$. Therefore, we find that the bivariate mass function $n(m_1, m_2; x)$ does not depend on the inter-shock distance x and merely factorizes as $n(m_1) \times n(m_2)$ (far from the origin $x_1 = 0$).

Thus, shocks are not correlated and there is no bias: knowing that there is a shock of mass m_1 at position x_1 does not bias in any way the shock multiplicity at position $x_2 = x_1 + x$. We can note that this is consistent with the fact that the densities within separate regions are uncorrelated, as seen in (114) and (115). In fact, from (115), which shows that the density fields over separate regions are completely independent, we can see that this must extend to all n-point shock mass functions, thus shocks at different positions are uncorrelated. The fact that shocks form a Poisson point process was also obtained in [9] for the case of one-sided Brownian velocity.

9 Conclusion

We have shown in this paper how to derive the equal-time statistical properties of the solution of the Burgers equation with Brownian initial velocity, using the transition kernel associated with Brownian particles over a parabolic absorbing barrier. This initial velocity field is not homogeneous, as the initial velocity is Gaussian with a variance $\langle v_0^2 \rangle \propto |x|$ at distance $|x|$. However, it has homogeneous increments. Then, although the one-point distributions, $p_x(v)$ and $p_x(q)$, of the velocity v and initial Lagrangian position q, depend on the position x, the two-point distributions exactly factorize provided that all spatial coordinates remain on the same side of $x = 0$, such as $p_{x_1,x_2}(v_1, v_2) = p_{x_1}(v_1)\overline{p}_{x_{21}}(v_{21})$ and $p_{x_1,x_2}(q_1, q_2) = p_{x_1}(q_1)\overline{p}_{x_{21}}(q_{21})$ for $q_i > 0$. A similar factorization holds for higher-order distributions. This agrees with the results that were obtained for the one-sided Brownian initial velocity by [9]. In the limit where we are far from the origin, this implies that we recover the invariance through translations for the distributions of velocity and Lagrangian

increments. Then, we have focussed on the properties of the system in this limit, where many simple explicit results can be derived.

As expected, we have found that on large scales, or at early times, all statistical properties converge to the Gaussian distributions set by the initial conditions (the nonlinear evolution being subdominant). On small scales, or at late times, the distributions of the velocity increment, Lagrangian increment, or mean overdensity η within a region of length x, increasingly depart from the Gaussian. They exhibit widely separated exponential cutoffs, of the form $e^{-\eta}$ and $e^{-1/\eta}$, while a power law $\eta^{-3/2}$ develops in the intermediate range. However, we find that the variance of these distributions remains unchanged by the nonlinear dynamics, that is, it is equal to the value that would be obtained by discarding collisions and shocks, and letting particles cross each other and always keep their initial velocity. In particular, the second-order velocity structure function and its energy spectrum do not evolve with time, while the density correlation remains a Dirac function with an amplitude that grows as t^2.

In fact, the densities within non-overlapping regions are uncorrelated and, at any order, the n-point connected density correlation can be written as a product of $n-1$ Dirac factors: it is non-vanishing only when all points coincide. Then, it can also be written as a product of $n-1$ two-point correlations, that connect the n points, with a constant amplitude that happens to be the number of heap ordered trees. This allows a combinatorial interpretation that is similar to the hierarchical tree models that were devised as a phenomenological tool in the cosmological context, with the difference that in our case we must consider ordered trees (note that in the present 1-D system, where particles do not cross, it is meaningful to order particles by their positions so that the concept of ordering appears rather natural). Then, the cumulants of the overdensity exactly scale as $\langle \eta^n \rangle_c \propto \langle \eta^2 \rangle_c^{(n-1)}$, with an amplitude that is independent of time and scale. Thus, they happen to exactly satisfy the so-called "stable-clustering ansatz". In fact, the density cumulant-generating function remains exactly equal to the one obtained at tree-order from a perturbative approach (which breaks down beyond leading order as next-to-leading corrections actually are divergent, which signals the need for a non-perturbative method that takes into account shocks).

We have also studied the Lagrangian displacement field, associated with a Lagrangian description of the dynamics. In the limit where we are far from the origin, we find that it satisfies a similar factorization and recovers the invariance through translations for the distributions of relative displacements. This also allows us to derive the properties of shocks. Thus, in agreement with previous works, we find that all of the mass is enclosed within shocks, at any time $t > 0$, and that the shock mass function has the very simple expression (154). It agrees with the asymptotic behaviors that were already obtained through analytical means or numerical simulations in [41, 43] or [51] and the exact result of [9]. Finally, shocks are not correlated as the bivariate multiplicity function $n(m_1, m_2; x)$, that counts shocks of mass m_1 and m_2 separated by the distance x, factorizes as $n(m_1) \times n(m_2)$, in agreement with the same lack of correlation obtained for the density field.

Thus, the equal-time statistical properties of the Burgers dynamics with Brownian initial velocity are remarkably simple. It appears that the nonlinear dynamics preserves some properties of the initial fields (e.g. the second-order structure functions, the independence and homogeneity of velocity increments and of the densities in separate domains) and that simple explicit expressions can be derived in the limit where we are far from the origin (or on the right side for one-sided initial conditions).

At finite distance from the origin, in addition to the quantities given here we need the two-point distribution associated with the case where the two particles are on different sides of the origin $x = 0$. Although we can obtain explicit expressions by the method presented in this article, this leads to multidimensional integrals that do not seem to greatly simplify

(although we obtained simple expressions for the one-point distributions). However, for practical purposes, one is mostly interested in the limit where we are far from the origin and homogeneity is recovered. From a physical point of view, the initial conditions (5) are meant to represent a system with homogeneous velocity increments, which scale as $\langle(\Delta v_0)^2\rangle \propto |\Delta q|$ as in (9) over a finite range, and an energy spectrum $E_0(k) \propto k^{-2}$ as in (10) over the range of interest. Thus, in practice there would be an infrared cutoff, Λ, below which $E_0(k)$ would grow more slowly than $1/k$ so that the velocity field is actually homogeneous (in an experimental setup there would actually be a finite lower wavenumber, set by the size of the box, and homogeneity would only apply far from the boundaries). Then, the initial conditions (5) studied in this article can be viewed as a convenient mathematical device to represent such a system, with the understanding that the special role played by the origin is a mathematical artifact and that only the properties far from the origin are meaningful in the physical sense described above. Note that this identification is possible because small scales are not strongly coupled to large scales, in agreement with the fact that over large scales we recover the initial fields and no strong correlations develop.

To put this study in a broader context, it may be useful to recall here the main properties of "decaying Burgers turbulence" for more general Gaussian initial conditions. It is customary to study the Burgers dynamics (1) for power-law energy spectra, $E_0(k) \propto k^n$ (here we focussed on the case $n = -2$, see (10)). Indeed, at late times the asymptotic statistical properties of the velocity field no longer depend on the details of the high-k spectrum (assuming a strong enough falloff) nor on the precise value of the viscosity ν, as a self-similar evolution develops [22, 35]. Then, depending on the exponent n, the integral scale of turbulence, $L(t)$, which measures the typical distance between shocks and the correlation length, and the shock and velocity probability distributions show the following behaviors.

For $-3 < n < -1$ (which includes the case $n = -2$ studied in this article, associated with a Brownian initial velocity), the initial velocity is not homogeneous but it has homogeneous increments, while for $-1 < n < 1$ (which includes the case $n = 0$ associated with a white-noise initial velocity), the initial velocity itself is homogeneous. In both cases, the integral scale grows as $L(t) \sim t^{2/(n+3)}$, and the tails of the cumulative shock distribution and velocity distribution satisfy $\ln[n(> m)] \sim -m^{n+3}$, $\ln[n(> |v|)] \sim -|v|^{n+3}$, for $m \to \infty$, $|v| \to \infty$, see [34, 41]. At low wavenumbers, below $1/L(t)$, the energy spectrum keeps its initial form, $E(k,t) \propto k^n$, whereas at high wavenumbers it shows the universal law, $E(k,t) \propto k^{-2}$, due to shocks [26, 36]. The preservation of the large-scale part, $E(k,t) \propto k^n$, is associated with the "principle of permanence of large eddies" [26]. Physically, this means that, at a given time t, structures of size larger than $L(t)$ have not had time to be strongly distorted by the dynamics (in agreement with the simple scaling argument $t\sigma_{v_0}(x) \ll x$ which gives $x \gg L(t)$). In particular, not only statistical properties but each random realization is stable against small-scale perturbations [2, 23]. Then, the tails of the shock and velocity distributions can be understood from the initial velocity field. Thus, the velocity difference between the left and right boundaries of a shock of mass $m = \rho_0 q$ is q/t, which leads to a probability $\sim e^{-(q/t)^2/\sigma_{v_0}(q)^2} \sim e^{-m^{n+3}/t^2}$ (where we did not write constants in the exponent) [51]. We can check that these properties agree with the results derived for $n = -2$ in this paper.

For $1 < n < 2$ the system shows a more complex behavior, since there are three scaling regions for the energy spectrum: first a k^n region at very low wavenumbers, below $k_s(t) \sim t^{-1/2(2-n)}$, next a k^2 region between $k_s(t)$ and $k_L(t) \sim t^{-1/2}$, and finally the standard k^{-2} region above $k_L(t)$ [26]. Therefore the evolution is no longer self-similar. For $n > 2$ the k^n region disappears (it gives subdominant corrections) and the leading-order evolution is again self-similar but independent of n [24, 26].

We can hope that the exact results presented in this article for the case of Brownian initial velocity could serve as a useful benchmark to test approximation schemes which could be devised to handle other initial conditions where no exact results are available. In particular, in the cosmological context, the Zeldovich approximation, which corresponds to removing the diffusive term altogether, has already been used to test for instance field-theoretic methods that attempt to resum perturbative series [47]. The Burgers equation in the inviscid limit, which corresponds to the more efficient adhesion model, might also be used for such purposes. In a similar fashion, the general properties of the Burgers dynamics (associated with shocks) have already been used to test approximation schemes devised for the study of turbulence [16].

Finally, we note that the method described in this article could also be applied to different-time statistics, where the parabolas used in the geometrical interpretations would now have different curvatures. However, we leave such studies for future works.

Appendix A: Some Properties of the Airy Functions

We recall here some properties of the Airy functions $\mathrm{Ai}(x)$ and $\mathrm{Bi}(x)$ that are used repeatedly in the calculations presented in this article. These two Airy functions are two linearly independent solutions to the second-order differential equation $y''(x) - xy(x) = 0$. The first one, $\mathrm{Ai}(x)$, is the only solution that vanishes at both ends, $x \to \pm\infty$, whereas $\mathrm{Bi}(x)$ grows to infinity at $x \to +\infty$ [1]. Both are entire functions and they are related through

$$\mathrm{Bi}(x) = e^{\mathrm{i}\pi/6}\mathrm{Ai}(e^{\mathrm{i}2\pi/3}x) + e^{-\mathrm{i}\pi/6}\mathrm{Ai}(e^{-\mathrm{i}2\pi/3}x), \tag{163}$$

while their Wronskian is constant and given by

$$\mathrm{Ai}(x)\mathrm{Bi}'(x) - \mathrm{Ai}'(x)\mathrm{Bi}(x) = \frac{1}{\pi}. \tag{164}$$

We also have the integral representation [1]

$$\mathrm{Ai}(x) = \int_{-\infty}^{\infty} \frac{\mathrm{d}t}{2\pi} e^{\mathrm{i}(\frac{t^3}{3}+xt)}. \tag{165}$$

At $x = 0$ we have

$$\frac{\mathrm{Bi}(0)}{\sqrt{3}} = \mathrm{Ai}(0) = \frac{1}{3^{2/3}\Gamma[2/3]}, \qquad \frac{-\mathrm{Bi}'(0)}{\sqrt{3}} = \mathrm{Ai}'(0) = \frac{-1}{3^{1/3}\Gamma[1/3]}, \tag{166}$$

and for $|x| \to \infty$:

$$|\mathrm{Arg}(x)| < \pi : \quad \mathrm{Ai}(x) \sim \frac{1}{2\sqrt{\pi}} x^{-1/4} e^{-\frac{2}{3}x^{3/2}}, \tag{167}$$

$$|\mathrm{Arg}(x)| < \frac{2\pi}{3} : \quad \mathrm{Ai}(-x) \sim \frac{1}{\sqrt{\pi}} x^{-1/4} \sin\left[\frac{2}{3}x^{3/2} + \frac{\pi}{4}\right], \tag{168}$$

$$|\mathrm{Arg}(x)| < \frac{\pi}{3} : \quad \mathrm{Bi}(x) \sim \frac{1}{\sqrt{\pi}} x^{-1/4} e^{\frac{2}{3}x^{3/2}}, \tag{169}$$

$$|\mathrm{Arg}(x)| < \frac{2\pi}{3} : \quad \mathrm{Bi}(-x) \sim \frac{1}{\sqrt{\pi}} x^{-1/4} \cos\left[\frac{2}{3}x^{3/2} + \frac{\pi}{4}\right]. \tag{170}$$

For $|\mathrm{Arg}(x)| < 2\pi/3$, the Airy function can also be expressed in terms of the modified Bessel function of the second kind K_ν as

$$|\mathrm{Arg}(x)| < \frac{2\pi}{3}: \quad \mathrm{Ai}(x) = \frac{1}{\pi}\sqrt{\frac{x}{3}} K_{1/3}\left(\frac{2}{3}x^{3/2}\right), \qquad \mathrm{Ai}'(x) = \frac{-x}{\pi\sqrt{3}} K_{2/3}\left(\frac{2}{3}x^{3/2}\right). \tag{171}$$

Four useful integrals, that may be obtained from the integral representation (165), are [50]

$$\int_{-\infty}^{\infty} \mathrm{d}x e^{\alpha x}\mathrm{Ai}(x) = e^{\alpha^3/3}, \quad \text{whence} \int_{-\infty}^{\infty} \mathrm{d}x e^{\alpha x} x\mathrm{Ai}(x) = \alpha^2 e^{\alpha^3/3}, \tag{172}$$

$$\nu_1 \neq \nu_2: \quad \int_{-\infty}^{\infty} \mathrm{d}u \mathrm{Ai}\left[\nu_1 u + \frac{s_1}{\nu_1^2}\right]\mathrm{Ai}\left[\nu_2 u + \frac{s_2}{\nu_2^2}\right]$$
$$= \frac{1}{|\nu_1^3 - \nu_2^3|^{1/3}}\mathrm{Ai}\left[(\nu_1^3 - \nu_2^3)^{-1/3}\left(\frac{\nu_1 s_2}{\nu_2^2} - \frac{\nu_2 s_1}{\nu_1^2}\right)\right], \tag{173}$$

and

$$\nu_1 \neq \nu_2: \quad \int_{-\infty}^{\infty} \mathrm{d}u u \mathrm{Ai}\left[\nu_1 u + \frac{s_1}{\nu_1^2}\right]\mathrm{Ai}\left[\nu_2 u + \frac{s_2}{\nu_2^2}\right]$$
$$= \frac{s_2 - s_1}{(\nu_1^3 - \nu_2^3)^{4/3}}\mathrm{Ai}\left[(\nu_1^3 - \nu_2^3)^{-1/3}\left(\frac{\nu_1 s_2}{\nu_2^2} - \frac{\nu_2 s_1}{\nu_1^2}\right)\right], \tag{174}$$

with the conventions: $(\nu_1^3 - \nu_2^3)^{-1/3} \to -(\nu_2^3 - \nu_1^3)^{-1/3}$ and $(\nu_1^3 - \nu_2^3)^{4/3} \to -(\nu_2^3 - \nu_1^3)^{4/3}$ if $\nu_1 < \nu_2$. This also implies the relation

$$\nu_1 \neq \nu_2: \quad \int_{-\infty}^{\infty} \mathrm{d}u u \mathrm{Ai}\left[\nu_1 u + \frac{s_1}{\nu_1^2}\right]\mathrm{Ai}\left[\nu_2 u + \frac{s_2}{\nu_2^2}\right]$$
$$= \frac{s_2 - s_1}{\nu_1^3 - \nu_2^3}\int_{-\infty}^{\infty} \mathrm{d}u \mathrm{Ai}\left[\nu_1 u + \frac{s_1}{\nu_1^2}\right]\mathrm{Ai}\left[\nu_2 u + \frac{s_2}{\nu_2^2}\right], \tag{175}$$

that could be obtained from the property $\mathrm{Ai}''(x) = x\mathrm{Ai}(x)$.

Finally, using the property [21]

$$\mu > \nu, \alpha + \beta > 0: \quad \int_0^{\infty} \mathrm{d}x x^{\mu-1} e^{-\alpha x} K_\nu(\beta x) = \frac{\sqrt{\pi}(2\beta)^\nu}{(\alpha+\beta)^{\mu+\nu}} \frac{\Gamma(\mu+\nu)\Gamma(\mu-\nu)}{\Gamma(\mu+\frac{1}{2})}$$
$$\times {}_2F_1\left(\mu+\nu, \nu+\frac{1}{2}; \mu+\frac{1}{2}; \frac{\alpha-\beta}{\alpha+\beta}\right), \tag{176}$$

and the relations (171), we obtain

$$\nu > 0, \alpha + \beta > 0: \quad \int_0^\infty \mathrm{d}x x^{\nu-1} e^{-\alpha x} \mathrm{Ai}\left[\left(\frac{3\beta x}{2}\right)^{2/3}\right]$$
$$= \frac{1}{\sqrt{\pi}} 3^{-1/6} \beta^{2/3} (\alpha+\beta)^{-\nu-\frac{2}{3}} \frac{\Gamma(\nu+\frac{2}{3})\Gamma(\nu)}{\Gamma(\nu+\frac{5}{6})}$$
$$\times {}_2F_1\left(\nu+\frac{2}{3}, \frac{5}{6}; \nu+\frac{5}{6}; \frac{\alpha-\beta}{\alpha+\beta}\right), \tag{177}$$

$$\nu > 0, \alpha + \beta > 0: \quad \int_0^\infty \mathrm{d}x x^{\nu-1} e^{-\alpha x} \mathrm{Ai}'\left[\left(\frac{3\beta x}{2}\right)^{2/3}\right]$$
$$= \frac{-1}{\sqrt{\pi}} 3^{1/6} \beta^{4/3} (\alpha+\beta)^{-\nu-\frac{4}{3}} \frac{\Gamma(\nu+\frac{4}{3})\Gamma(\nu)}{\Gamma(\nu+\frac{7}{6})}$$
$$\times {}_2F_1\left(\nu+\frac{4}{3}, \frac{7}{6}; \nu+\frac{7}{6}; \frac{\alpha-\beta}{\alpha+\beta}\right). \tag{178}$$

Appendix B: Half-Range Expansion and Useful Integrals

We show in this appendix how to obtain the solution (34) to the half-range expansion problem (32)–(33). The same method also allows us to derive other useful identities that we need to perform the calculations presented in this article. Thus, we consider the function $f(p)$ of the complex variable p defined by

$$s \geq 0, u \geq 0, |\mathrm{Arg}(p)| < \pi: \quad f(p) = p^{-1/6} e^{\frac{2}{3}s^{3/2}/p} \mathrm{Ai}\left[p^{1/3}u + \frac{s}{p^{2/3}}\right]. \tag{179}$$

This function is regular over the complex plane except for a branch cut along the negative real axis. Moreover, from the asymptotic behavior (167) of the Airy function we obtain

$$u > 0: \quad f(p) \sim \frac{u^{-1/4}}{2\sqrt{\pi}} p^{-1/4} e^{-\frac{2}{3}u^{3/2}p^{1/2}} \quad \text{as } |p| \to \infty \text{ with } |\mathrm{Arg}(p)| < \pi, \tag{180}$$

and

$$u = 0: f(p) \sim \mathrm{Ai}(0) p^{-1/6} \quad \text{as } |p| \to \infty \text{ with } |\mathrm{Arg}(p)| < \pi. \tag{181}$$

Next, we introduce the general integral $F_{k,\ell}(\nu_1, \ldots, \nu_k; \lambda_1, \ldots, \lambda_\ell)$ defined by

$$F_{k,\ell}(\nu_i; \lambda_j) = \int_{c-\mathrm{i}\infty}^{c+\mathrm{i}\infty} \frac{\mathrm{d}p}{2\pi \mathrm{i}} \frac{f(p)}{\prod_{i=1}^k (p-\nu_i^3) \prod_{j=1}^\ell (p+\lambda_j^3)} \quad \text{with } c > \max_i\{\nu_i^3\}, \tag{182}$$

with the conditions

$$\nu_i > 0, \quad \nu_i \neq \nu_{i'} \quad \text{for } i \neq i'; \qquad \lambda_j > 0, \quad \lambda_j \neq \lambda_{j'} \quad \text{for } j \neq j'; \qquad k + \ell \geq 1. \tag{183}$$

If $k=0$ or $\ell=0$ one of the products in (182) is removed and replaced by a factor 1. If $k=0$ the contour in (182) again runs to the right of all singularities, that is $c>0$.

Then, from the asymptotics (180)–(181), we can see that we can push the contour in (182) to the right, as $c\to+\infty$, which shows that $F_{k,\ell}=0$ (using $k+\ell\geq 1$). On the other hand, by pushing the contour to the left, using again the asymptotics (180)–(181), we can see that $F_{k,\ell}$ is the sum of the k residues at $p=\nu_i^3$ and of the contribution associated with the branch cut along the negative real axis. This yields

$$0=\sum_{i=1}^{k}\frac{\nu_i^{-\frac{1}{2}}e^{\frac{2}{3}s^{3/2}\nu_i^{-3}}\mathrm{Ai}[\nu_i u+\frac{s}{\nu_i^2}]}{\prod_{j\neq i}(\nu_i^3-\nu_j^3)\prod_j(\nu_i^3+\lambda_j^3)}+\int_{\mathcal{C}}\frac{\mathrm{d}p}{2\pi\mathrm{i}}\frac{p^{-\frac{1}{6}}e^{\frac{2}{3}s^{3/2}/p}\mathrm{Ai}[p^{1/3}u+\frac{s}{p^{2/3}}]}{\prod_j(p-\nu_j^3)\prod_j(p+\lambda_j^3)}, \tag{184}$$

where $\mathcal{C}$ is the anticlockwise Hankel contour that bends around the negative real axis. Then, pushing the contour towards both sides of the negative real axis, making the change of variable $p=-\mu^3\pm\mathrm{i}\epsilon$ with $\mu>0$ and $\epsilon\to 0^+$, and using [1]

$$\mathrm{Ai}[e^{\pm\mathrm{i}2\pi/3}x]=\frac{1}{2}e^{\pm\mathrm{i}\pi/3}[\mathrm{Ai}(x)\mp\mathrm{i}\mathrm{Bi}(x)], \tag{185}$$

as well as the Sokhatsky-Weierstrass theorem, written here in concise form as

$$\lim_{\epsilon\to 0^+}\frac{1}{\mu^3-\nu^3+\mathrm{i}\epsilon}=\mathrm{p.v.}\frac{1}{\mu^3-\nu^3}-\frac{\mathrm{i}\pi}{3\mu^2}\delta(\mu-\nu), \tag{186}$$

we obtain

$$\begin{aligned} u\geq 0:\quad \mathrm{p.v.}\int_0^\infty\frac{\mathrm{d}\mu}{2\pi}&\frac{3\mu^{3/2}e^{-\frac{2}{3}s^{3/2}\mu^{-3}}\mathrm{Ai}[-\mu u+\frac{s}{\mu^2}]}{\prod_{j=1}^{k}(\mu^3+\nu_j^3)\prod_{j=1}^{\ell}(\mu^3-\lambda_j^3)}\\ &=\sum_{i=1}^{k}\frac{\nu_i^{-\frac{1}{2}}e^{\frac{2}{3}s^{3/2}\nu_i^{-3}}\mathrm{Ai}[\nu_i u+\frac{s}{\nu_i^2}]}{\prod_{j\neq i}(-\nu_i^3+\nu_j^3)\prod_j(-\nu_i^3-\lambda_j^3)}\\ &\quad+\frac{1}{2}\sum_{i=1}^{\ell}\frac{\lambda_i^{-\frac{1}{2}}e^{-\frac{2}{3}s^{3/2}\lambda_i^{-3}}\mathrm{Bi}[-\lambda_i u+\frac{s}{\lambda_i^2}]}{\prod_j(\lambda_i^3+\nu_j^3)\prod_{j\neq i}(\lambda_i^3-\lambda_j^3)}. \end{aligned} \tag{187}$$

Here, the symbol p.v. stands for the Cauchy principal value and must be understood with respect to μ^3 (rather than μ). That is, the integrals are regularized by cutting around each pole λ_j the interval $[\mu_-,\mu_+]$, with $\mu_\pm^3=\lambda_j^3\pm\epsilon$, which is symmetric in terms of μ^3 around λ_j^3, and taking the limit $\epsilon\to 0^+$. If $\ell=0$ the integral is regular and there is no need to introduce the principal value. In particular, the case $k=1$ and $\ell=0$ yields, with $\nu>0$,

$$u\geq 0:\quad \int_0^\infty\frac{\mathrm{d}\mu}{2\pi}\frac{3\mu^{3/2}}{\mu^3+\nu^3}e^{-\frac{2}{3}s^{3/2}\mu^{-3}}\mathrm{Ai}\left[-\mu u+\frac{s}{\mu^2}\right]=\nu^{-1/2}e^{\frac{2}{3}s^{3/2}\nu^{-3}}\mathrm{Ai}\left[\nu u+\frac{s}{\nu^2}\right]. \tag{188}$$

This implies that $\phi_{s,\nu}(r,u)$ defined by (34) is the solution of the form (32) that satisfies the constraint (33). Note that the restriction to $u\geq 0$ is essential. For instance, as $\mathrm{Arg}(u)$ grows from 0, the function $f(p)$ displays an exponential growth for $\pi-3\mathrm{Arg}(u)<\mathrm{Arg}(p)<\pi$ and we can no longer bend the integration contour onto the negative real axis.

Alternatively, as in [11], we can obtain (188) from the analysis of [31] and [32], or of [27], who studied several problems associated with the Klein-Kramers equation, by taking the limit of zero friction. However, these problems lead to discrete spectra and require a sophisticated analysis that involves infinite products to handle the poles associated with all eigenvalues.

Finally, making the change $k \to k+1$ and taking the limit $\nu_{k+1} \to 0^+$ in (187) gives the useful identity

$$u \geq 0: \quad \text{p.v.} \int_0^\infty \frac{\mathrm{d}\mu}{2\pi} \frac{3\mu^{-3/2} e^{-\frac{2}{3}s^{3/2}\mu^{-3}} \mathrm{Ai}[-\mu u + \frac{s}{\mu^2}]}{\prod_{j=1}^k (\mu^3 + \nu_j^3) \prod_{j=1}^\ell (\mu^3 - \lambda_j^3)}$$
$$= \frac{s^{-\frac{1}{4}} e^{-\sqrt{s}u}}{2\sqrt{\pi} \prod_j \nu_j^3 \prod_j (-\lambda_j^3)} - \sum_{i=1}^k \frac{\nu_i^{-\frac{7}{2}} e^{\frac{2}{3}s^{3/2}\nu_i^{-3}} \mathrm{Ai}[\nu_i u + \frac{s}{\nu_i^2}]}{\prod_{j\neq i} (-\nu_i^3 + \nu_j^3) \prod_j (-\nu_i^3 - \lambda_j^3)}$$
$$+ \frac{1}{2} \sum_{i=1}^\ell \frac{\lambda_i^{-\frac{7}{2}} e^{-\frac{2}{3}s^{3/2}\lambda_i^{-3}} \mathrm{Bi}[-\lambda_i u + \frac{s}{\lambda_i^2}]}{\prod_j (\lambda_i^3 + \nu_j^3) \prod_{j\neq i} (\lambda_i^3 - \lambda_j^3)}. \tag{189}$$

Equation (189) now applies to any $k \geq 0$, $\ell \geq 0$. In particular, the case $k = \ell = 0$ yields

$$u \geq 0: \quad e^{-\sqrt{s}u} = s^{1/4} \int_0^\infty \frac{\mathrm{d}\mu}{\sqrt{\pi}} 3\mu^{-3/2} e^{-\frac{2}{3}s^{3/2}\mu^{-3}} \mathrm{Ai}\left[-\mu u + \frac{s}{\mu^2}\right]. \tag{190}$$

Note that s can be absorbed in (190) through the change of variables $v = \sqrt{s}u$ and $\nu = \mu/\sqrt{s}$. By letting m parameters ν_i going to zero in a sequential manner, we could derive a series of similar identities for integrals of the form of (189) with a prefactor $\mu^{3/2-3m}$ for any $m \geq 0$. However, in this article we do not need to go beyond $m = 1$ as in (189)–(190).

In a similar fashion, we now consider the function $\hat{f}(p)$ of the complex variable p defined for $s_i \geq 0$, $u_i \geq 0$, by

$$\hat{f}(p) = e^{\frac{2}{3}(s_1^{3/2} - s_2^{3/2})/p} \mathrm{Ai}'\left[p^{1/3}u_1 + \frac{s_1}{p^{2/3}}\right] \mathrm{Ai}\left[e^{-\mathrm{i}\pi/3} p^{1/3} u_2 + e^{\mathrm{i}2\pi/3} \frac{s_2}{p^{2/3}}\right]. \tag{191}$$

It has a branch cut along the negative real axis and it grows as most as $p^{1/12}$ for $|p| \to \infty$ and $0 < \mathrm{Arg}(p) < \pi$. Then, in a manner similar to (182), we introduce the integral $\hat{F}_{k,\ell}(\nu_1, \ldots, \nu_k; \lambda_1, \ldots, \lambda_\ell)$ defined by

$$\hat{F}_{k,\ell}(\nu_i; \lambda_j) = \int_{-\infty+\mathrm{i}c}^{\infty+\mathrm{i}c} \frac{\mathrm{d}p}{2\pi} \frac{\hat{f}(p)}{\prod_{i=1}^k (p - \nu_i^3) \prod_{j=1}^\ell (p + \lambda_j^3)} \quad \text{with } c > 0, \tag{192}$$

with the conditions

$$\nu_i > 0, \qquad \nu_i \neq \nu_{i'} \qquad \text{for } i \neq i'; \qquad \lambda_j > 0, \quad \lambda_j \neq \lambda_{j'} \quad \text{for } j \neq j'; \qquad k + \ell \geq 2. \tag{193}$$

Note that the integration contour is now parallel to the real axis, in the upper half-plane, and that the asymptotic behavior of $\hat{f}(p)$ for large $|p|$, with $0 < \mathrm{Arg}(p) < \pi$, now requires $k + \ell \geq 2$. Pushing the contour upward, as $c \to +\infty$, we can see that $\hat{F}_{k,\ell} = 0$. Next, pushing the contour towards the real axis, by making the change of variable $p = \pm\mu^3 + \mathrm{i}\epsilon$ with $\mu > 0$ and $\epsilon \to 0^+$, and using (185), that also yields

$$\mathrm{Ai}'[e^{\pm\mathrm{i}2\pi/3} x] = \frac{1}{2} e^{\mp\mathrm{i}\pi/3} [\mathrm{Ai}'(x) \mp \mathrm{i}\mathrm{Bi}'(x)], \tag{194}$$

as well as (186), we obtain after taking the real part

$$u_i \geq 0: \quad \text{p.v.} \int_{-\infty}^{\infty} \frac{\mathrm{d}\mu}{2\pi} \frac{3\mu^2 e^{-\frac{2}{3}(s_1^{3/2}-s_2^{3/2})\mu^{-3}} \mathrm{Ai}'[-\mu u_1 + \frac{s_1}{\mu^2}]\mathrm{Ai}[\mu u_2 + \frac{s_2}{\mu^2}]}{\prod_{j=1}^k (\mu^3+\nu_j^3)\prod_{j=1}^\ell (\mu^3-\lambda_j^3)}$$

$$= -\frac{1}{2}\sum_{i=1}^k \frac{e^{\frac{2}{3}(s_1^{3/2}-s_2^{3/2})\nu_i^{-3}} \mathrm{Ai}'[\nu_i u_1 + \frac{s_1}{\nu_i^2}]\mathrm{Bi}[-\nu_i u_2 + \frac{s_2}{\nu_i^2}]}{\prod_{j\neq i}(-\nu_i^3+\nu_j^3)\prod_j(-\nu_i^3-\lambda_j^3)}$$

$$+ \frac{1}{2}\sum_{i=1}^\ell \frac{e^{-\frac{2}{3}(s_1^{3/2}-s_2^{3/2})\lambda_i^{-3}} \mathrm{Bi}'[-\lambda_i u_1 + \frac{s_1}{\lambda_i^2}]\mathrm{Ai}[\lambda_i u_2 + \frac{s_2}{\lambda_i^2}]}{\prod_j(\lambda_i^3+\nu_j^3)\prod_{j\neq i}(\lambda_i^3-\lambda_j^3)}. \tag{195}$$

Taking the imaginary part gives another identity, that involves the integral over μ of products $\mathrm{Bi}'\mathrm{Ai}$ and $\mathrm{Ai}'\mathrm{Bi}$, which we do not need for the present calculations. Again, in (195) the Cauchy principal value is understood with respect to μ^3. Exchanging the derivative in expression (191), we obtain an identity similar to (195) where the derivatives are exchanged:

$$u_i \geq 0: \quad \text{p.v.} \int_{-\infty}^{\infty} \frac{\mathrm{d}\mu}{2\pi} \frac{3\mu^2 e^{-\frac{2}{3}(s_1^{3/2}-s_2^{3/2})\mu^{-3}} \mathrm{Ai}[-\mu u_1 + \frac{s_1}{\mu^2}]\mathrm{Ai}'[\mu u_2 + \frac{s_2}{\mu^2}]}{\prod_{j=1}^k (\mu^3+\nu_j^3)\prod_{j=1}^\ell (\mu^3-\lambda_j^3)}$$

$$= -\frac{1}{2}\sum_{i=1}^k \frac{e^{\frac{2}{3}(s_1^{3/2}-s_2^{3/2})\nu_i^{-3}} \mathrm{Ai}[\nu_i u_1 + \frac{s_1}{\nu_i^2}]\mathrm{Bi}'[-\nu_i u_2 + \frac{s_2}{\nu_i^2}]}{\prod_{j\neq i}(-\nu_i^3+\nu_j^3)\prod_j(-\nu_i^3-\lambda_j^3)}$$

$$+ \frac{1}{2}\sum_{i=1}^\ell \frac{e^{-\frac{2}{3}(s_1^{3/2}-s_2^{3/2})\lambda_i^{-3}} \mathrm{Bi}[-\lambda_i u_1 + \frac{s_1}{\lambda_i^2}]\mathrm{Ai}'[\lambda_i u_2 + \frac{s_2}{\lambda_i^2}]}{\prod_j(\lambda_i^3+\nu_j^3)\prod_{j\neq i}(\lambda_i^3-\lambda_j^3)}. \tag{196}$$

Next, making the change $k \to k+1$ and taking the limit $\nu_{k+1} \to 0$ gives, for $k+\ell \geq 1$,

$$u_i \geq 0: \quad \text{p.v.} \int_{-\infty}^{\infty} \frac{\mathrm{d}\mu}{2\pi} \frac{3\mu^{-1} e^{-\frac{2}{3}(s_1^{3/2}-s_2^{3/2})\mu^{-3}}}{\prod_j(\mu^3+\nu_j^3)\prod_j(\mu^3-\lambda_j^3)}$$

$$\times \left[\mathrm{Ai}'\left(-\mu u_1 + \frac{s_1}{\mu^2}\right)\mathrm{Ai}\left(\mu u_2 + \frac{s_2}{\mu^2}\right) - \mathrm{AiAi}'\right]$$

$$= \frac{1}{4\pi}\left[\left(\frac{s_1}{s_2}\right)^{1/4} + \left(\frac{s_1}{s_2}\right)^{-1/4}\right] \frac{e^{-\sqrt{s_1}u_1 - \sqrt{s_2}u_2}}{\prod_j \nu_j^3 \prod_j(-\lambda_j^3)}$$

$$+ \frac{1}{2}\sum_{i=1}^k \frac{\nu_i^{-3} e^{\frac{2}{3}(s_1^{3/2}-s_2^{3/2})\nu_i^{-3}}}{\prod_{j\neq i}(-\nu_i^3+\nu_j^3)\prod_j(-\nu_i^3-\lambda_j^3)}$$

$$\times \left[\mathrm{Ai}'\left(\nu_i u_1 + \frac{s_1}{\nu_i^2}\right)\mathrm{Bi}\left(-\nu_i u_2 + \frac{s_2}{\nu_i^2}\right) - \mathrm{AiBi}'\right]$$

$$+ \frac{1}{2}\sum_{i=1}^\ell \frac{\lambda_i^{-3} e^{-\frac{2}{3}(s_1^{3/2}-s_2^{3/2})\lambda_i^{-3}}}{\prod_j(\lambda_i^3+\nu_j^3)\prod_{j\neq i}(\lambda_i^3-\lambda_j^3)}$$

$$\times \left[\mathrm{Bi}'\left(-\lambda_i u_1 + \frac{s_1}{\lambda_i^2}\right)\mathrm{Ai}\left(\lambda_i u_2 + \frac{s_2}{\lambda_i^2}\right) - \mathrm{BiAi}'\right]. \tag{197}$$

Here we combined both (195)–(196), and in each bracket the second product, such as AiAi', is equal to the first product where we exchange the derivative. Next, for the case $u_1 = u_2 = 0$, we again make the change $k \to k+1$ and take the limit $\nu_{k+1} \to \infty$. This yields for any $k \geq 0$, $\ell \geq 0$,

$$\begin{aligned}
\text{p.v.} \int_{-\infty}^{\infty} \frac{\mathrm{d}\mu}{2\pi} \frac{3\mu^{-1} e^{-\frac{2}{3}(s_1^{3/2} - s_2^{3/2})\mu^{-3}}}{\prod_j (\mu^3 + \nu_j^3) \prod_j (\mu^3 - \lambda_j^3)} \left[\mathrm{Ai}'\left(\frac{s_1}{\mu^2}\right) \mathrm{Ai}\left(\frac{s_2}{\mu^2}\right) - \mathrm{AiAi}' \right] \\
= -\frac{\delta_{k+\ell,0}}{2\pi} + \frac{\left(\frac{s_1}{s_2}\right)^{1/4} + \left(\frac{s_1}{s_2}\right)^{-1/4}}{4\pi \prod_j \nu_j^3 \prod_j (-\lambda_j^3)} + \frac{1}{2} \sum_{i=1}^{k} \frac{\nu_i^{-3} e^{\frac{2}{3}(s_1^{3/2} - s_2^{3/2})\nu_i^{-3}}}{\prod_{j \neq i} (-\nu_i^3 + \nu_j^3) \prod_j (-\nu_i^3 - \lambda_j^3)} \\
\times \left[\mathrm{Ai}'\left(\frac{s_1}{\nu_i^2}\right) \mathrm{Bi}\left(\frac{s_2}{\nu_i^2}\right) - \mathrm{AiBi}' \right] \\
+ \frac{1}{2} \sum_{i=1}^{\ell} \frac{\lambda_i^{-3} e^{-\frac{2}{3}(s_1^{3/2} - s_2^{3/2})\lambda_i^{-3}}}{\prod_j (\lambda_i^3 + \nu_j^3) \prod_{j \neq i} (\lambda_i^3 - \lambda_j^3)} \left[\mathrm{Bi}'\left(\frac{s_1}{\lambda_i^2}\right) \mathrm{Ai}\left(\frac{s_2}{\lambda_i^2}\right) - \mathrm{BiAi}' \right], \qquad (198)
\end{aligned}$$

where we used the Wronskian property (164) and $\delta_{k+\ell,0}$ is the Kronecker symbol. In particular, for $k = \ell = 0$ we obtain

$$\int_{-\infty}^{\infty} \frac{\mathrm{d}\mu}{\mu} e^{-\frac{2}{3}(s_1^{3/2} - s_2^{3/2})\mu^{-3}} \left[\mathrm{Ai}'\left(\frac{s_1}{\mu^2}\right) \mathrm{Ai}\left(\frac{s_2}{\mu^2}\right) - \mathrm{AiAi}' \right] = \frac{1}{6} \left[\left(\frac{s_1}{s_2}\right)^{1/4} + \left(\frac{s_1}{s_2}\right)^{-1/4} - 2 \right]. \qquad (199)$$

Since the integral is convergent at $\mu = 0$ there is no need to use the principal value.

Appendix C: Computation of the Two-Point Distribution

We present here the computation of the two-point distribution (82) from the two contributions $p^{>}$ and $p^{<}$ described in Figs. 4 and 5.

Let us first consider the contribution $p^{>}$. In a fashion similar to (55), using the Markovian character of the process $q \mapsto \{\psi, v\}$, it reads as

$$\begin{aligned}
& p^{>}_{x_1,x_2}(0 \leq q_1' \leq q_1, c_1; q_2' \geq q_2) \mathrm{d}c_1 \\
&= \lim_{q_\pm \to \pm\infty} \int \mathrm{d}\psi_- \mathrm{d}v_- K_{x_1,c_1}(0,0,0; q_-, \psi_-, v_-) \\
&\quad \times \int \mathrm{d}\psi_1 \mathrm{d}v_1 [K_{x_1,c_1}(0,0,0; q_1, \psi_1, v_1) - K_{x_1,c_1+\mathrm{d}c_1}(0,0,0; q_1, \psi_1, v_1)] \\
&\quad \times \left\{ \int \mathrm{d}\psi_+ \mathrm{d}v_+ K_{x_1,c_1}(q_1, \psi_1, v_1; q_+, \psi_+, v_+) - \int \mathrm{d}\psi_2 \mathrm{d}v_2 K_{x_1,c_1}(q_1, \psi_1, v_1; q_2, \psi_2, v_2) \right. \\
&\quad \left. \times \int \mathrm{d}\psi_+ \mathrm{d}v_+ K_{x_2,c_2}(q_2, \psi_2, v_2; q_+, \psi_+, v_+) \right\}. \qquad (200)
\end{aligned}$$

Then, we recognize $p_{x_1}(0 \leq q_1' \leq q_1)$ in the contribution associated with the first term in the bracket, and we can write

$$p^{>}_{x_1,x_2}(0 \leq q_1' \leq q_1; q_2' \geq q_2) = p_{x_1}(0 \leq q_1' \leq q_1) - \hat{p}^{>}_{x_1,x_2}(0 \leq q_1' \leq q_1; q_2' \geq q_2), \quad (201)$$

where we introduced the remaining part

$$\begin{aligned}
&\hat{p}^{>}_{x_1,x_2}(0 \leq q_1' \leq q_1, c_1; q_2' \geq q_2)\mathrm{d}c_1 \\
&= \lim_{q_\pm \to \pm\infty} \int \mathrm{d}\psi_- \mathrm{d}v_- \mathrm{d}\psi_1 \mathrm{d}v_1 \mathrm{d}\psi_2 \mathrm{d}v_2 \mathrm{d}\psi_+ \mathrm{d}v_+ \\
&\quad \times K_{x_1,c_1}(0,0,0;q_-,\psi_-,v_-)[K_{x_1,c_1}(0,0,0;q_1,\psi_1,v_1) - K_{x_1,c_1+\mathrm{d}c_1}(0,0,0;q_1,\psi_1,v_1)] \\
&\quad \times K_{x_1,c_1}(q_1,\psi_1,v_1;q_2,\psi_2,v_2) K_{x_2,c_2}(q_2,\psi_2,v_2;q_+,\psi_+,v_+). \quad (202)
\end{aligned}$$

In (201) we have also integrated $\hat{p}^{>}$ over c_1.

We can note that $p^{>}_{x_1,x_2}$ and $\hat{p}^{>}_{x_1,x_2}$ satisfy the following boundary conditions. First, taking the derivative with respect to q_1 to obtain the probability density $p^{>}_{x_1,x_2}(q_1; q_2' \geq q_2)$, we have

$$\lim_{q_2 \to q_1^+} p^{>}_{x_1,x_2}(q_1; q_2' \geq q_2) \to p_{x_1}(q_1), \quad \text{whence} \quad \lim_{q_2 \to q_1^+} \hat{p}^{>}_{x_1,x_2}(q_1; q_2' \geq q_2) = 0. \quad (203)$$

Indeed, following the discussion at the beginning of Sect. 5.1, if $\psi_0(q)$ is tangent to $\mathcal{P}_{x_1,c_1}$ at q_1, the second parabola $\mathcal{P}_{x_2,c_2}$ can only cross the first one at a point $q_* > q_1$ (otherwise, ψ_0' being continuous, if we had $q_* = q_1$ the curve $\psi_0(q)$ would go below $\mathcal{P}_{x_2,c_2}$ just beyond q_1). Then, all curves tangent to $\mathcal{P}_{x_1,c_1}$ at q_1 satisfy both properties $q_* > q_1$ and $q_2 > q_1$, so that they are all included in the contribution $p^{>}_{x_1,x_2}$ as we take the limit $q_2 \to q_1^+$ and we must recover $p_{x_1}(q_1)$, as stated in (203). Second, for large q_2 we obviously have the asymptotics

$$\lim_{q_2 \to +\infty} p^{>}_{x_1,x_2}(0 \leq q_1' \leq q_1; q_2' \geq q_2) = 0, \qquad \lim_{q_2 \to +\infty} \hat{p}^{>}_{x_1,x_2}(0 \leq q_1' \leq q_1; q_2' \geq q_2) = p_{x_1}(q_1). \quad (204)$$

This latter constraint can be directly checked on (202).

Using the transformations (17) and (20), we obtain

$$\begin{aligned}
&\hat{p}^{>}_{x_1,x_2}(0 \leq q_1' \leq q_1; q_2' \geq q_2) \\
&\quad = e^{\frac{\hat{u}_{21}}{\gamma} - \frac{q_2}{\gamma^2}} \int \mathrm{d}r_1 \mathrm{d}u_1 \mathrm{d}r_2 \mathrm{d}u_2 \mathrm{d}r_3 H_\infty(r_3, \hat{u}_1) \\
&\qquad \times \Delta(q_1; r_3, -\hat{u}_1; r_1, u_1) G(q_2 - q_1; r_1, u_1; r_2, u_2 + \hat{u}_{21}) H_\infty(r_2, u_2), \quad (205)
\end{aligned}$$

where we introduced as in (57) the quantities

$$\hat{u}_i = \sqrt{\frac{2}{D}} \frac{x_i}{t}, \qquad \hat{u}_{21} = \hat{u}_2 - \hat{u}_1. \quad (206)$$

Next, taking the derivative with respect to q_1, using the backward equation (37) for G and the forward equation (22) that is also satisfied by Δ, we obtain a total differential over r_1, which only leaves the boundary term at $r_1 = 0$:

$$\begin{aligned}
\hat{p}^{>}_{x_1,x_2}(q_1; q_2' \geq q_2) = e^{\frac{\hat{u}_{21}}{\gamma} - \frac{q_2}{\gamma^2}} &\int \mathrm{d}u_1 \mathrm{d}r_2 \mathrm{d}u_2 \mathrm{d}r_3 H_\infty(r_3, \hat{u}_1) u_1 \Delta(q_1; r_3, -\hat{u}_1; 0, u_1) \\
&\times G(q_2 - q_1; 0, u_1; r_2, u_2 + \hat{u}_{21}) H_\infty(r_2, u_2). \quad (207)
\end{aligned}$$

We can check from the explicit expressions of Δ and G that the integrations by parts leading to (207) are valid. The expression (207) clearly satisfies the property (203). Indeed, for $q_2 \to q_1^+$ the factor G implies $r_2 \to 0$, using the first boundary condition (23), which in turns leads to $u_2 + \hat{u}_{21} \le 0$ because of the second boundary condition in (23). However, the last factor H_∞ also implies $u_2 \ge 0$, using the boundary condition (39) applied to H_∞. Since $\hat{u}_{21} > 0$ both constraints on u_2 cannot be simultaneously satisfied which leads to (203). This can also be checked on (207) using the explicit expressions of Δ and H_∞.

Then, using the explicit expressions of G, Δ, and H_∞, and the results of Appendices A and B, it is possible to greatly simplify (207). Indeed, the integrals over r_i are immediate (they only involve factors of the form $e^{-v^3 r}$) whereas the integral over u_1 can be transformed using (175). Next, integrals over u_i are typically split over $u_i \le 0$ and $u_i \ge 0$, and each factor of the form $\mathrm{Ai}(-\mu u_i + s/\mu^2)$ with $u_i \ge 0$, or $\mathrm{Ai}(\mu u_i + s/\mu^2)$ with $u_i \le 0$, can be integrated over μ using the results (187)–(190) of Appendix B. This leads to products of the form $\mathrm{Ai}(\mu u_i + s_1/\mu^2)\mathrm{Ai}(\mu u_i + s_2/\mu^2)$ that can be integrated over u_i using the primitive (63), that also extends to the second Airy function Bi. Then, these terms can be further simplified using the Wronskian (164) and the results (195)–(199) of Appendix B. We eventually obtain in terms of dimensionless variables

$$\hat{P}^{>}_{X_1,X_2}(Q_1, Q_2' \ge Q_2) = \int_{-i\infty}^{+i\infty} \frac{\mathrm{d}s_1 \mathrm{d}s_2}{(2\pi \mathrm{i})^2} e^{(s_1-1)Q_1 + (s_2-1)Q_{21}} J(s_1, 2X_1) I(s_2, 2X_{21}), \quad (208)$$

with

$$Q_1 \ge 0, \quad Q_{21} = Q_2 - Q_1 \ge 0, \quad \text{and} \quad I(s, 2X) = \frac{1}{s-1} e^{-(\frac{2}{3}s^{3/2} - s + \frac{1}{3})2X/(s-1)}. \quad (209)$$

We can check that (208) agrees with both constraints (203)–(204). Then, taking the derivative with respect to Q_2 we obtain the full probability density associated with $q_* > q_2$ as

$$P^{>}_{X_1,X_2}(Q_1, Q_2) = \int_{-i\infty}^{+i\infty} \frac{\mathrm{d}s_1 \mathrm{d}s_2}{(2\pi \mathrm{i})^2} e^{(s_1-1)Q_1 + (s_2-1)Q_{21}} J(s_1, 2X_1)(s_2 - 1) I(s_2, 2X_{21}), \quad (210)$$

since the derivative with respect to Q_2 of the first term in the right hand side of (201) vanishes.

We now consider the second contribution, $p^{<}$, associated with the intersection q_* between both parabolas, $\mathcal{P}_{x_1,c_1}$ and $\mathcal{P}_{x_2,c_2}$, being in the range $q_1 < q_* < q_2$. Proceeding as for (55) and (200) it reads as

$$\begin{aligned}
&p^{<}_{x_1,x_2}(0 \le q_1' \le q_1, c_1; q_2' \ge q_2, c_2)\mathrm{d}c_1\mathrm{d}c_2 \\
&\quad = \lim_{q_\pm \to \pm\infty} \int \mathrm{d}\psi_- \mathrm{d}v_- K_{x_1,c_1}(0,0,0; q_-, \psi_-, v_-) \\
&\qquad \times \int \mathrm{d}\psi_1 \mathrm{d}v_1 [K_{x_1,c_1}(0,0,0; q_1, \psi_1, v_1) - K_{x_1,c_1+\mathrm{d}c_1}(0,0,0; q_1, \psi_1, v_1)] \\
&\qquad \times \int \mathrm{d}\psi_* \mathrm{d}v_* K_{x_1,c_1}(q_1, \psi_1, v_1; q_*, \psi_*, v_*) \int \mathrm{d}\psi_2 \mathrm{d}v_2 K_{x_2,c_2}(q_*, \psi_*, v_*; q_2, \psi_2, v_2) \\
&\qquad \times \int \mathrm{d}\psi_+ \mathrm{d}v_+ [K_{x_2,c_2}(q_2, \psi_2, v_2; q_+, \psi_+, v_+) - K_{x_2,c_2+\mathrm{d}c_2}(q_2, \psi_2, v_2; q_+, \psi_+, v_+)],
\end{aligned} \quad (211)$$

which we must integrate over both c_1 and c_2. We can note that it satisfies the boundary conditions

$$\lim_{q_2\to q_1^+} p^<_{x_1,x_2}(q_1;q_2'\geq q_2)\to 0, \quad \text{and} \quad \lim_{q_2\to+\infty} p^<_{x_1,x_2}(0\leq q_1'\leq q_1;q_2'\geq q_2)=0. \tag{212}$$

Using again (17), (20), we obtain

$$\begin{aligned} &p^<_{x_1,x_2}(0\leq q_1'\leq q_1;q_2'\geq q_2)\\ &\quad= e^{\frac{\hat{u}_{21}}{\gamma}-\frac{q_2}{\gamma^2}}\int \mathrm{d}r_1\mathrm{d}u_1\mathrm{d}r_*\mathrm{d}u_*\mathrm{d}r_2\mathrm{d}u_2\mathrm{d}r_3\mathrm{d}r_4 H_\infty(r_3,\hat{u}_1)\\ &\qquad\times\Delta(q_1;r_3,-\hat{u}_1;r_1,u_1)G(q_*-q_1;r_1,u_1;r_*,u_*)\\ &\qquad\times G(q_2-q_*;r_*,u_*-\hat{u}_{21};r_2,u_2)\frac{\partial H_\infty}{\partial r_2}(r_2,u_2). \end{aligned} \tag{213}$$

Next, taking again the derivative with respect to q_1 and using the forward and backward equations (22), (37), gives

$$\begin{aligned} &p^<_{x_1,x_2}(q_1;q_2'\geq q_2)\\ &\quad= e^{\frac{\hat{u}_{21}}{\gamma}-\frac{q_2}{\gamma^2}}\int \mathrm{d}u_1\mathrm{d}r_*\mathrm{d}u_*\mathrm{d}r_2\mathrm{d}u_2\mathrm{d}r_3\mathrm{d}r_4 H_\infty(r_3,\hat{u}_1)u_1\Delta(q_1;r_3,-\hat{u}_1;0,u_1)\\ &\qquad\times G(q_*-q_1;0,u_1;r_*,u_*)G(q_2-q_*;r_*,u_*-\hat{u}_{21};r_2,u_2)\frac{\partial H_\infty}{\partial r_2}(r_2,u_2). \end{aligned} \tag{214}$$

As for the derivation of (208), using the explicit expressions of G, Δ, and H_∞, and the results of Appendices A and B, as well as the property (28), we obtain

$$\begin{aligned} P^<_{X_1,X_2}(Q_1,Q_2'\geq Q_2) &= 2X_{21}e^{2X_{21}-Q_2}\int_{Q_1}^{Q_2}\mathrm{d}Q_*\int_{-i\infty}^{+i\infty}\frac{\mathrm{d}s_1\mathrm{d}s\mathrm{d}s_2}{(2\pi\mathrm{i})^3}e^{s_1Q_1+s(Q_*-Q_1)+s_2(Q_2-Q_*)}\\ &\quad\times J(s_1,2X_1)\frac{1}{s_2-1}[L(1,s;2X_{21})-L(s_2,s;2X_{21})], \end{aligned} \tag{215}$$

with

$$L(s_1,s_2;2X)=\frac{1}{2X}e^{-\frac{2}{3}(s_1^{3/2}-s_2^{3/2})2X/(s_1-s_2)}, \quad \text{whence } L(s,s;2X)=\frac{1}{2X}e^{-\sqrt{s}2X}. \tag{216}$$

We now have three inverse Laplace transforms because of the three terms ΔGG in (214). The integration over Q_* is associated with r_4 in (214) and c_2 in (211) (q_* being related to c_2 through (81)). It gives a factor $[e^{sQ_{21}}-e^{s_2Q_{21}}]/(s-s_2)$. Then, choosing for instance a contour such that $\Re(s_2)>\Re(s)>1$, we can integrate the first term over s_2, which gives zero by pushing the contour to the right, $\Re(s_2)\to+\infty$, and the second term over s, which gives the contribution associated with the pole at $s=s_2$. This yields

$$\begin{aligned} P^<_{X_1,X_2}(Q_1,Q_2'\geq Q_2) &= 2X_{21}e^{2X_{21}}\int_{-i\infty}^{+i\infty}\frac{\mathrm{d}s_1\mathrm{d}s_2}{(2\pi\mathrm{i})^2}e^{(s_1-1)Q_1+(s_2-1)Q_{21}}\\ &\quad\times J(s_1,2X_1)\frac{1}{s_2-1}[L(1,s_2;2X_{21})-L(s_2,s_2;2X_{21})]. \end{aligned} \tag{217}$$

We can check that (217) agrees with the constraints (212). Then, taking the derivative with respect to Q_2 we obtain the probability density

$$P^{<}_{X_1,X_2}(Q_1, Q_2) = 2X_{21}e^{2X_{21}} \int_{-i\infty}^{+i\infty} \frac{\mathrm{d}s_1 \mathrm{d}s_2}{(2\pi \mathrm{i})^2} e^{(s_1-1)Q_1+(s_2-1)Q_{21}} \times J(s_1, 2X_1)[L(s_2, s_2; 2X_{21}) - L(1, s_2; 2X_{21})]. \quad (218)$$

Finally, combining (210) and (218) we find that two terms cancel out and we are left with the total probability density (82).

References

1. Abramowitz, M., Stegun, I.A.: Handbook of Mathematical Functions. Dover, New York (1970)
2. Aurell, E., Gurbatov, S.N., Wertgeim, I.I.: Self-preservation of large-scale structures in Burgers' turbulence. Phys. Lett. A **182**, 109–113 (1993)
3. Aurell, E., Frisch, U., Noullez, A., Blank, M.: Bifractality of the devil's staircase appearing in the Burgers equation with Brownian initial velocity. J. Stat. Phys. **88**, 1151–1164 (1997)
4. Balian, R., Schaeffer, R.: Scale-invariant matter distribution in the universe. I—Counts in cells. Astron. Astrophys. **220**, 1–29 (1989)
5. Balian, R., Schaeffer, R.: Scale-invariant matter distribution in the universe. II—Bifractal behaviour. Astron. Astrophys. **226**, 373–414 (1989)
6. Bec, J., Khanin, K.: Burgers turbulence. Phys. Rep. **447**, 1–66 (2007)
7. Bernardeau, F.: The effects of smoothing on the statistical properties of large-scale cosmic fields. Astron. Astrophys. **291**, 697–712 (1994)
8. Bernardeau, F., Colombi, S., Gaztaaga, E., Scoccimarro, R.: Large-scale structure of the universe and cosmological perturbation theory. Phys. Rep. **367**, 1–248 (2002)
9. Bertoin, J.: The inviscid Burgers equation with Brownian initial velocity. Commun. Math. Phys. **193**, 397–406 (1998)
10. Burgers, J.M.: The Nonlinear Diffusion Equation. Reidel, Dordrecht (1974)
11. Burkhardt, T.W.: Semiflexible polymer in the half plane and statistics of the integral of a Brownian curve. J. Phys. A **26**, L1157–L1162 (1993)
12. Carraro, L., Duchon, J.: Equation de Burgers avec conditions initiales a accroissements independants et homogenes. Ann. Inst. Henri Poincare **15**, 431–458 (1998)
13. Cole, J.D.: On a quasi-linear parabolic equation occuring in aerodynamics. Q. Appl. Math. **9**, 225–236 (1951)
14. Colombi, S., Bouchet, F.R., Schaeffer, R.: Large scale structure statistics: Finite volume effects. Astron. Astrophys. **281**, 301–313 (1994)
15. Davis, M., Peebles, P.J.E.: On the integration of the bbgky equations for the development of strongly nonlinear clustering in an expanding universe. Astrophys. J. Suppl. S. **34**, 425–450 (1977)
16. Fournier, J.-D., Frisch, U.: L'equation de Burgers deterministe et statistique. J. Mec. Theor. Appl. **2**, 699–750 (1983)
17. Frachebourg, L., Martin, Ph.A.: Exact statistical properties of the Burgers equation. J. Fluid Mech. **417**, 323–349 (2000)
18. Frisch, U., Bec, J.: "Burgulence". In: Lesieur, M., Yaglom, A., David, F. (eds.) Les Houches 2000: New trends in turbulence. Springer, Berlin (2001)
19. Frisch, U., Bec, J., Aurell, E.: "Locally homogeneous turbulence" is it an inconsistent framework? Phys. Fluids **17**, 081706 (2005)
20. Fry, J.N.: Galaxy n-point correlation functions—theoretical amplitudes for arbitrary n. Astrophys. J. **277**, L5–L8 (1984)
21. Gradshteyn, I.S., Ryzhik, I.M.: Table of Integrals, Series, and Products. Academic Press, New York (1965)
22. Gurbatov, S., Malakhov, A., Saichev, A.: Nonlinear Random Waves and Turbulence in Nondispersive Media: Waves, Rays and Particles. Manchester University Press, Manchester (1991)
23. Gurbatov, S.N., Pasmanik, G.V.: Self-preservation of large-scale structures in a nonlinear viscous medium described by the Burgers equation. Sov. Phys. JETP **88**, 309–319 (1999)
24. Gurbatov, S.N., Saichev, A.I.: Degeneracy of one-dimensional acoustic turbulence at large Reynolds numbers. Sov. Phys. JETP **53**, 347–354 (1981)

25. Gurbatov, S.N., Saichev, A.I., Shandarin, S.F.: The large-scale structure of the universe in the frame of the model equation of non-linear diffusion. Mon. Not. R. Astron. Soc. **236**, 385–402 (1989)
26. Gurbatov, S.N., Simdyankin, S.I., Aurell, E., Frisch, U., Toth, G.: On the decay of Burgers turbulence. J. Fluid Mech. **344**, 339–374 (1997)
27. Hagan, P.S., Doering, C.R., Levermore, C.D.: The distribution of exit times for weakly colored noise. J. Stat. Phys. **54**, 1321–1352 (1989)
28. Hopf, E.: The partial differential equation $u_t + uu_x = u_{xx}$. Commun. Pure Appl. Mech. **3**, 201–230 (1950)
29. Kida, S.: Asymptotic properties of Burgers turbulence. J. Fluid Mech. **93**, 337–377 (1979)
30. Le Doussal, P.: Exact results and open questions in first principle functional rg. arXiv:0809.1192 (2008)
31. Marshall, T.W., Watson, E.J.: A drop of ink falls from my pen... it comes to earth, I know not when. J. Phys. A, Math. Gen. **18**, 3531–3559 (1985)
32. Marshall, T.W., Watson, E.J.: The analytic solutions of some boundary layer problems in the theory of Brownian motion. J. Phys. A, Math. Gen. **20**, 1345–1354 (1987)
33. Melott, A.L., Shandarin, S.F., Weinberg, D.H.: A test of the adhesion approximation for gravitational clustering. Astrophys. J. **428**, 28–34 (1994)
34. Molchan, G.M.: Burgers equation with self-similar Gaussian initial data: tail probabilities. J. Stat. Phys. **88**, 1139–1150 (1997)
35. Molchanov, S.A., Surgailis, D., Woyczynski, W.A.: Hyperbolic asymptotics in Burgers' turbulence and extremal processes. Commun. Math. Phys. **168**, 209–226 (1995)
36. Noullez, A., Gurbatov, S.N., Aurell, E., Simdyankin, S.I.: Global picture of self-similar and non-self-similar decay in Burgers turbulence. Phys. Rev. E **71**, 056305 (2005)
37. Peebles, P.J.E.: The Large Scale Structure of the Universe. Princeton University Press, Princeton (1980)
38. Press, W., Schechter, P.: Formation of galaxies and clusters of galaxies by self-similar gravitational condensation. Astrophys. J. **187**, 425–438 (1974)
39. Prodinger, H., Urbanek, F.J.: On monotone functions of tree structures. Discrete Appl. Math. **5**, 223–239 (1983)
40. Schaeffer, R.: The probability generating function for galaxy clustering. Astron. Astrophys. **144**, L1–L4 (1985)
41. She, Z.-S., Aurell, E., Frisch, U.: The inviscid Burgers equation with initial data of Brownian type. Commun. Math. Phys. **148**, 623–641 (1992)
42. Sheth, R.K., Tormen, G.: Large-scale bias and the peak background split. Mon. Not. R. Astron. Soc. **308**, 119–126 (1999)
43. Sinai, Ya.G.: Statistics of shocks in solutions of inviscid Burgers equation. Commun. Math. Phys. **148**, 601–621 (1992)
44. Valageas, P.: Non-linear gravitational clustering: smooth halos, substructures and scaling exponents. Astron. Astrophys. **347**, 757–768 (1999)
45. Valageas, P.: Dynamics of gravitational clustering. II. Steepest-descent method for the quasi-linear regime. Astron. Astrophys. **382**, 412–430 (2002)
46. Valageas, P.: Dynamics of gravitational clustering. IV. The probability distribution of rare events. Astron. Astrophys. **382**, 450–476 (2002)
47. Valageas, P.: Using the Zeldovich dynamics to test expansion schemes. Astron. Astrophys. **476**, 31–58 (2007)
48. Valageas, P.: Ballistic aggregation for one-sided Brownian initial velocity. Physica A **388**, 1031–1045 (2009). arXiv:0809.1192
49. Valageas, P., Munshi, D.: Evolution of the cosmological density distribution function: a new analytical model. Mon. Not. R. Astron. Soc. **354**, 1146–1158 (2004)
50. Vallée, O., Soares, M.: Les Fonctions d'Airy pour la Physique. Diderot, Paris (1998)
51. Vergassola, M., Dubrulle, B., Frisch, U., Noullez, A.: Burgers'equation, devil's staircases and the mass distribution for large-scale structures. Astron. Astrophys. **289**, 325–356 (1994)
52. Zeldovich, Y.B.: Gravitational instability: An approximate theory for large density perturbations. Astron. Astrophys. **5**, 84–89 (1970)